Personalized musculoskeletal modeling

Bone morphing, knee joint modeling, and applications

Dzialo, Christine Mary

DOI (link to publication from Publisher):
10.5278/vbn.phd.eng.00076

Publication date:
2018

Document Version
Publisher's PDF, also known as Version of record

PERSONALIZED MUSCULOSKELETAL MODELING

BONE MORPHING, KNEE JOINT MODELING, AND APPLICATIONS

BY
CHRISTINE MARY DZIALO

DISSERTATION SUBMITTED 2018

AALBORG UNIVERSITY
DENMARK

PERSONALIZED MUSCULOSKELETAL MODELING–

BONE MORPHING, KNEE JOINT MODELING, AND APPLICATIONS

by

Christine Mary Dzialo

Dissertation submitted December 2018

Dissertation submitted:	December 2018
PhD supervisor:	Associate Prof. Michael Skipper Andersen Aalborg University
Assistant PhD supervisor:	Associate Prof. Mark de Zee Aalborg University
PhD committee:	Clinical Professor Søren Kold (chairman) Aalborg University
	Senior Researcher Raphaël Dumas Université Lyon
	Professor Elena M. Gutierrez-Farewik KTH Mechanics
PhD Series:	Faculty of Engineering and Science, Aalborg University
Department:	Department of Materials and Production

ISSN (online): 2446-1636
ISBN (online): 978-87-7210-373-0

Published by:
Aalborg University Press
Langagervej 2
DK – 9220 Aalborg Ø
Phone: +45 99407140
aauf@forlag.aau.dk
forlag.aau.dk

Typeset in Word and printed Denmark by Rosendahls, 2019

KNEEMO
Initial Training Network in
Knee Osteoarthritis Research

The work presented in this PhD dissertation was carried out at Aalborg University in the Biomechanics Group of the Department of Materials and Production. This research was part of the KNEEMO Initial Training Network and has received funding from the European Union's Seventh Framework Programme for research, technological development and demonstration under grant agreement no 607510.

Publications in peer-reviewed scientific journals

1. Dzialo, C.M., Pedersen Heide, P., Simonsen, C.W., Krogh, K., de Zee, M., Andersen, M.S., 2018. Development and validation of subject-specific moving-axis tibiofemoral joint model using MRI and EOS imaging during a quasi-static lunge. Journal of Biomechanics. https://doi.org/10.1016/j.jbiomech.2018.02.032
2. Dzialo, C.M., Pedersen, P.H., Krogh, K., de Zee, M., Andersen, M.S. (2018) Evaluation of predicted patellofemoral joint kinematics with a moving-axis joint model, *Medical Engineering and Physics*, under review.
3. Dzialo, C.M., Mannisi, M., Halonen, K.S., de Zee M., Woodburn, J., Andersen, M.S. (2018) Comparison of generic vs patient-specific musculoskeletal model-scaling techniques for identification of personalized gait alteration for individuals diagnosed with medial compartment knee osteoarthritis, *International Biomechanics*, under review.

Co-authored publications in peer-reviewed scientific journals

1. Halonen, K.S., **Dzialo, C.M.**, Mannisi, M., Venäläinen, M.S., Zee, M. De, Andersen, M.S., 2017. Workflow assessing the effect of gait alterations on stresses in the medial tibial cartilage – combined musculoskeletal modelling and finite element analysis. Scientific Reports. 7, 17396. https://doi.org/10.1038/s41598-017-17228-x
2. Andersen, M.S., **Dzialo, C.M.**, Marra, M.A., Pedersen, D. (2018) The effect of measurement uncertainties on estimated knee ligament properties from laxity measurements, *Journal of Biomechanics*, under review.
3. Dejtiar, D.L., **Dzialo, C.M.**, Pedersen, P.H., Jensen, K.K., Fleron, M.K., Andersen, M.S. (2018) Development and evaluation of a subject-specific lower limb model with an 11 DOF natural knee model using MRI and EOS during a quasi-static lunge, *Journal of Biomechanical Engineering*, under review.
4. Crabolu, M., Cereatti, A., Pani, D., Raffo, L., Croce, U.D., Konrath, J., **Dzialo, C.M.**, Hol, J., Schepers, M., Bellusci, G. (2019) Automatic lower body segment length calibration using wearable inertial measurement units. *Manuscript in preparation phase.*

Publications in proceedings and monographs

1. C.M. Dzialo, M. Mannisi, M. Marra, R. Richards, S. Telfer, J. Woodburn, et al.
   A subject-specific analysis framework to investigate gait alterations
   Osteoarthritis & Cartilage, 24 (2016), p. S126, 10.1016/j.joca.2016.01.247
2. C.M. Dzialo, P.H. Pedersen, C.W. Simonsen, K.K. Jensen, M. de Zee, M.S. Andersen (2017). Development of subject-specific moving-axis knee model. Presented at XVI International Symposium on Computer Simulation in Biomechanics, Gold Coast, Australia, Computer
3. C.M. Dzialo, P.H. Pedersen, C.W. Simonsen, K.K. Jensen, M. de Zee, M.S. Andersen (2017). Development and validation of subject-specific moving-axis knee model using MRI and EOS imaging during quasi-static movements. Presented at XXVI Congress of the International Society of Biomechanics, Brisbane, Australia
4. C. M. Dzialo, M. Mannisi, K. Halonen, J. Woodburn, M. de Zee, M. S. Andersen (2018). Patient-Specific Musculoskeletal Modelling Influence of model scaling on clinical outcomes. Presented at Peacocks Medical Group Symposium, Liverpool, UK
5. A. Culvenor, **C. Dzialo**, K. Halonen, J.Kemnitz, M. Mannisi, W.Wirth. (2018). Musculoskeletal Modelling and the Role of Thigh Muscles in Knee OA Presented at Osteoarthritis Research Society International, Liverpool, UK
6. Halonen, K., Galibarov, P.E., **Dzialo, C.M.**, Damsgaard, M., Andersen, M.S. (2017) Multiscale Simulation Framework as a Research Tool for Clinical Gait Alteration Strategies, Presented at Congress of the European Society of Biomechanics, Seville, Spain

ENGLISH SUMMARY

This PhD study was part of a greater collaborative effort, funded by the EU within an initial training network called KNEEMO; which worked towards a step change in early detection of knee osteoarthritis (OA) and non-pharmacological management of the disease through personalized interventions. This dissertation focused on personalized musculoskeletal modeling, with emphasis on bone morphing, knee joint modeling, and clinical applications. The main aims of the PhD project were to (1) develop and validate a computationally efficient novel knee joint model, while capturing the subject-specific kinematics and bone geometries. (2) To establish a subject-specific multi-scale model, ultimately allowing clinicians to investigate how varying biomechanics and orthoses interventions can affect the internal loads of the body and influence the stresses/strains on anatomical features. (3) Determine if treatment outcomes, based on individual patients and a patient group as a whole are influenced by different musculoskeletal model scaling techniques.

First, an introduction chapter outlines the general information and state-of-the-art studies relevant to the dissertation. Here, the epidemiology of knee osteoarthritis (KOA) is described, including current diagnosis procedures and common treatment methods for early and late stage KOA. Next, computational modeling, with an emphasis on lower limb and knee joint anatomy, is introduced; focusing on musculoskeletal and finite element modeling genres. Then, various model validation approaches are discussed that (1) have already been established and (2) should be considered more in the future in regard to computational modeling. Finally, the importance of personalized models is considered, covering how these models are typically developed, and what they can be used for with respect to model application.

In the second chapter, subject-specific moving-axis tibiofemoral joint models using MRI and EOS imaging during a quasi-static lunge are developed and validated. In the literature, musculoskeletal tibiofemoral joint models can range from simple generic (hinge) to complex subject-specific (multi-body contact models) depending on their generic qualities and computational time. The main aims of this study were to create a novel subject-specific tibiofemoral joint model that is computationally efficient and can predict anatomically accurate secondary joint kinematics. The model utilized a moving-axis concept that is based upon a linear relationship between two tibiofemoral flexion positions. Validation of this approach is performed by measuring the secondary joint kinematics from a quasi-static lunge obtained using biplanar EOS Imaging, segmented 2D EOS contours and 3D MRI bone geometries, and custom written MATLAB registration software. Additionally, the study compared the model against a commonly used subject-specific hinge model in attempt to show the advantages and advancements of the proposed model. The resulting secondary joint kinematics proved to be better predicted when employing a moving-axis tibiofemoral model as compared to a hinge, with an average mean difference and standard error of

(translations: 2.84 ± 0.31 mm, rotations: 1.25 ± 0.43^0) and higher coefficients of determination (R^2) for each clinical measure. The commonly used hinge model resulted in an average mean difference and standard error of (3.87 ± 0.39 mm, 7.39 ± 0.87^0). No significant differences were found between the moving-axis model and the experimentally observed tibiofemoral joint rotations from the EOS data, while this was not the case for the hinge model. Achieving our initial aims, it was concluded that the moving-axis joint can better predict experimentally observed rotations and translations when compared to the commonly used subject-specific hinge model.

Chapter 3 expands upon the work done in Chapter 2 by applying the moving-axis principal to the patellofemoral joint and evaluating the predicted patellar motion derived from 6 combinations of tibiofemoral (hinge, moving-axis, interpolated) and patellofemoral (hinge and moving-axis) models against experimental in vivo kinematics from a series of biplanar EOS images. In addition to the novel moving-axis patellofemoral joint, this study introduces an interpolated tibiofemoral joint calibrated from the five EOS quasi-static lunge positions. In this particular model, error is only permitted from the patellofemoral model when compared against the EOS experimental data. The results from this paper show that a moving-axis tibiofemoral joint in combination with a hinge patellofemoral joint offer (-5.12 ± 1.23 mm, 5.81 ± 0.97 mm, 14.98 ± 2.30°, -4.35 ± 1.95°) mean differences when compared to the experimental EOS data in terms of lateral-shift, superior translation, patellofemoral-flexion, and patellar-rotation respectively. While when using a moving-axis patellofemoral joint in exchange for the hinge a mean difference of (-2.69 ± 1.04 mm, 1.13 ± 0.80 mm, 12.63 ± 2.03°, 1.74 ± 1.46°) was achieved. As to be expected, the model predictive capabilities increased as a direct result of adding more calibrated positions to the tibiofemoral model (hinge-1, moving-axis-2, and interpolated-5) for most patellofemoral kinematic measures. Overall, the aim of establishing a novel subject-specific moving-axis patellofemoral model was achieved; that produces realistic patellar motion for certain kinematic measures and is computationally efficient enough for clinical applications. However, the error arising from patellar tilt, rotation, and medial-lateral translation is not ideal and the introduction of ligaments and contact (in 2 DOF), giving the model a force response along the directions where the major external influences are expected to be, in the future might be an added benefit.

Chapter 4 presents a workflow that combines motion capture, ground reaction forces, MRI, bone morphing, multibody dynamics, and finite element analysis to assess the effect of gait modifications and lateral wedge insoles on the stresses and strains in the medial tibial cartilage. The goal of this multi-scale model was to simultaneously estimate net joint loads from a musculoskeletal model and stresses in soft tissues of the knee during normal and modified gait through finite element analyses. Only one subject was modeled due to the methodological nature of this study and the focus of establishing a method to investigate the outcomes of various gait alterations effects

(rather than proving or disproving the benefits of a particular technique). In order to achieve the multi-scale model, full lower limb and detailed MRI images were needed to establish the bone and ligament architecture of the musculoskeletal model and the soft tissue structures of the finite element model. Various gait alterations (normal shod walking, 5° and 10° lateral wedge insole walking, toe-in, and toe-out wide walking) were first recorded in a gait laboratory. Then processed through the musculoskeletal model, were output forces were obtained and used as boundary conditions for the finite element knee model; ultimately tibial articular cartilage stresses and strains were achieved. What was found for this particular individual was that during the stance phase, the LWI failed to reduce medial peak pressures apart from the second loading peak during the insole-10° trial. While the toe-in modification achieved reduced peak pressures of -11% during the first peak, the opposite effect occurred during the second peak increasing the pressures by nearly 12%. Additionally, when the subject walked with toe-out gait, the peak pressures reduced by -15% during the first peak and increased by 7% during the second peak. Overall, a workflow was established during this study allowing researchers to assess the effect of low-cost clinical interventions aimed at reducing loads in the medial tibial cartilage on a subject-specific basis. Furthermore, the groundwork necessary to develop patient-specific models has been created to better optimize treatments based on an individual patient rather than cohort.

The last paper for this dissertation is presented in Chapter 5, comparing generic vs patient-specific musculoskeletal model-scaling techniques for identification of personalized gait alteration for individuals diagnosed with medial compartment knee osteoarthritis. Gait alterations, such as gait modifications and lateral wedged insoles, are a controversial topic due to the success of these interventions not always being exclusive. So, the purpose of this study was to analyze the effect gait alterations on medial contact forces through use of patient-specific musculoskeletal models, exploring what might contribute to these inconsistencies in patient responses. One hypothesis of why these inconsistences are observed is that the whole study group is provided with the same intervention, although each patient may require individualized interventions, which on a group level can lead to a no response average. Additionally, the type of musculoskeletal model scaling approach may influence the outcomes. To answer these questions, motion capture was recorded of five patients with clinical evidence of medial knee osteoarthritis during normal walking, walking with patient-specific lateral wedged insoles (0°, 5°, and 10°), walking with a gait modification (toe-in, toe-out, wide stance). Then two kinds of patient-specific musculoskeletal models were constructed for each patient (1) by manually segmenting MRI images of the patients that were then used to morph a generic model to the patient-specific bone geometries and (2) through use of a simple linear scaling technique, that utilizes the marker placements from the motion capture data. The main parameters investigated during this study were the medial contact force peak and impulse values during stance phase of walking. What was found as a result from this study was that a ‘one-size-fits-all’ gait alteration aimed at minimizing medial contact loading does not exist for these five patients, which suggests the importance of individually assigned interventions.

Moreover, the different scaling and morphing techniques used on the musculoskeletal models lead to differences in medial contact forces. Highlighting the importance of further investigation of scaling approaches prior to being able to use such models in the clinical setting to assist in prescribing gait alterations. With the small sample size being a main limitation, detection of meaningful clinical results was beyond the scope of this study.

The final chapter provides a summary of key results from the publications making up this dissertation and a discussion regarding the outcomes of this PhD research. Additionally, the limitations of these studies are addressed and recommendations for future research outlined. The research conducted during this PhD study is merely a starting point in hopes of future researchers better validating personalized knee joint models and directing patient-specific musculoskeletal modeling into to the clinical setting. In order to further validate various personalized knee models, more extensive in vivo dynamic data sets are needed to explore various motions of daily living, to make sure these models are capable of predicating kinematics from movements other than lunging. Additionally, more efficient computational building methods are needed for these models to be used in the clinical setting, the main hold up is occurring when obtaining personalized bone geometries. Thus, effort needs to be focused on (1) automatic segmentation and or (2) determining how accurate is good enough with respect to bone geometries and computational modeling.

DANSK RESUME

Dette PhD projekt var del af en større samarbejdsindsats med midler fra EU indenfor et initielt træningsnetværk kaldet KNEEMO, som har arbejdet for en radikal ændring i tidlig opdagelse af knæartrose (KA) og ikke-farmakologisk behandling af sygdommen igennem individualiserede interventioner. Denne afhandling fokuserede på individualiseret muskuloskeletal modellering med vægt på knogleforandringer, knæledsmodellering, og klinisk anvendelse. Hovedmålene med PhD projektet var (1) at udvikle og validere en ny beregningseffektiv knæledsmodel baseret på individspecifik kinematik og knoglegeometri. (2) At etablere en individspecifik multiskala model, der ultimativt tillader klinikere at undersøge, hvordan varierende biomekanik og ortoseinterventioner kan påvirke kroppens interne belastninger og spændinger/tøjninger på anatomiske strukturer. (3) Afgøre om behandlingsresultater, baseret på individuelle patienter og en patientgruppe som helhed, bliver påvirket af forskellige muskuloskeletalmodellerings skaleringsteknikker.

Først kommer et introduktionskapitel, der beskriver den generelle information og de nyeste studier relevante for afhandlingen. Her beskrives epimiologien bag KA samt nuværende diagnoseprocedurer og almindelige behandlingsmetoder ved tidlig og senstadie KA. Derefter introduceres computermodellering, der ligger vægt på undereskstremitet- og knæledsanatomi; med fokus på muskuloskeletal og finite element modelling. Derfra følger en diskussion af forskellige tilgange til modelvalidering der (1) allerede er etableret og (2) burde benyttes mere i fremtiden med hensyn til computermodellering. Til sidst vil vigtigheden af individualiserede modeler betragtes, samt hvordan disse modeller typisk udvikles og hvordan de kan anvendes.

I andet afsnit præsenteres udviklingen og valideringen af individuelt tilpassede modeller af det tibiofemorale led med en flytbar knæakse ved benyttelse af MRI og EOS skanninger, under kvasi-statisk lunge. I den muskuloskeletale litteratur varierer tibiofemorale ledmodeller fra simple generiske hængseler til komplekse individ-specifikke (multi-legeme kontaktmodeller) alt afhængigt af deres generiske egenskaber og beregningstid. Hovedmålet med dette studie var at skabe en ny individ-specifik tibiofemoral ledmodel der er beregningseffektiv og kan forudsige anatomisk nøjagtig sekundær ledkinematik. Modellen benytter et flytbart knæakse koncept, der er baseret på et linært forhold mellem to tibiofemoral fleksionspositioner. Validering af denne tilgang foretages ved at måle den sekundære ledkinematik under et kvasi-statisk lunge indsamlet ved brug af toplansrøngten med EOS teknologien, segmenterede 2D konturer og 3D MRI knoglegeometrier og tilpasset MATLAB registreringssoftware. Derudover sammenligner studiet modellen med en alment brugt individ-specifik hængselmodel i et forsøg på at vise fordele og fremskridt ved den nærværende model. Den resulterende sekundære ledkinematik blev forudsagt bedre ved brug af en flytbar knæakse model, sammenlignet med et hængsel, med en gennemsnitlig forskel og standardfejl på (translationer: 2.84 ± 0.31 mm, rotationer:

1.25 ± 0.43°) og højere korrelationskoefficienter (R^2) for hver klinisk varibel. De alment brugte hængselsmodeller resulterede i en gennemsnitlig forskel og standardfejl på (3.87 ± 0.39 mm, 7.39 ± 0.87°). Der blev ikke findet en signifikant forskel mellem den flytbare knæakse model og de eksperimentielt observerede tibiofemorale ledrotationer fra EOS data, mens dette ikke var tilfældet for hængselsmodellen. Da vi opnåede vores oprindelige mål, blev det konkluderet at det flytbare knæakseled bedre kan forudsige eksperimentielt observerede rotationer og translationer, når denne sammenlignes med den alment brugte individuelt tilpassede hængselsmodel.

Kapitel 3 bygger oven på arbejdet lavet i kapitel 2 ved at anvendte det flytbare akse princip på det patellofemorale led og evaluerer den forudsagte patella bevægelse ved seks kombinationer af tibiofemoral(hængsel, flytbar akse, interpoleret) og patellofemorale (hængsel og flytbar akse) modeller mod eksperimentielt in vivo kinematik fra en serie af toplans EOS røntgenbilleder. Ud over det nye patellofemorale led med flytbar akse introducerer dette studie et interpoleret tibiofemoral led kalibreret fra de fem EOS kvasi-statiske lunge positioner. I denne specifikke model er fejl begrænset til den patellofemorale model, når denne sammenlignes med det eksperimentelle EOS data. Resultatet af dette studie viser, at et flytbar akse tibiofemoral led i kombination med et hængsel patellofemoralt led giver (-5.12 ± 1.23 mm, 5.81 ± 0.97 mm, 14.98 ± 2.30°, -4.35 ± 1.95°) gennemsnitsforskelle sammenlignet med det eksperimentelle EOS data i forhold til henholdsvis lateral-shift, superior translation, patellofemoral-fleksion, og patellar-rotation. Når et flybar akse patellofemoral led blev brugt istedet for et hængsel blev der opnået en gennemsnitsforskel på (-2.69 ± 1.04 mm, 1.13 ± 0.80 mm, 12.63 ± 2.03°, 1.74 ± 1.46°). Modellens prædiktive kapaciteter blev øget som et resultat af at tilføje flere kalibrerede positioner til den tibibiofemorale model (hængsel-1, flytbar akse-2, og interpoleret-5) for de fleste af de patellofemorale kinematiske målinger. Samlet set blev målet med at etablere en ny individ-specifik flytbar patellofemoral model opnået; den producerer realistisk patella bevægelse for nogle af de kinematiske variable og er beregningseffektiv nok til klinisk anvendelighed. Imidlertid er fejlen som opstår fra patellar tilt, rotation, og medial lateral translation ikke ideal og introduktionen af ligamenter og kontakt (i 2 frihedsgrader) kan måske være gavnlig, da dette giver modellen en mulig kraftpåvirkning langs retningerne, hvor den største påvirkning af de eksterne belastninger forventes.

Kapitel 4 præsenterer et workflow, der kombinerer bevægelsesmålinger, underlagsreaktionskræfter, MRI, knogleforandringer, multilegeme dynamik, og finite element analyser til at vurdere effekten af gangartmodifikationer og lateral kileindlæg på spændingspåvirkningerne i det mediotibiale bruskvæv. Målet med denne multiskalamodel var at samtidigt estimere den samlede ledbelastning med en muskuloskeletal model og spændingspåvirkningen i det bløde væv i knæet under normal og modificeret gang vha. finite element analyser. Kun én forsøgsperson blev modeleret på grund af dette studies metodologiske karakter og fokus på at etablere en metode til at undersøge resultaterne af forskellige gangartændringer (i stedet for at be- eller afkræfte de gavnlige effekter af en bestemt gangart eller lateral kile). For at skabe

multiskalamodellen var detaljerede MRI billeder af undereskremiteterne nødvendige for at bestemme knogle- og ledbåndsarkitekturen til den muskuloskeletale model og blødvævsstrukturerne i finite element modellen. Forskellige gangartændringer (normal gang med sko, gang med 5° and 10° lateral kileindlæg, tå-ind, og tå-ud bred gang) blev first optaget i et gangartslaboratorie. Derefter blev det kørt igennem den muskuloskeletale model hvor de resulterende kræfter og momenter blev brugt som randbetingelser til finite element knæmodellen, hvilket ultimativt førte til at tibiale ledbrusk spændingspåvirkninger opnås. For dette individ blev der fundet, at under standfasen kunne LWI ikke reducere det maksimale medial-tryk bortset fra det andet belastningsmaksimum under indlæg-10° forsøget. Mens tå-in modifikationen reducerede det maksimale tryk med -11% under det første belastningsmaksimum, så opstod den modsatte effekt under det andet belastningsmaksimum, hvilket øgede trykket med næsten 12%. Desuden, når forsøgspersonen gik med tå-ud gang, blev det maksimale tryk reduceret med -15% under det første belastningsmaksimum, og øget med 7% under det andet. Alt i alt blev et workflow etableret i dette studie, som gør det muligt for forskerne at vurdere effekten af lav-omkostnings kliniske interventioner rettet mod at reducere belastninger i det mediotibiale brusk på en individ-specifik basis. Endvidere er det nødvendige grundlag lagt for at udvikle patient-tilpassede modeller til at optimere behandling baseret på en individuel patient i stedet for en kohorte.

Det sidste studie i denne afhandling præsenteres i kapitel 5. Her sammenlignes generiske og patient-specifikke muskuloskeletal modelskaleringsteknikker for identificering af personaliserede gangartændringer for individer diagnosticeret med medial kompartement KA. Gangartændringer, såsom gangartmodifikationer og laterale kileindlæg, er et kontroversielt emne som følge af, at successen med disse interventioner ikke er entydig. Formålet med dette studie var dermed at analysere den effekt som gangartændringer havde på den mediale kontaktkraft gennem brug af patientspecifikke muskuloskeletale modeller, og udforsker hvad der kunne bidrage til disse inkonsistente patientresponser. Én hypotese om hvorfor denne inkonsistens observeres er, at hele undersøgelsesgruppen er forsynet med den samme intervention, selvom hver patient givetvis kræver individualiserede interventioner, og på gruppe-niveau kan dette føre til et gennemsnit, der ikke viser respons. Derudover kan typen af musculoskeletal modelskalering påvirke resultatet. For at besvare disse spørgsmål blev bevægelsesdata indsamlet fra fem patienter med klinisk evidens for medial KA ved normal gang, gang med patient-specifikke laterale kileindlæg (0°, 5°, and 10°), gang med en gangartsmodification (tå-ind, tå-ud, bred stand). Derefter blev to slags patient-specifikke muskuloskeletale modeller konstrueret for hver patient (1) ved manualt at segmentere MRI billeder fra patienterne, som så blev brugt til at tilpasse en generisk model til den patient-specifikke knoglegeometri og (2) gennem brug af en simpel lineær skaleringsteknik, der benytter markørplacering fra bevægelsesdata. Hovedparametrene undersøgt under dette studie var den maksimale mediale kontaktkraft og impulsen under standfasen af gang. Det der blev fundet som et resultat af dette studie var, at en 'one-size-fits-all' gangartændring målrettet mod minimering af den mediale kontaktkraft ikke eksisterer for disse fem patienter, hvilket tyder på vigtigheden af individuelt tildelte interventioner. I øvrigt fører brugen af forskellige

skalerings- og tilpasningsteknikker af de muskuloskeletale modeller til forskelle i den medial kontaktkraft. Hermed fremhæves vigtigheden af videre undersøgelser af skaleringstilgange før brugen af sådanne modeller kan anvendes klinisk til at assistere med at ordinere gangartsændringer. Med den lille stikprøvestørrelse var opdagelse af meningsfyldte kliniske resultater udenfor studiets rækkevidde.

Det sidste kapitel giver et resumé af hovedresultaterne fra publikationerne i denne afhandling samt en diskussion af resultaterne fra denne PhD's forskning. Derudover bliver begrænsningerne adresseret og anbefalinger til fremtidig forskning angivet. Forskningen udført under dette PhD-studie er kun en start i håbet om at fremtidige forskere bedre kan validere personaliserede knæledsmodeller og føre patient-specifik muskuloskeletale modeller ud i klinikken. For yderlige at kunne validere forskellige personaliserede knæmodeller skal der gøres brug af mere omfattende in vivo dynamiske datasæt for at udforske forskellige dagligdagsbevægelser for at sikre sig, at disse modeller er i stand til at forudsige kinematik fra andre bevægelser end lunge. Desuden er der behov for hurtigere modeludvikling for at disse modeller kan anvendes klinisk, og den primære flaskehals er at opnå individuelle knoglegeometrier. Derfor skal der fokuseres en indsats på (1) automatisk segmentering og eller (2) bestemmelse af hvor stor nøjagtighed, der kræves mht. knoglegeometri og computermodelleringen.

PREFACE

This dissertation has been submitted to the Faculty of Engineering and Science at Aalborg University in partial fulfillment of the requirements for the degree of Doctor of Philosophy in Mechanical Engineering. The work was carried out at the Department of Materials and Production, AAU from January 2015 until December 2018 under the supervision of Professors Michael Skipper Andersen and Mark de Zee. This PhD study was completed as part of the KNEEMO project; an Initial Training Network for knee osteoarthritis research funded by the European Union's Seventh Framework Programme. I would like to acknowledge those who envisioned the KNEEMO project, for without your perseverance of this grant proposal I would not have had the chance to be part of such an amazing network or to move to Denmark for the pursuit of my PhD.

First and foremost, I would like to thank my supervisor, Michael Skipper Andersen, for the endless support and leadership. It has been a privilege to work with you, I have learned so much and hope to have great collaborations in the future. I would also like to thank my co-supervisor, Mark de Zee for all the help in the motion capture lab and invaluable guidance, especially in the realm of work life balance. Additionally, I'd like to thank the head of our research group, John Rasmussen, for all the knowledge you have shared with me, whether it was regarding biomechanics, Danish culture, or life in general; there has never been a dull conversation.

I'd like to extend my gratitude to Dr. Jens Brøndum Frøkjær, Carsten Wiberg Simonsen, and Kenneth Krogh Jensen of the Department of Radiology and Dr. Peter Heide Pedersen from the Department of Orthopedic Surgery at Aalborg Universitetshospital for their time and effort in developing imaging protocols and collecting data used for Papers I and II in this PhD dissertation. Furthermore, I am deeply thankful for the external supervision from Prof Jim Woodburn and all the hard work and data collections performed by Marco Mannisi of Glasgow Caledonian

University. Without this effort, Papers III and IV of this dissertation would not have been possible. Additional thanks goes out to the radiologists at Queen Elizabeth University Hospital in Glasgow Scotland for their advice in developing the optimal MR imaging protocol for constructing multiscale models of patients with knee osteoarthritis. I'd like to take this opportunity to thank all the members of Anybody Technology for their endless help and recommendations throughout this PhD research. Finally, I would like to recognize Sjoerd Kolk and the rest of the engineers I worked with from Materialise, thank you for your support and granting access to the necessary research licenses needed for the completion of this PhD.

A big thank you to my office mates at the AnyBody Research group for the ample amount of cake, swim sessions, potluck dinners, and pep talks. In addition, I greatly appreciate that you never hesitated to spend an hour or more of your time in an MRI scanner for the sake of my research. To my fellow early stage researchers, the experienced researchers, and bonus supervisors of KNEEMO, thank you for the amazing meetups, collaborative efforts, and network we established.

To my family and friends, near and far, thank you so much for helping me through this journey. Finally, I would like to express my gratitude to Henrik, for the abundance of love, encouragement, and patience.

CONTENTS

CHAPTER 1. INTRODUCTION

1.1. BACKGROUND AND MOTIVATION

1.1.1. THE KNEEMO INITIAL TRAINING NETWORK

The research presented in this PhD dissertation was completed as part of the KNEEMO project ("KNEEMO: Initial Training Network in Knee Osteoarthritis Research," n.d.); an Initial Training Network (ITN) for knee osteoarthritis research funded by the European Union's Seventh Framework Programme for research technological development, and demonstrations under Grant agreement No. 607510. The project consisted of 15 research fellows (4 experienced researchers and 11 early stage researchers) employed across 8 institutions (Aalborg University, Glasgow Caledonia University, Paracelsus Medical University, Peacocks, University of Münster, University of Southern Denmark, VU University Medical Center Amsterdam, and Xsens) and ran from April 2014-2018. The main theme of KNEEMO was "towards targeted and tailored interventions for KOA", and focused on identifying the right patients for the right treatment at the right time. The objectives of KNEEMO ITN were:

1. Understanding the epidemiology, impact, burden and cost of osteoarthritis of the knee including disease mechanisms and biomechanical paradigms.
2. Understanding the structure and function of the knee joint, its constituent anatomy and complex function in health and OA diseased states.
3. Performing imaged-based reconstruction of the knee joint anatomy including bone, cartilage, muscle and soft-tissue in health and OA diseased states.
4. Performing 3-D measurements of knee joint function including motion, forces, muscle strength and proprioception during activities of daily living.
5. Understanding and applying the basic principles of computational modelling employing anatomical (3) and functional (4) data to better understand disease processes and pathology.
6. Understanding the need for early identification of patients and preventative action
7. Understanding of current non-pharmacological interventions, their biomechanical basis and limitations.
8. Translating knowledge gained in (3) and (4) towards the development of novel, personalized biomechanical-based interventions.
9. Effective dissemination of scientific findings to peers, policy makers, the private sector and lay public.

The objectives were accomplished by employing research methodology in the forms of: computer simulation modeling, observational patient-based studies, product development, primary analysis of prospective cohort data, evidence synthesis through systematic review of the literature and meta-analysis, and secondary analysis of existing data sets. In addition, to the transferable skills learned during the project: research leadership, organizing and planning, entrepreneurship and innovation, ethics of human research, using information technology, intellectual property rights, and finally, effective communication skills through various mediums of dissemination and outreach. Overall, the KNEEMO ITN achieved a better understanding of non-pharmacological conservative management of knee OA through early identification and tailored interventions.

1.1.2. KNEE OSTEOARTHRITIS

Osteoarthritis (OA) is a slow degenerative disease of diarthrosis (synovial) joints, with the knee joint being the most commonly affected (Martel-Pelletier et al., 2016) and currently, without a cure (Egloff et al., 2012). Symptoms of knee OA (KOA) include: stiffness of joint causing limited range-of-motion, inflammation, pain, and grinding sensation and or sound; often resulting in reduced participation daily physical activities and an overall reduced quality-of-life (Heidari et al., 2016). However, the diagnosis of KOA should not be determined solely upon symptomatic findings, it is possible for patients with KOA to have radiographic evidence, while not experiencing any of the above symptoms (asymptomatic patients) and vice versa (Bedson and Croft, 2008; Finan et al., 2013).

Knee osteoarthritis is normally diagnosed using a variety of tools, including medical history report, physical examination, medical imaging such as radiography or magnetic resonance imaging (MRI), and questionnaires for example the Western Ontario and McMaster Universities Osteoarthritis Index (WOMAC) (Bellamy et al., 2005; Felson, 2006). Radiography is predominantly used for structural assessment of KOA due to its low cost and availability (Demehri et al., 2015; Roemer et al., 2011). The x-ray is taken in the coronal plane (anteroposterior) and produces a high contrast image of the bone tissue, however it is unable to capture the structure of the articular cartilage (Roemer et al., 2011). Instead, the x-ray has been used for over 60 years in combination with the Kellgren & Lawrence (KL) grading scale, which mainly evaluates the knee for joint space narrowing, subchondral sclerosis, presence of osteophytes and or cysts (Altman and Gold, 2007; Lawrence, 1957; Roemer et al., 2011). More recently, MRI has become increasingly prevalent in KOA diagnosis (Figure 1-1) due to its capability to capture soft tissue contrast, no radiation exposure, and ability to conduct 3D assessment of all structures of the knee (Wang et al., 2012). It has been found that the structural changes in cartilage can be detected earlier when using MRI (Javaid et al., 2010) than x-ray, and furthermore the thickness and overall health of the cartilage is better identified through use of MRI (Gold et al., 2006;

Stammberger et al., 1999). Quantitative scoring systems have been established for MRI in the diagnosis of KOA including: Boston-Leeds Osteoarthritis Knee Score (BLOKS), Knee Osteoarthritis Scoring System (KOSS), Whole-Organ MRI Score (WORMS), Multicenter Osteoarthritis Study (MOST), and most recently the MRI Osteoarthritis Knee Score (MOAKS) (Guermazi et al., 2011; Hunter et al., 2011, 2008; Kornaat et al., 2005; Peterfy et al., 2004). MOAKS subdivides the knee into 14 articular subregions for evaluation of bone marrow legions (BML), cysts, articular cartilage, osteophytes, Hoffa's synovitis and synovitis-effusion, meniscus, ligaments,

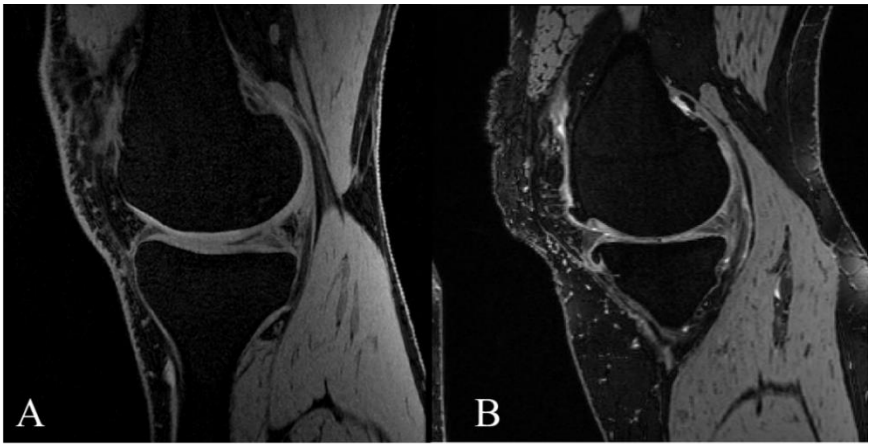

and periarticular features with respect to the patella (2 subregions), femur (6 subregions), and tibia (6 subregions). Overall, although MRI grading has far greater specificity and sensitivity, the cost of a MR scanner is incredibly high, in addition to the scan itself which is a rather lengthy procedure when compared to radiology.

Figure 1-1. Sagittal plane MRI of (A) healthy and (B) osteoarthritic knee joint.

Due to the irreversible deterioration, KOA has been recognized as one of the leading causes of global disabilities (Cross et al., 2014). A particular study highlights that KOA has an incidence of 240 per 100 000 person-years (Bijlsma et al., 2011; Oliveria et al., 1995). Prevalence of KOA in the United states alone has been recorded at roughly 19-28%, 37% those aged 45, 60 years and older respectively (Dillon et al., 2006; Felson et al., 1987; Jordan et al., 2007; Lawrence et al., 2008). In the Nordic region (Figure 1-2), persons aged 75 and older have a prevalence of about 22 % for women, and for men 17% (Kiadaliri et al., 2018). Furthermore, a recent study concluded that there is a prevalence of 30% in former athletes (Madaleno et al., 2018). With the incidence and prevalence of KOA on the rise, partially due to an increased life expectancy, causes KOA to be one of the largest health care burdens (Egloff et al., 2012; Turkiewicz et al., 2014). The burden of OA, especially in the knee and the hip, is not only of a physical nature, it also has psychological, social, and economical

burdens, and furthermore causes a reduction in life expectancy (A. Chen et al., 2012; Kiadaliri et al., 2018; Kingsbury et al., 2014; Litwic and Edwards, 2013; Palazzo et al., 2016).

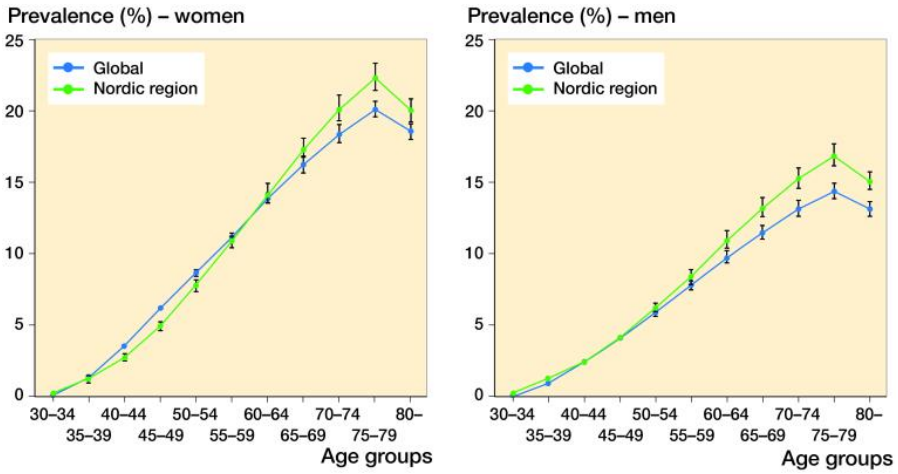

Figure 1-2. Age- and sex-specific prevalence (%) of osteoarthritis in the Nordic region and the world, 2015. Figure and caption from Kiadaliri et al (2018) (Kiadaliri et al., 2018).

Various risk factors have been identified that may speed up the process, and systematic risk factors for KOA include: age, sex, race/ethnicity, genetics. While biomechanical risk factors of KOA include: obesity, joint deformity, muscle weakness, malalignment, and previous injury or trauma (Bijlsma et al., 2011; Martel-Pelletier et al., 2016; Tunen et al., 2016). The concept of phenotyping has made it possible to divide patients with KOA of similar observable characteristics into multiple subgroups (Bierma-Zeinstra and van Middelkoop, 2017; Dell'Isola et al., 2016; Deveza et al., 2017; Felson, 2010; Isola and Steultjens, 2018; Nelson, 2018), with each group likely to respond different to individualized intervention (Felson, 2010). Recent studies (Dell'Isola et al., 2016; Deveza et al., 2017) have reviewed the literature to identify *clinical phenotypes* such as: chronic pain (psycological profile such as depression, comorbid symptom profile), inflammatory, metabolic syndrome, metabolic bone/cartilage, mechanical overload (knee joint alignment, gait parameters), and minimal joint disease, *imaging phenotypes* such as: knee chondrocalcinosis, MRI-detected denuded bone areas, imaging features with clinical symptoms, and knee joint compartment evidence, and *laboratory phenotypes* such as: biochemical marker patterns, inflammatory profile, synovial fluid profile, serum biochemical markers of bone and cartilage metabolism, and profile of gene expression in peripheral blood leukocytes. Dell'Isola and Steultjens (2018) went one step further classifying a large patient group from the Osteoarthritis Initiative (OAI), into the

predefined phenotypes from Dell'Isola et al (2016), resulting in roughly 84% classifications of cases with merely 20% overlap (Isola and Steultjens, 2018). Finally, the phenotypes found by the systematic reviews above were then organized into aetiological, structural, pain, joint function-related, and disability-related phenotypes by Bierma-Zeinstra and van Middelkoop (2017) in hopes of simplifying and bringing light to the KOA phenotypes that may influence how the clinics allocate treaments (Bierma-Zeinstra and van Middelkoop, 2017). Ultimately, KOA patient classification may prove to be a useful tool for the future in the attempt to tailor treatements to the individual patients and patient groups.

1.1.3. COMMON TREATMENT METHODS IN KOA

Spite the significant burden of KOA, there seems a lack in effective treatment methods at early stages of the disease, which is essential in furthering the prevention and management of KOA. Most often, KOA treatments begins with some form of nonpharmacological management, which could be any combination of: biomechanical interventions (knee sleeve, brace, foot orthoses), exercise (land or water), strength training, self-management and education, and or weight management, (McAlindon et al., 2014; Yusuf, 2016). If non-pharmacological treatments cease to benefit the patients, clinicians then may combine them with pre-existing treatments or solely prescribe pharmacological interventions such as paracetamol, oral/topical nonsteroidal anti-inflammatory drugs, and or intra-articular corticosteroid injections (McAlindon et al., 2014; Yusuf, 2016). As a last resort, surgical treatments for KOA come into play, including arthroscopy, joint lavage, and partial/total knee arthroplasty (Glyn-Jones et al., 2015; Yusuf, 2016). However, common invasive treatment options for example, total knee replacement (TKR) and osteochondral graft transplantation, are rather costly and often used as a last resort when the non-invasive pharmacological or pharmacological therapies cease to be viable options (Bruyère et al., 2014; Murawski and Kennedy, 2013). Knee replacements have both proven to be effective treatments for end-stage KOA (Carr et al., 2012). Roughly 50% of the patients diagnosed with KOA in the US will undergo TKR surgery (Weinstein et al., 2013). Nevertheless, the rate of knee replacement surgeries is on the rise (Chawla et al., 2017; Pabinger et al., 2013) with increasing human life expectancy and decreasing age at which patients receive the replacement (Goudie et al., 2017; Losina et al., 2012). The lifetime risk of revision (LTRR) is significantly higher for patients under 70 years old, particularly for men in the 50-54 age range (Bayliss et al., 2017). It is known that if a patient has a TKA earlier on in life, they will have more wear on their implant when compared to that of an older patient (Fernandez-Fernandez and Rodriguez-Merchan, 2015). Contributing to the need for non-invasive interventions aimed at treating early-stage KOA which will ultimately delay the onset of late-stage KOA which may require joint replacement surgery.

KOA most often develops in the medial tibial plateau (Bruns et al., 1994; Eckstein et al., 2014; Mills et al., 2013), with excessive loading believed to be a major contributor development of KOA and its progression. Thus many non-surgical interventions have been proposed to decrease the knee adduction moment (KAM) in hopes of reducing medial knee compartment loading: lateral wedged insoles (LWI), gait modification (toe in, toe out wide, medial knees, wide stance, and trunk sway) unloading knee braces, use of walking poles, and ankle orthoses (Ardestani et al., 2014b; Shull et al., 2013a; van den Noort et al., 2013). Yet, the success of these treatments has not always been consistent (Arnold, 2016; Bennell et al., 2011; Hinman et al., 2012; Penny et al., 2013). Studies have shown a reduction in average peak KAM during both toe toe-in and toe-out walking (Hunt and Takacs, 2014; Shull et al., 2013a, 2013b). However, not all patients have responded positively to these treatments, triggering the need for more tailored treatments based on an individual patient's biomechanics (Favre et al., 2016; Gerbrands et al., 2014; Shull et al., 2015). One such study aimed at assigning patient-specific toe-in and toe-out angles when walking which resulted in greater reductions in peak KAM when compared to assigning uniform angles to the entire group (Uhlrich et al., 2018). Another popular treatment option, lateral wedge insoles, introduces a wedge to the lateral side of the insole trying to shift the load from medial to the lateral tibial compartment, the outcome which is debatable. Some studies have resulted in a 5–7% reduction in knee adduction moment (Butler et al., 2007; Hinman et al., 2012; Kakihana et al., 2005), while a meta-analysis concluded that despite a statistically significant association between the use of insoles and reduced pain in the medial KOA, the findings did not support the use of LWIs as a conservative treatment option (Parkes et al., 2013). The best treament for an individual and or patient group, has been explored through optimizational methods (Ackermann and van den Bogert, 2010; Anderson and Pandy, 2001) and real-time feedback. Recent gait alteration studies that utilize biofeedback techniques investigate gait alteration effects in terms of KAM, and or knee flexion moment (KFM) with software that uses rescaled generic models (Barrios et al., 2010; Fregly, 2007; Hunt et al., 2008; Liu et al., 2016; Miller et al., 2015; Ogaya et al., 2014; Richards et al., 2017; Shull et al., 2013a; van den Noort et al., 2015). However, it has been showed that a reduction in knee adduction moment (KAM) does not directly relate to decreased loads in medial tibial compartment (Kirking et al., 2006; Richards et al., 2018; Walter et al., 2010). And furthermore, it is speculated that solely focusing on KAM may not give the whole portrayal of medial knee loading (Walter et al., 2010).

However, direct measurements of knee contact forces can only be achieved in an individually with an instrumented TKA, and at this point the KOA patient would have already hit late stage osteoarthritis and opted for a knee replacement. Thus, we need a non-invasive surrogate to estimate knee contact loads, which is where musculoskeletal modeling comes into play. With musculoskeletal modeling, the medial contact forces in the knee can be estimated.

1.2. COMPUTATIONAL MODELING OF THE KNEE JOINT

The knee is composed of four bones (femur, tibia, fibula and patella) which function as synovial joints (tibiofemoral, patellofemoral, and superior tibiofibular). The bones of a synovial joint are in contact, but not connected by fibrous structures or cartilage, and are able to move with respect to each other (Herzog, 2006). The patella is the body's largest sesamoid bone, nestled within the femoral trochlear groove. The patella serves as a bony shield protecting the tibiofemoral joint (Tecklenburg et al., 2006) while also engaging as a lever arm translating force from the quadriceps muscle across the tibiofemoral joint. The knee is a non-conforming joint, meaning that along with the obvious flexion/extension Degree-of-Freedom (DOF), there are small translations and rotations, which are guided and stabilized by muscles, ligaments, articular cartilage and menisci (Benoit et al., 2006). Within the knee, the major *ligaments* are the posterior cruciate ligament (PCL), anterior cruciate ligament (ACL), medial collateral ligament (MCL), lateral collateral ligament (LCL), patellar tendon (PT) medial PF ligament (MPFL), lateral epicondylopatellar ligament (LEPL), lateral transverse ligament (LTL), popliteofibular ligament (PFL), posteromedial capsule (pmCAP), the posterior capsule (CAP), and the iliotibial band (ITB), *muscles* are: vastus lateralis, vastus medialis, satorious, rectus femoris, biceps femoris, gastrocnemius, peroneus longus, extensor digitorum longus, tibialis anterior, and *fat pads* infrapatellar (Hoffa), posterior suprapatellar, anterior suprapatellar. It is important to understand that the articular cartilage is not the only structure degenerating in response to KOA, and attention also needs to also be paid to the menisci, ligaments, muscles, synovial, and bone structures KOA (Bijlsma et al., 2011). Stresses, strains, and forces parameters cannot be directly measured in these structures due to ethical reason and therefore researchers have to rely on estimates of these loads. Computational models of the knee joint are used to investigate knee joint kinematics, contact forces, stresses in the soft tissue structures without having to deal with the ethics of conducting direct measurements using invasive techniques and furthermore, to make systematic investigations that you may not be able to in the laboratory. Varying magnetic resonance imaging (MRI) techniques have been established to best view the unique structures of the knee and lower limb (Balamoody et al., 2010; Handsfield et al., 2014; Peterfy et al., 2008; Roemer et al., 2014). In order to clearly distinguish between bone, articular cartilage, and various soft tissue structures, both fat suppression (Figure 1-3.A) and fat saturated (Figure 1-3.B) scans are required.

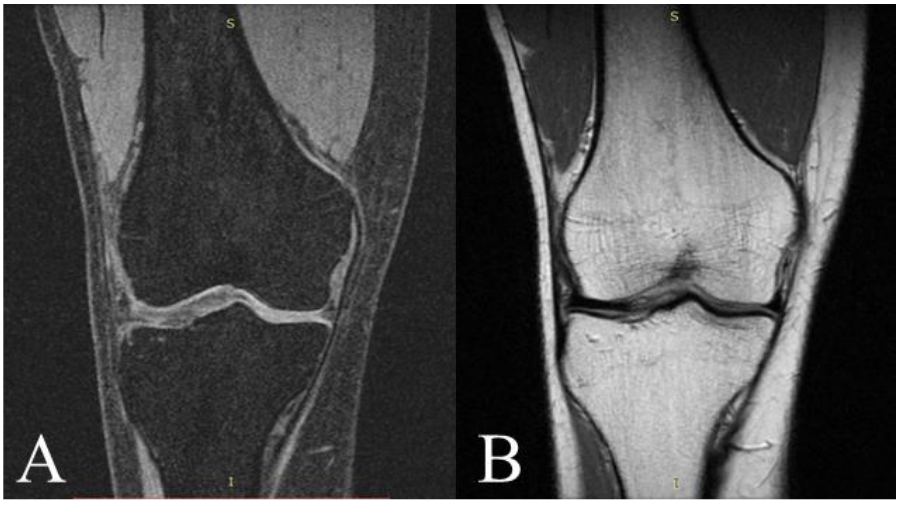

Figure 1-3. MRI acquisitions of the knee, in coronal plane using (A) 3D spoiled gradient recalled acquisition in the steady state (SPGR) with fat suppressed where the articular cartilage (white) can be clearly distinguished from the bone (black) and (B) proton density (PD) with fat saturated sequences where the menisci and ligaments are clearly depicted in black, while it is more difficult distinguishing the boarders of the bone due to the fact cortical bone shows up as black and the trabecular bone in white.

These scans have been used in developing subject-specific musculoskeletal and finite element (FE) models that require more than just bone geometries and for research who would like to avoid the CT radiation exposure for their subjects. Musculoskeletal models can be used to estimate the joint loads, while finite element models estimate tissue stresses and strains. It is important to note that the results obtained from a computational model are only as reliable as the input data. The outputs from these models are known to be sensitive to input parameters, with regards to MS the muscle-tendon moment arm, tendon slack length, nominal muscle fiber length, maximal isometric muscle force (Carbone et al., 2012) are some to consider; and regards to FEA, the model geometry, mesh density, material properties, and loading conditions (Carey et al., 2014; Erdemir et al., 2012; Pianigiani et al., 2017) are also important to take into account.

1.2.1. MUSCULOSKELETAL MODELING

A musculoskeletal model is made up of bones, muscles, joints and ligaments (**Error! Reference source not found.**). The anatomical segments of the model are linked together by joints, which are often idealized but also sometimes exchanged for more advanced forms. The skeletal system gains motion actively from muscles and passively through ligaments and other soft tissue structures. Musculoskeletal (MS)

modeling estimates internal loading conditions of anatomical structures related to specific motion. Although the entire body can be modeled using musculoskeletal techniques, often in research that focuses on the knee, solely the lower limbs are included for sake of simplicity. The most commonly use musculoskeletal software systems include: Software for Interactive Musculoskeletal Modeling (SIMM) (Delp and Loan, 2000), AnyBody Modeling System (AMS) (Damsgaard et al., 2006), and OpenSim (Seth et al., 2011). The complexity of the musculoskeletal model is derived from the nature of the research question. Model complexity can vary in model dimension (2D vs 3D), how many segments and joints are modeled and to what subject specificity, DOF of joint movement, and finally how the muscles are modeled and driven. In 3D musculoskeletal modeling, each body segment is a rigid body with six DOF (3 translational and 3 rotational) and specific anthropometric properties: mass, center of mass position, and principle moments of inertia (Robertson et al., 2014). The muscles that are modeled in a musculoskeletal model act on at least two rigid body segments, spanning one or more joints. Muscle-tendon models are connected to bones at origin and insertion points, passing through one or more joint. The most commonly used muscle model (m) was introduced by Hill et al (1938) and expanded on by Zajac (1989) stating that a given muscle produces a force (F_m) described by the following formula:

$$F_m = a_f F_{max} F_1\big(L_f(t)\big) F_2\big(V_f(t)\big) + F_p\big(L_f\big) \qquad [1\text{-}1]$$

in which both active (contractile element) and passive elements are included and a_f denotes the muscle activity, F_{max} is the muscle's maximum isometric force, $F_1(L_f)$ is the force length relationship, and $F_2(V_f)$ represents the force-velocity relationship of the muscle, and and $F_p\big(L_f\big)$ is the passive force-length the muscle, and $F_p\big(L_f\big)$ is the passive force-length relationship describing the elasticity of the muscle-tendon and connective tissue (Delp et al., 1990; Hoy et al., 1990; Millard et al., 2013; Robertson et al., 2014; Romero and Alonso, 2016; Zajac, 1989).

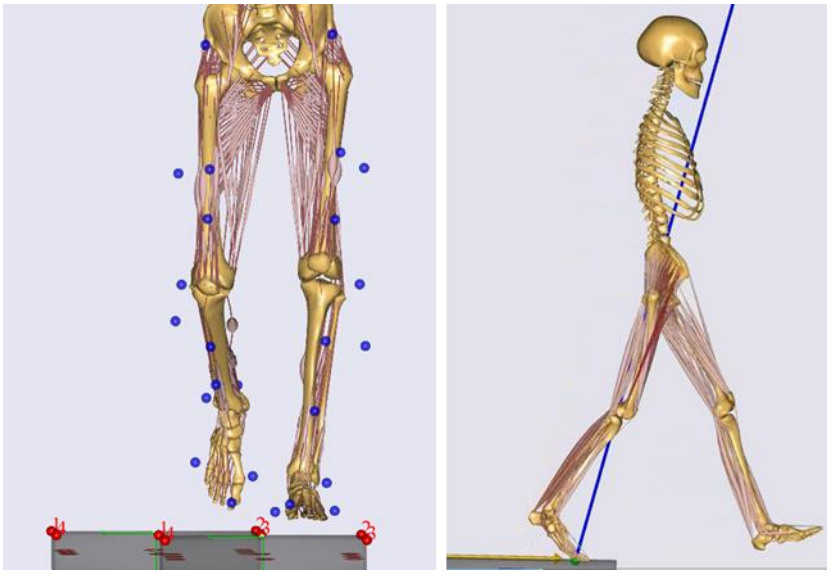

Figure 1-4. Examples of musculoskeletal models with focus on the lower limbs

Depending on the available experimental data and the given research problem, MS models are simulated using: tracking methods based on forward dynamics (Neptune et al., 2010; Neptune and Bogert, 1998; Thelen and Anderson, 2006), inverse dynamics (Crowninshield, 1978; Rasmussen et al., 2001), electromyography-driven models (Buchanan et al., 2006), or dynamic optimization (Anderson and Pandy, 2001). Forward dynamic, predicting movements through muscle forces, can be broken up into two categories (1) forward dynamic-assisted data tracking and (2) optimal control strategy. In the former, simulations of muscle activations are used as inputs (primarily EMG-driven) and the MS model calculates the movement of the body (Kia et al., 2014; Piazza, 2006; Sartori et al., 2014; Thelen et al., 2014). While optimal control strategy, often coined as dynamic optimization, predicts motion with respect to an optimality criteria (Anderson and Pandy, 2001). The forward dynamic-based tracking method, computed muscle control (CMC), was first introduced by Thelen, Anderson, & Delp, (2003). CMC estimates a set of muscle excitation levels that drive the generalized coordinates of a MS model towards a desired kinematic trajectory by employing muscle recruitment, feedforward, and feedback controls (Gerus et al., 2013; Hast and Piazza, 2013; Lloyd and Besier, 2003; Manal and Buchanan, 2013; Sandholm et al., 2011; Sartori et al., 2014; Thelen et al., 2014). Inverse dynamics uses kinematics, inertial properties of moving bodies, and external forces to solve for joint reaction and muscle forces by applying muscle recruitment, ensuring equilibrium with all the other forces and moments in the model (Fregly, 2007; Hast and Piazza, 2013; Lerner et al., 2015; Manal and Buchanan, 2013). The reader can find an extensive literary review of forward dynamics optimization and inverse dynamics methods in Erdemir et al., (2007). It is essential to use the

appropriate number of DOF in the MS model with respect to the number of segments modeled to avoid overestimation of muscle forces (Erdemir et al., 2007). However, the more muscles added to the system, each adding an additional force, the more of a risk of redundancy (if the number of muscles exceeds the total DOF in the model). To solve this, in inverse dynamics problems, a general optimization problem (Damsgaard et al., 2006; Rasmussen et al., 2001) is defined to minimize the objective function (G):

$$\underset{f}{\text{minimize}}\ G\left(\mathbf{f}^{(\mathrm{M})}\right) \tag{1-2.a}$$

$$\text{subject to } \mathbf{Cf} = \mathbf{d}, \tag{1-2.b}$$

$$N_i \geq f_i^{(M)} \geq 0, \quad i \in \left\{1, \dots, n^{(M)}\right\}, \tag{1-2.c}$$

where, $\boldsymbol{f}^{(M)}$, is a vector of all the muscle forces, $\mathbf{C}$ is the coefficient-matrix of all unknown forces, $\mathbf{f}$ contains all unknown forces coming from muscle forces and joint reaction, $\mathbf{d}$ is a vector of all the known applied loads, and the instantaneous muscle strength is denoted by N_i. Finally, the optimization problem is subjected to a non-negativity constraint, stating that the fact that muscles can only pull and that the maximal muscle force must remain lower than the instantaneous muscle strength. Commonly used objective functions are: polynomial, soft saturation, min/max (Rasmussen et al., 2001), and the subdivided muscle criterion (Marra et al., 2015). The polynomial criteria allows for researchers to try different polynomial forms:

$$\underset{f}{\text{minimize}}\ G\left(\mathbf{f}^{(\mathrm{M})}\right) = \sum_{i=1}^{n^M} \left(\frac{f_i^{(M)}}{N_i}\right)^p \tag{1-3}$$

and the muscle strength, N_i, can be taken from maximum strength tests, physiological cross-sectional area (PCSA), or instantaneous muscle strength values. The soft saturation criteria:

$$\underset{f}{\text{minimize}}\ G\left(\mathbf{f}^{(\mathrm{M})}\right) = -\sum_{i=1}^{n^M} \sqrt[p]{1 - \left(\frac{f_i^{(M)}}{N_i}\right)^p} \tag{1-4}$$

was introduced to avoid overloading muscles during the inverse dynamic simulations of the musculoskeletal model, which can be achieved by eliminating unnecessary constraints. The min/max criterion introduces an artificial criterion function $B(\beta) = \beta$, and following a well-known technique in engineering design optimization, takes the original formula:

$$G\left(\mathbf{f}^{(\mathrm{M})}\right) = \max\left(\frac{f_i^{(M)}}{N_i}\right) \tag{1-5}$$

and reformulates it into:

$$\underset{f,\beta}{\text{minimize}}\ \beta \qquad \text{[1-6.a]}$$

subject to

$$\frac{f_i^{(M)}}{N_i} \leq \beta,\ i \in \{1, \dots, n^{(M)}\}, \qquad \text{[1-6.b]}$$

$$\mathbf{Cf} = \mathbf{d}, \qquad \text{[1-6.c]}$$

$$f_i^{(M)} \geq 0,\ i \in \{1, \dots, n^{(M)}\} \qquad \text{[1-6.d]}$$

This objective function is essentially the polynomial criterion using a very high order (p). Recently muscle force predictions have improved by updating the objective function has been enhanced to account for muscle subdividing (Marra et al., 2015; Richards et al., 2018):

$$\underset{f}{\text{minimize}}\ G(\mathbf{f}^{(\mathrm{M})}) = \sum_{i=1}^{n^M} V_i \left(\frac{f_i^{(M)}}{N_i}\right)^3 \qquad \text{[1-7]}$$

where V_i is a normalized factor reflected the subdivided muscle model, typically the fraction of muscle volume or PCSA.

Most musculoskeletal models have the ability to be scaled and morphed from generic cadaver geometries. There are various levels of subject-specific scaling and geometric morphing techniques available between the different MS software packages. For instance, the Twente Lower Extremity Model 2.0 (TLEM 2.0) was developed in AMS to use in combination with novel image-based morphing techniques (Carbone et al., 2015). For a MS model to obtain subject-specific architecture, geometric morphing techniques are applied to the TLEM 2.0 cadaver-based model to scale the bones, joints, and muscles attachments relative to the subject. Advancements in these techniques are explained in greater detail in the literature (Andersen et al., 2010b; Lund et al., 2015; Marra et al., 2015; Pellikaan et al., 2013; Reinbolt et al., 2005). Marra et al., (2015) morphed the TLEM 2.0 model to the patients-specific geometry of a total knee arthroplasty patient based on a pre-operative CT scan ranging from the hip to the ankle joint. Musculoskeletal models have also been previously scaled directly based on MRI scans (Allison S Arnold et al., 2000; Allison S. Arnold et al., 2000; Carbone et al., 2015; Scheys et al., 2008), which however remain a time-consuming process due to the technically challenging task of segmenting muscles and identifying their origin and insertions.

The tibiofemoral and patellofemoral joints in MS models often range from simple (1 or 2 DOF) to very complex (with up to 12 DOF) varying with respect to computational time required to run and their generic qualities. Despite the complex knee structure, researchers often idealize the tibiofemoral joint as a revolute/hinge/pin joint with a fixed position and orientation (Anderson and Pandy, 2001; Fregly, 2007; Klein Horsman et al., 2007; Marra et al., 2015). In addition, pure kinematic models often exclude the patellofemoral joint (Moissenet et al., 2017), and when included, its most often as a hinge joint with an additional rigid patella tendon (Brito da Luz et al., 2017; Carbone et al., 2015; Habachi et al., 2015; Lund et al., 2015; Marra et al., 2015; Moissenet et al., 2016, 2014; Sancisi and Parenti-Castelli, 2011; Thelen et al., 2014). When studying knee biomechanics, a hinge is often too simplified, so researchers have included coupling constraints based on tibiofemoral flexion to allow for more DOF (Delp et al., 1990; Donnelly et al., 2012; Feikes et al., 2003; Pontonnier and Dumont, 2010; Tsai and Lung, 2014), additionally: parallel spatial mechanisms (Duprey et al., 2010, 2009, Moissenet et al., 2014, 2012; Wilson et al., 1998; Xavier Gasparutto et al., 2015), and sphere-on-plane contact models (Clément et al., 2015; Duprey et al., 2010, 2009; Habachi et al., 2015). The properties of these models are typically derived from cadaver studies; however, some have adopted subject-specific characteristics (Brito da Luz et al., 2017; Clément et al., 2015; Delp et al., 1990; Donnelly et al., 2012; Marra et al., 2015; Tsai and Lung, 2014). The most complex 11-12 DOF multibody contact knee joint models (Guess et al., 2014; Hast and Piazza, 2013; Lenhart et al., 2015; Marra et al., 2017, 2015; Serrancolí et al., 2016; Smith et al., 2017, 2016; Thelen et al., 2014; Walter et al., 2014) utilize various methods of solving gross body dynamics and detailed joint dynamics. These models allow for quantifying contact and ligaments forces; however, they are quite computationally slow so use in the clinical setting is currently a challenge. Commonly in multibody contact knee models, two separate contact models are defined between the femoral articular cartilage (or femoral TKR component) surface and (1) the medial and (2) lateral tibial articular (or tibial TKR component) surfaces. When the menisci is included, four additional contact models are defined between the articular cartilages (femoral and tibial) and the corresponding medial and lateral menisci. Finally, when appropriate, contact models are established between the various articular cartilages and their respective bony surfaces. Furthermore, with respect to the patellofemoral joint, the two contacts are defined between the patella cartilage (or TKR button) and (1) femoral cartilage (or femoral TKR component) and (2) patella bone. The most common ligaments that are modeled include the: (PCL), anterior cruciate ligament (ACL), medial collateral ligament (MCL), lateral collateral ligament (LCL), patellar tendon (PT) medial PF ligament (MPFL), lateral epicondylopatellar ligament (LEPL), and lateral transverse ligament (LTL). Some models also include the popliteofibular ligament (PFL), posteromedial capsule (pmCAP), the posterior capsule (CAP), and the iliotibial band (ITB). Each ligament is divided into bundles depending on the geometry with each bundle modeled with as a nonlinear elastic spring running from a given origin to the respective insertion. Various methods have been established to enable detailed joint models including (Andersen et al., 2017; Guess et al., 2014;

Smith et al., 2018; Thelen et al., 2014), but not limited to, Force dependent kinematics (FDK) (Andersen et al., 2017; Marra et al., 2015), CMC (Thelen et al., 2014), and concurrent optimization of muscle activations and kinematics (COMAK) (Smith et al., 2018). Force-dependent kinematics (FDK) solves for the internal forces and secondary joint kinematics at the same time (Andersen et al., 2017). The concept expands upon inverse dynamics by using a quasi-static force-equilibrium to compute the small secondary movements in the joint (Andersen et al., 2017; Marra et al., 2015). The COMAK algorithm uses ray casting with oriented bounding boxes (OBB), which allows for quicker collision detection (important for calculating contact pressure between articular cartilage), to ultimately solve for cartilage contact pressures during dynamic gait. A prominent advantage of FDK compared to these other methods is that it does not require any manually tuned nonphysiological controller parameters.

The importance of personalized computational modeling has been highlighted as of late (Clément et al., 2015; Benjamin J Fregly et al., 2012; Gerus et al., 2013). More personalized models and methods have also been used although most often on patients with implanted knees (Ardestani et al., 2014b, 2014a; Fregly et al., 2009) or on healthy subjects (Caldwell et al., 2013; Halonen et al., 2017; Miller et al., 2015; Mündermann et al., 2008; Pizzolato et al., 2017; Shull et al., 2011; Uhlrich et al., 2018; van den Noort et al., 2013; Wheeler et al., 2011; Willson et al., 2001). This leaves a gap in the knowledge pertaining to personalized musculoskeletal models of earlystage patient (pre-surgical interventions) that need to be filled. It is known that patients with knee osteoarthritis have altered biomechanics for a variety of reasons which may or may not be linked to each other: increased pain, stiffening of the joint, malalignment, previous injuries, instability, etc. For instance, instability often occurs in the tibiofemoral joint when there is presence of knee osteoarthritis (Farrokhi et al., 2015, 2014, 2012; Hoshi et al., 2016; Maly et al., 2015; Yue et al., 2011; Zeng et al., 2017), meniscectomy (Perez-blanca et al., 2016; Sturnieks et al., 2008; Yang et al., 2009), and ligament injuries (C. H. Chen et al., 2012; DeFrate, 2006; Dennis et al., 2005; Gill et al., 2009). The laxity that may arise from instability and potential coexisting pain contributes to loss of function of the knee joint and in turn can be very debilitating (National Institute for Health and Clinical Excellence, 2014). KOA patients have been known to adjust their gait in hopes of alleviating pain (Heiden et al., 2009), and excessive laxity (Gustafson et al., 2015) increasing the need to more subject-specific modeling. Additionally, it has been shown that patients with tibiofemoral KOA tend to have greater adduction angles, and furthermore a more medially positioned femur relative to tibia (Zeighami et al., 2017). With various patients deviating from norm with respect to biomechanics, and more attention to phenotyping of patients with KOA, there is a greater need for personalized musculoskeletal models with regards to anatomy and gait in hopes of capturing the differences kinematics and kinetics in order to investigate pathologies, such as KOA progression. Dell'Isola et al (2016) and De et al (2017) have shown the complexity of subgrouping patients with KOA, patients differ with respect to so many aspects, requiring the need for individualized interventions. To this end, we need tools capable of assessing how these interventions

affect the individual's biomechanics, which motivates some of the work performed for this PhD. It should be noted, although contact forces can be achieved, these musculoskeletal models are unable to investigate stresses and strains at the soft tissue level, thus affirming the need for finite element modeling.

1.2.2. FINITE ELEMENT MODELING

Finite element analysis (FEA) is used to predict the performance of a given structure subjected to loading, and furthermore investigate the stresses and strains of the system using a numerical technique called the finite element method (FEM). The main components of FEA include the creating the model geometry, assigning material properties, and establishing boundary conditions. In 3-dimensional FE models, the geometry is transformed into a volumetric mesh structure made up of small ('finite') solid elements (Figure 1-5

Figure 1-5. Femoral articular cartilage represented as (left) a solid surface geometry and (right) a volumetric mesh divided into elements

). When considering 1- or 2-dimensional geometries, these structures are divided into shell or line elements. Each element is made up of a given number of nodes, which depend on the shape and dimension of the element (for instance a solid 4-noded tetrahedral vs 10-noded tetrahedral) and reside at the element's interconnected elements. Depending on the chosen element type, particular polynomial base functions, also called shape functions **N**, are interpolated with respect to the nodal DOFs **d** to solve for displacements $\mathbf{f} = \{u, v, w\}$.

$$\mathbf{f} = \mathbf{Nd} \qquad [1\text{-}8]$$

The geometry complexity is often directly proportional to the computational time and how well the model mimics reality, hence the reason convergence tests are often performed for geometric mesh refinement prior to final analyses. A convergence test can be conducted simply by taking a given model and increasing the mesh density

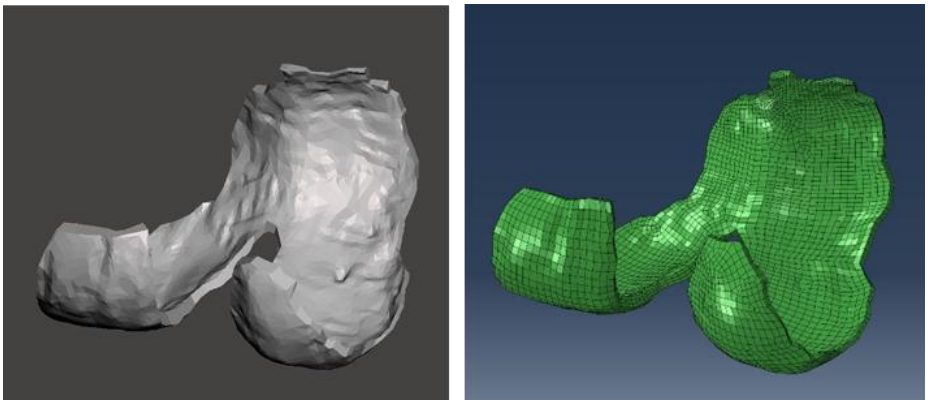

until a threshold is reached for a given output measure, most often Max. Von. Mises stress, at this point the model has converged and a more complex mesh would be meaningless (Cook et al., 2002; Rayfield, 2007; Richmond et al., 2005). Additionally, these convergence tests can be done by increasing the order of polynomial base functions during interpolation defining the displacement field of each element (Cook et al., 2002).

Figure 1-5. Femoral articular cartilage represented as (left) a solid surface geometry and (right) a volumetric mesh divided into elements

Prior to running FEA, boundary conditions and material properties need to be assigned to the geometric structure via elements and nodes. Boundary conditions are set up to mimic the loading conditions interest by the study, for example dynamic knee bending or a single static axial load along the long axis of the femur, this also includes any displacement or rotational constraints needed to be applied to the system, and or any existing contact between tissues (for example, bone, cartilage, and meniscus interactions). Assigning of material properties poses the greatest challenge, especially in FE models of human body systems such as the knee joint, and thus not often modeled realistically due to ethical reasoning. The material model selected for the model geometry will dictate how the structure changes as a function of time, thus influencing the order (linear, quadradic, etc.) of differential equation required to be solved (Cook et al., 2002).

The solution found in FEA gives a prediction how a given structure will behave with respect to physical loads. Common parameters of interest include stresses, strains, contact pressure, etc. The definition for average stress $\left(\sigma = \frac{F}{A}\right)$ is the applied force (F) over the contact area (A). While the average strain, $\varepsilon = \left(\frac{\Delta l}{l}\right)$, is defined as the change of length (Δl) over the original length (l). For small stains in linearly elastic materials, stresses and strains are related linearly $\sigma = E\varepsilon$ though the elastic modulus (E), or Young's modulus. The relation can be rewritten as:

$$F = \frac{EA}{l}(\Delta l) \qquad [1\text{-}9]$$

Consider an overly simplified one-dimensional line element (Figure 1-6) with compressive and tensile forces acting on nodes 1 and 2 respectively.

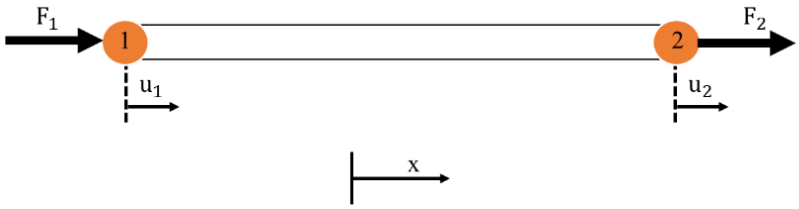

Figure 1-6. Overly simplified example of a one-dimensional FE model of a single line element. Forces (F) are applied to nodes (1 and 2) and result in displacements u_1 and u_2. The element has an area of (A^e), length (l^e), and elastic modulus (E^e). Modified from Richard et al 2005.

By manipulating equation 1-2 we achieve:

$$F_1 = \frac{E^e A^e}{l^e}(u_1 - u_2) \quad [1\text{-}10]$$

$$F_2 = \frac{E^e A^e}{l^e}(u_2 - u_1) \quad [1\text{-}11]$$

Which can be expressed in matrix notation:

$$\mathbf{f} = \mathbf{Kd} \quad [1\text{-}12]$$

Where **K** is the global stiffness matrix of the entire model, **f** is a vector of all nodal forces, and **d** is a vector containing all nodal displacements in the model (Cook et al., 2002; Richmond et al., 2005). Thus, depending on the stiffness matrix, derived from the material properties and the geometry of the model, the displacements caused by forces applied to the model can be calculated. In turn, the strains are derived from nodal displacements and finally the stresses are calculated using the stress-strain relationship introduced above. A more rigorous set of mathematical equations are required to (1) describe material properties that are anisotropic, bi-phasic, etc., and or (2) solve complex three-dimensional geometries, so researchers most often resort to commercial software such as, but not limited to: Abaqus, ANSYS, and LS-DYNA.
Finite element analysis of the knee joint has been implemented by researchers to gain insight on the inner workings of the knee and furthermore; aiding in the development of orthopedic devices such as hip and knee implants. One of the main reasons FEA was adopted is because of ethical restrictions and the technical challenges that direct strain measurements pose when dealing with human subjects. Some of the earliest FEM studies, estimating stresses and strains found within the femur (Brekelmans et al., 1972; Rybicki et al., 1972; Viano and Khalil, 1976) in two-dimensions and the tibia (Hayes et al., 1978) in three-dimensions, date back to the 1970s. Some of the first three-dimensional knee models complete with soft tissue structures were based on cadaveric specimens and developed by (Bendjaballah et al., 1995; Blankevoort et

al., 1991; Li et al., 1999). These models were constructed from either CT/MRI image segmentation or a stereophotogrammetric method, with linear elastic material properties assigned to the articular cartilages and one-dimensional spring element ligaments. Prestrained hyperelastic and transversely isotropic ligaments were introduced in a full tibiofemoral-patellofemoral knee joint model (Peña et al., 2006) and based from a human subject. Linear elastic materials, although, commonly used, cannot represent time dependent behavior of cartilage, only the short-term response; which is not accurate due to the biphasic properties of articular cartilage (Mow, 1989). More complex cartilage models with multiple material constants including: biphasic linear elastic (Mow et al., 1984, 1980), isotropic poroelastic (Donahue et al., 2002; Yang et al., 2010), transversely isotropic poroelastic (Cohen et al., 1998; Disilvestro and Suh, 2001; Suh and Bai, 1998; Vaziri et al., 2008; Wilson et al., 2003), and fibril-reinforced biphasic/poroelastic/poroviscoelastic models can predict time-dependent properties (Li and Herzog, 2004; Wilson et al., 2005, 2004). By introducing a fibral and non-fibral part to the bi-phasic models, this accounts for the lack of anisotrophy in the cartilage and better represents to mechanical roles the collagen plays. Although computationally heavy, many researchers have begun adding the fibril-reinforced biphasic material models to FEA of the knee joint (Gu and Li, 2011; Halonen et al., 2013; K S Halonen et al., 2016; K.S. Halonen et al., 2016, 2014, Mononen et al., 2015, 2013, 2012; Shirazi, 2009; Shirazi et al., 2008).

1.2.3. MULTISCALE MODELING

Technological advances have utilized MS model outputs: forces moments, rotations, and translations, as boundary conditions for FEA models. This method allows researchers to estimate soft tissue stresses and strains during activities beyond simple compression loading trials, such as activities of daily living such as walking (Adouni and Shirazi-Adl, 2014). A recent effort at building a multi-scale (MS and FEA) model attempted to take loads resulting from MS motion trials and input them into a patient-specific model of a femur (Seo et al., 2014), however the soft tissue structures were excluded and the MS model was not scaled to patient-specific geometry. Additional studies that have attempted to combine MS and FEA often exclude patient-specific muscle and or ligament attachments (Godest et al., 2002; Mononen et al., 2013; Peña et al., 2006; Tanska et al., 2015). Moreover, other studies do not use subject-specific MS output data (Adouni and Shirazi-Adl, 2014; Ardestani et al., 2014b; Guess et al., 2010; Halonen et al., 2013; Mononen et al., 2013) and/or have been based on cadaveric data (Adouni and Shirazi-Adl, 2014; Godest et al., 2002; Guess et al., 2010). In one of the most advanced multi-scale models, complete with subject-specific MS output data and subject-specific FEM of the knee, the articular cartilage is modelled as a biphasic fibril-reinforced poroviscoelastic consisting of superficial, middle, and deep zones (K S Halonen et al., 2016). In this study, the meniscus was modeled as a transversely isotropic and elastic material. The bone is excluded from the study assuming infinite stiffness when compared to soft tissues (K S Halonen et al., 2016).

The boundary conditions consisted of a reference point midway between the medial and lateral femoral epicondyles which the femur cartilage-bone interface can rotate around. The nodes on the tibia cartilage-bone interface were assumed to be fixed. Interactions between surfaces were assigned to femoral-tibia and femoral-patella cartilage surfaces; in addition to the cartilage-meniscus surfaces eliminating the possibility of fluid flow through the cartilage surfaces during the gait cycle. Ligament, tendon, and meniscal attachments were all represented by linear springs of varying stiffness. The model was run by implementing knee joint moments, translational forces, corresponding motions (rotations and translations), and quadriceps forces during stance phase obtained through simulating kinematic and inverse dynamic simulations of a musculoskeletal model using motion capture data. However, the musculoskeletal model was not personalized beyond linear scaling with respect to skin markers. To the best of our knowledge, the estimation of cartilage stresses and strains using both subject-specific MS and FEA models has not been developed before.

1.2.4. VALIDATION OF COMPUTATIONAL MODELS

The validation of subject-specific models is a significant challenge researchers have been trying to overcome to allow for broader acceptance and use in the clinical setting (Kinney and Besier, 2013; Lund et al., 2012). A model is considered validated when accurate enough to perform the task or research question it has be designed to accomplish. Since the result obtained from the model will never completely agree with reality, researchers have to establish acceptable error margins which depends on the model application and the associated risk if the simulations are incorrect. Most commonly, to evaluate a model one can compare the estimated results of the model using direct, indirect, and or trend validation. An extensive review of practices for verification and validation of MS models can be found in (Hicks et al., 2015; Lund et al., 2012), FEA models (Erdemir et al., 2012; Halonen, 2015), and overall computational modeling of solids mechanics and fluid dynamics (The American Society of Mechanical Engineers, 2009, 2006).

In order to perform a direct validation on a model, first the desired properties need to be identified. In the case of lower limb MS and knee FEA models, common parameters are typically tibiofemoral and patellofemoral: joint kinematics, contact forces and or pressures, and articular cartilage stresses and strains. Technology has been developed in the form of: EOS Imaging (Azmy et al., 2010; Clement et al., 2014), bi-planar fluoroscopy (Li et al., 2008; Myers et al., 2012), dynamic MRI (Borotikar et al., 2017; Gilles et al., 2005), and or dynamic radiostereometric analysis (Carey et al., 2014; Stentz-Olesen et al., 2017), to evaluate in vivo knee joint motion (static, quasi-static, or dynamic) under varying loading conditions, by recording bi-planar images and reconstructing the three dimensional bone trajectory by pairing with bone geometry from MRI, CT, or statistical shape models (Li et al., 2008; Michael J Rainbow, Ph.D, Daniel L Miranda, Ph.D, Roy T.H. Cheung, Ph.D, Joel B Schwartz,

Sc.B., Joseph J Crisco, Ph.D., Irene S Davis, Ph.D, P.T. and Fleming, 2013; Miranda et al., 2010; Van de Velde et al., 2010). These methods can be used to directly validate the joint kinematics of computation models.

The EOS bi-plane x-ray system (EOS Imaging SA, Paris, France) shown in Figure 1-7 uses a low-dose x-ray to scan the entire body collecting a continuous, distortion-free image in two orthogonal planes (Illés and Somoskeöy, 2012; Wybier and Bossard, 2013). Researchers have already used this relatively new technology to evaluate subject-specific musculoskeletal knee joint models, although the motion is collected in a quasi-static manner (Clément et al., 2015). It has also been used to produce more reliable inter- and intra-observer assessment of limb length and angle measurements compared to 2D x-ray results (Guenoun et al., 2012; Viel et al., 2013) and considered a valid alternative to the reference standard, computed tomography (CT), for lower-limb torsion measurements while also decreasing patient radiation exposure (Folinais et al., 2013). Pedersen et al (2018) recently conducted a study comparing an EOS reconstruction method aligning CT segmented bone geometries to EOS biplanar scans and comparing this to 'Gold Standard' bone pin methods and

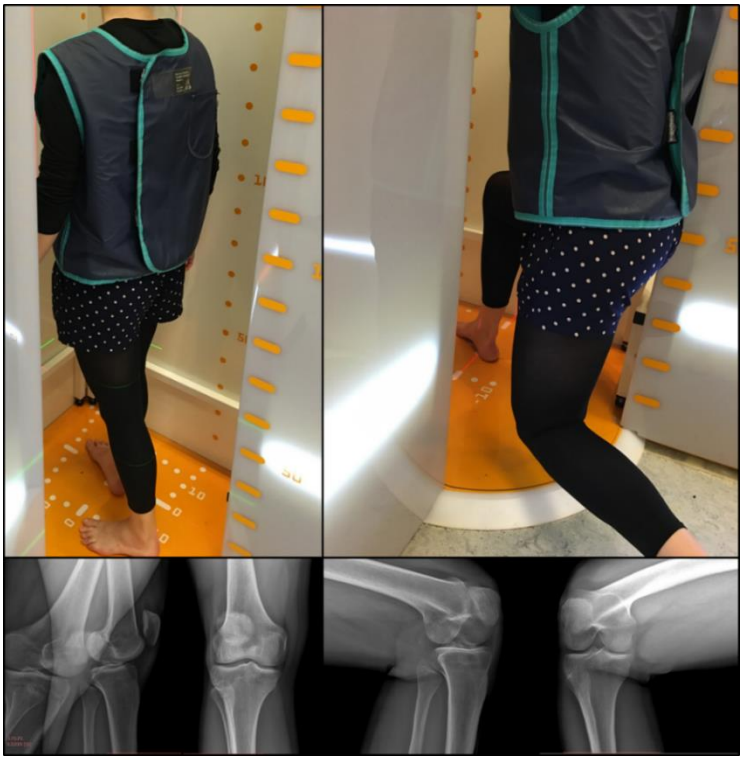

found a RMSE difference of 0.49° for rotations and 0.88 mm (Pedersen et al., 2018).

Figure 1-7. EOS Imaging biplanar x-ray System. Examples of quasi-static lunge (0° and 90° tibiofemoral flexion) with corresponding pairs of lateral and frontal biplanar x-rays.

Bi-planar fluoroscopy uses x-rays from two planes to recreate the motion of a 3D object in real-time. The imaging process has been used to investigate the translations and rotations of the patellofemoral and tibiofemoral joints during dynamic movements (Li et al., 2008; Myers et al., 2012). It is nearly impossible to obtain accurate measurements such as tibiofemoral and patellofemoral translations using traditional motion capture methods (optical-based reflective markers). Due to these limitations, researchers have started measuring secondary kinematic rotations and translations using bi-planar fluoroscopy (Kozanek, 2010; Li, 2004; Li et al., 2009, 2008, 2007, Myers et al., 2012, 2011). Many researchers have utilized the extensive datasets available through 'Orthoload' and 'Grand Challenge competition to predict in vivo knee loads' (Bergmann, 2008; Bergmann et al., 2014; Benjamin J. Fregly et al., 2012; Kinney and Besier, 2013). Some of the available data includes fluoroscopy imaging of knee joint mechanics and direct contact force measurements taken from a limited number of subjects implanted with a telemetric TKA (Heinlein et al., 2007). Various publications pertaining to the prediction of knee joint mechanics and the techniques used to perform extensive validations of the proposed MS models have resulted from these databases (Guess et al., 2014; Hast and Piazza, 2013; Lerner et al., 2015; Lundberg et al., 2013; Marra et al., 2015; Sandholm et al., 2011; Thelen et al., 2014). The validation of subject-specific MS models is a significant challenge researchers have been trying to overcome to allow for broader acceptance and use in the clinical setting (Kinney and Besier, 2013; Lund et al., 2012). Similarly, The CAMS-Knee data set has recently been established to provide researchers with combine bi-planar fluoroscopy and motion capture data of 6 subjects with an instrumented tibial insert (TKR) performing a variety of daily living activities (Taylor et al., 2017). It should be stressed that the entirety of these works only applies to joint replacement and that the results cannot be generalized to the healthy or OA knee. Hence, we need to explore other options in hopes of validating such models.

Obtaining contact pressures, stresses, and strains measurements of various knee joint structures is very difficult and restricted to invasive techniques, such as inserting a pressure sensor between the joint (Anderson et al., 2008) or implanting a strain gage directly on the bone's surface (Burr et al., 1996; Hoshaw et al., 1997). Therefore, researchers are drawn to using non-invasive techniques such as FEA to examine internal stresses/strains, especially on structures whose material properties cannot be obtained simply from strain gauge readings. However, the FE model first needs proper validation to determine if the results are reliable (Erdemir et al., 2012), which is often with cadaver models (Mootanah et al., 2014). As statement prior, the three most important parts of FEA are the model geometry, loading conditions, and material

properties, with the material properties posing the greatest challenge. Some material models of cartilage (Julkunen et al., 2007; Wilson et al., 2005, 2004) and knee joint cartilage strains (K S Halonen et al., 2014) have even been validated against experimental results.

Direct measurements cannot always be used in human research studies because they are often invasive and thus require an extensive ethical review process. Thus, measurements of another variable can be recorded and then compared with the value predicted for this variable by the model (Herzog, 2006; Lund et al., 2012). If this comparison is favorable, a leap of faith is then necessary to trust the prediction of the variable of interest. This is termed indirect validation. For instance, if the model predicts well the joint kinematics (direct measurement) then potentially it can also estimate accurately the joint reaction forces, ligament forces, muscle forces, etc as the joint kinematics is a function of these unknown forces. A common use of indirect validation in musculoskeletal modeling is judging how well the model can predict joint compressive forces though a comparison of EMG measurements and the muscle forces output by the musculoskeletal model (de Zee et al., 2007; Gaspar et al., 2017; Hug, 2011).

Additionally, trend validation can be conducted to investigate whether the output of the computational model increases or decreases correctly as a function of a systematic change in the model inputs (Herzog, 2006; Lund et al., 2012; Zee et al., 2010). One purpose of a model is to describe the general behavior of the system of interest. An acceptable agreement is one that consists of similar trends. This validation technique depends on how well the trends that are predicted agree with the trends that are measured. It is important to note that trend validation can be executed using direct and indirect measurements. If a model shows a trend, similar changes in model and experimental inputs will produce similar changes in outputs, thus leading to high confidence in a model's prediction. If the goal behind a personalized knee model is to design optimal patient-specific interventions, it is important that the model responds accurately to the specific interventions. For example, one particular study investigates whether the EMG activations and the MS model predicted muscle activations follow the same trend when analyzing a meat cutting task at an increasing table height (Pontonnier et al., 2011). Another example looks at various chair positions and examines whether the shear forces present between the chair and the human body follow the same trend when (1) collected in an experimental setup and (2) predicted by a musculoskeletal model (Olesen et al., 2014).

1.3. LIMITATIONS

The simplified generic and personalized knee joint models are computationally efficient but often do not capture the complex joint mechanics that are needed to

govern secondary joint movements. However, it has been shown that these simple subject-specific tibiofemoral models display secondary joint kinematics better than their generic counter parts (Clément et al., 2015). Granted, sometimes adding more subject-specific properties to knee models may prove to be a more time-consuming process due to required tuning to avoid singularities with respect to parallel mechanisms and/or coupling constraints (Brito da Luz et al., 2017) and/or full range of motion data (Tsai and Lung, 2014). While at the other end of the modeling spectrum, complex joint mechanics such as contact and ligament forces can be captured by the detailed 11-12 DOF joint models. However, the computational efficiency of this level of modeling if often too slow to be used for clinical applications.

A common limitation for the existing studies attempting to combine MS and FEA is that either they are based on cadaveric data, exclude important soft tissue structures, the MS output is not personalized for the given subject/patient, and finally the ligament and muscle insertions are not based on the individual's bony geometry. In order for MS to be useful in a clinical setting, the models need to reflect a patient's musculoskeletal architecture and properties as accurately as possible. To the best of my knowledge, a multi-scale model combining the use of subject-specific MS modeling and FEM of the subject's knee joint reflecting bones, meniscus, ligaments, and tendons has yet to be created. This research advances current state-of-the-art techniques by allowing scientists to simultaneously estimate net joint loads (resulting from knee joint kinematics, external loads and ligament/muscle forces) and the stresses/strains present in the soft tissue of the knee.

The first step in expanding this proposed multiscale workflow to a patient cohort is to capture the net joint loads more accurately using patient-specific models. The goal of personalized models being utilized in the clinical setting will call for better model calibration with respect to patient data (Benjamin J Fregly et al., 2012). Currently, clinical gait analysis software uses generic stick-figure models only capable of obtaining KAM measurements, and if researchers attempt musculoskeletal modeling to investigate optimal treatment methods through means of knee contact forces, they rarely stray from simple linear scaling. This should raise the question on whether differences exist between linearly scaled models and patient-specific models with regards to the evaluation of knee contact forces and consequently the identification of patient-specific interventions for KOA.

1.4. AIMS AND OUTLINE OF DISSERATION

The main aims of this PhD project are to (1) develop and validate a novel joint model which captures the subject-specific kinematics and bone geometry while also being computationally efficient. (2) To establish a subject-specific multi-scale model that

ultimately allows clinicians to investigate how varying biomechanics and orthosis interventions will affect the internal loads of the body and influence the stresses/strains on anatomical features of the knee. (3) Determine if treatment outcomes, based on individual patients and a patient group as a whole are influenced by different musculoskeletal modelling scaling techniques. The results from these objectives are presented in the following chapters:

Chapter 2 presents the development and validation of subject-specific moving-axis tibiofemoral joint models using MRI and EOS imaging during a quasi-static lunge. The main aims of this study are to create a subject-specific tibiofemoral joint model that is computationally efficient and can display anatomically correct secondary joint kinematics. The model utilizes a moving-axis concept that is based upon a linear relationship between two tibiofemoral flexion positions. Validation of this approach is done by measuring the secondary joint kinematics from a quasi-static lunge obtained using biplanar EOS Imaging, segmented 2D EOS contours and 3D MRI bone geometries, and custom written MATLAB registration software.

Subsequently, in **Chapter 3,** the work established in **Chapter 2** is expanded to the patellofemoral joint by applying a moving-axis concept, which utilizes a linear relationship between two known patellar positions (consequently when the tibiofemoral joint is flexed and extended). Subject-specific patellofemoral joint kinematics are then extracted from combinations of tibiofemoral (hinge, moving-axis, interpolated) and patellofemoral (hinge and moving-axis) joint models and evaluated against experimental in vivo kinematics from a series of biplanar EOS images. Overall a computationally efficient patellofemoral model was established that captures subject-specific patellar motion.

In **Chapter 4,** a workflow to assess the effect of gait modifications and lateral wedge insoles on the stresses and strains in the medial tibial cartilage is presented through combining musculoskeletal modeling and finite element analysis. The main aim was to simultaneously estimate net joint loads from a musculoskeletal model and stresses in soft tissues of the knee during normal and modified gait through finite element analyses. Full lower limb and detailed MRI images were needed to establish the bone and ligament architecture of the musculoskeletal model and the soft tissue structures of the finite element model. Output forces from various gait alterations (normal shod walking, 5° and 10° lateral wedge insole walking, toe-in, and toe-out wide walking) were obtained through musculoskeletal model simulations and used as boundary conditions for the finite element knee model to achieve tibial articular cartilage stresses and strains. Overall, this study established a workflow allowing researchers to assess the effect of low-cost clinical interventions on a subject-specific basis. This paper provides the necessary groundwork to develop patient-specific models and furthermore, better optimize treatments based on an individual patient rather than cohort.

Chapter 5 partially applies the workflow established in **Chapter 4** to a small patient cohort. This study compared generic vs patient-specific musculoskeletal model-scaling techniques for identification of personalized gait alteration for individuals diagnosed with medial compartment knee osteoarthritis. The main objectives of the study were to first analyze the effect gait alterations such as lateral wedge insoles or gait modifications have on medial contact forces through use of patient-specific musculoskeletal models. Secondly, the research aimed to identify which of the various alterations result in the greatest reduction in peak medial compressive force and or impulse with respect to the patients individually and as a group. Last, this study investigated whether the same conclusions would have been reached by using a simple linear scaling technique as opposed to an advanced MRI morphing method.

The final **Chapter (6)** provides a general overview of key results and a discussion regarding the outcomes of this PhD dissertation. It lays out recommendations for future research in the subject-specific multiscale modeling field. Chapters 2-5 are scientific journal publications that have been (1) granted permissions by the journal to reprint in this dissertation document or (2) submitted to a journal and awaiting publication.

CHAPTER 2. PAPER I

Development and validation of a subject-specific moving-axis tibiofemoral joint model using MRI and EOS imaging during a quasi-static lunge

Dzialo, C.M., Pedersen, P.H., Simonsen, C.W., Krogh, K., de Zee, M., Andersen, M.S. *Journal of Biomechanics (2018), Volume 72, Pages 71-80. https://doi.org/10.1016/j.jbiomech.2018.02.032*

ABSTRACT

The aims of this study were to introduce and validate a novel computationally-efficient subject-specific tibiofemoral joint model. Each subject performed a quasi-static lunge while micro-dose radiation bi-planar x-rays (EOS Imaging, Paris, France) were captured at roughly 0, 20, 45, 60, and 90 degrees of tibiofemoral flexion. Joint translations and rotations were extracted from this experimental data through 2D-to-3D bone reconstructions, using an iterative closest point optimization technique, and employed during model calibration and validation. Subject-specific moving-axis and hinge models for comparisons were constructed in the AnyBody Modeling System (AMS) from Magnetic Resonance Imaging (MRI)-extracted anatomical surfaces and compared against the experimental data. The tibiofemoral axis of the hinge model was defined between the epicondyles while the moving-axis model was defined based on two tibiofemoral flexion angles at about 0 and 90 degrees and the articulation modeled such that the tibiofemoral joint axis moved linearly between these two positions as a function of the tibiofemoral flexion. Outside this range, the joint axis was assumed to remain stationary. Overall, the secondary joint kinematics were better approximated by the moving-axis tibiofemoral model with an average mean difference and standard error of (translations: 2.84 ± 0.31 mm, rotations: 1.25 ± 0.43^0) and higher coefficients of determination (R^2) for each clinical measure. While the hinge model achieved an average mean difference and standard error of (3.87 ± 0.39 mm, 7.39 ± 0.87^0). Unlike the hinge model, no significant differences were found between the moving-axis model and the experimentally observed tibiofemoral joint rotations.

2.1 INTRODUCTION

Musculoskeletal (MS) models are utilized by the scientific community to gain insight on how external forces and movements influence the human body internally, allowing for quantification of muscle, ligament, and joint contact forces without using invasive methods. Studies have shown that subjects with knee osteoarthritis (KOA) in the tibiofemoral joint tend to have greater adduction angles, and a more medially positioned femur relative to tibia (Zeighami et al., 2017). Researchers require MS tibiofemoral joint models that capture kinematics properly if the end goal is to investigate pathologies, such as KOA progression, through use of models. Emphasizing the importance of proper model validation.

Existing MS tibiofemoral joint models range from simple to complex depending on their generic qualities and computational time. On one end of the spectrum, researchers often idealize the tibiofemoral joint as a hinge joint with a fixed position and orientation (Anderson and Pandy, 2001; Fregly, 2007; Klein Horsman et al., 2007; Marra et al., 2015). More detailed models include coupling constraints allowing for additional degrees of freedom (DOF) based on tibiofemoral flexion (Delp et al., 1990; Donnelly et al., 2012; Feikes et al., 2003; Pontonnier and Dumont, 2010; Tsai and Lung, 2014), parallel spatial mechanisms (Duprey et al., 2010, 2009, Moissenet et al., 2014, 2012; Wilson et al., 1998; Xavier Gasparutto et al., 2015), and sphere-on-plane contact models (Clément et al., 2015; Duprey et al., 2010, 2009; Habachi et al., 2015). These models are often based off cadaveric geometries and properties, though some models have been given subject-specific properties. These simplified generic and subject-specific models allow for computational convenience; however, they do not capture the complex joint mechanics that govern the secondary joint movements. At the other end of the spectrum exists computationally complex, 11-12 DOF multibody contact tibiofemoral models (Guess et al., 2014; Hast and Piazza, 2013; Marra et al., 2017, 2015; Smith et al., 2016; Thelen et al., 2014) utilizing varying methods of solving gross body dynamics and the detailed joint dynamics.

The existing computationally efficient subject-specific tibiofemoral models capture secondary joint kinematics better than their generic counter parts (Clément et al., 2015). However, these models require intensive tuning to avoid singularities and/or require full range of motion data which is time consuming to collect. Our aim is to develop a subject-specific tibiofemoral model that avoids these issues, is computationally efficient, and can display anatomically correct secondary joint kinematics. This paper presents a novel subject-specific tibiofemoral model utilizing a moving-axis based on a linear relationship between two tibiofemoral flexion positions. To validate this approach, we compare the estimates against measured secondary joint kinematics during a quasi-static lunge obtained from EOS^{TM} Imaging biplanar x-rays.

2.2 METHODS

Ten male subjects (age 33 ± 10 years, body mass 79 ± 11 kg, height 1.82 ± 0.07 m, body mass index (BMI) 23.81 ± 2.66 kg/m^2) participated in this study. Subjects were categorized as healthy, without pre-existing knee injuries. The following procedures were approved by the Scientific Ethical Committee for the Region of Nordjylland and informed consent was obtained prior to data collection.

1.1 Magnetic Resonance Imaging

Each subject underwent magnetic resonance imaging (MRI) from pelvis to the feet. The 1.5T *OptimaTM MR450w - 70cm* (General Electric Healthcare, Chicago, Illinois, USA) scanner was utilized running a T1W-LAVA-XV-IDEAL, coronal plane scan. To create the lower limb series, each subject was scanned in 3 overlapping sections, moving the table further into the bore, and then stitching the water-only scans together using GE software (Figure 2-1.A).

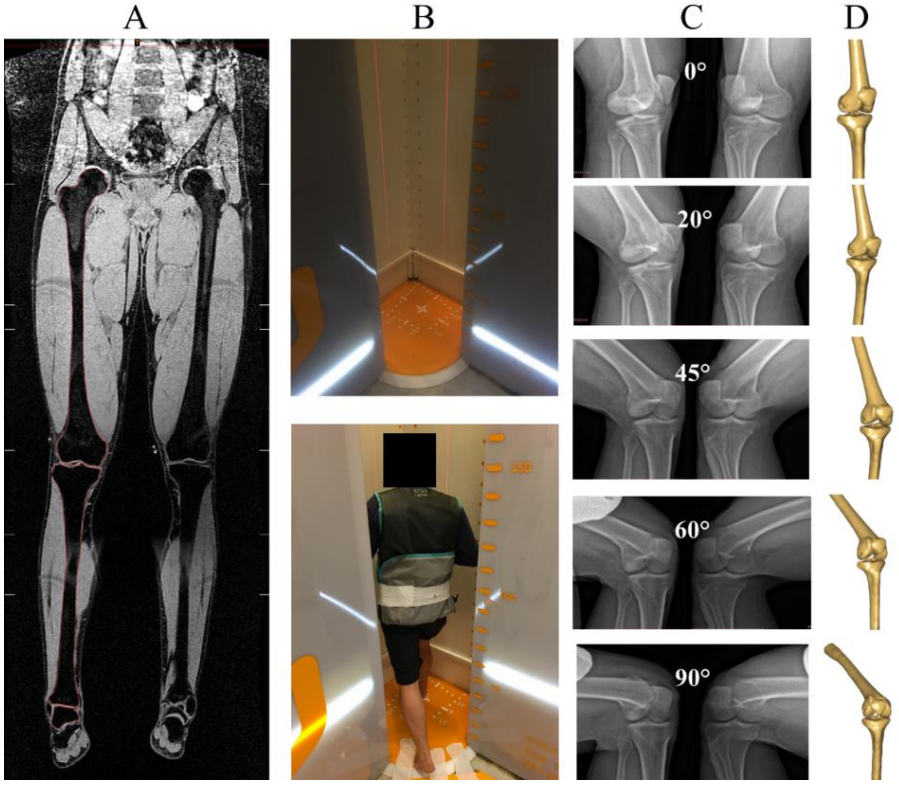

Figure 2-1. A method of combining MR and EOS Imaging technology: A, Development of 3D knee geometry using a stack of coronal MR images; B, and acquisition of quasi-static lunge (lower image) using two orthogonally positioned low dose x-rays (top image). C, Bi-planar EOS images were taken at roughly 0^0, 20^0, 45^0, 60^0, and 90^0 tibiofemoral flexion. D, Bone positions were determined by combining the 3D knee model with the bi-planar contours and applying optimization methods.

1.2 Bi-planar X-ray images

The EOS^{TM} bi-plane x-ray system, shown in the top of Figure 2-1.B, uses a low-dose biplanar slot-scanning technology, which allows for partial- or full-body imaging collecting a continuous, distortion-free image in two orthogonal planes (Illés and Somoskeöy, 2012; Wybier and Bossard, 2013). Researchers have used this new technology to investigate tibiofemoral contact during a quasi-static squat in healthy and KOA patients (Zeighami et al., 2017). We used this system to obtain in-vivo data for model development and validation. Five pairs of orthogonal x-rays images were taken, focusing on the tibiofemoral joint, as the subject performed a quasi-static lunge holding tibiofemoral flexion at roughly 0, 20, 45, 60, and 90 degrees (Figure 1.B bottom). Due to the structural limitations of the EOS scanner, the anterior posterior (AP) and lateral (LAT) images were taken at approximately 45-degree to the x-ray tubes (Figure 2-1.C).

1.3 Segmentation and Registration

The right femur, tibia, and talus bones were manually segmented from the lower limb MRI (Figure 2-1.A) using Mimics Research 19.0 (Materialise, Belgium). Post-processing was done in Meshmixer (Autodesk, United States of America) and using the contour editing toolbox in Mimics. Stereolithography (STL) surfaces were exported of each bone to obtain subject-specific anatomical landmarks, contact surfaces, and joint centers. In addition, femur and tibia contours were segmented from all biplane x-ray images (Figure 2-1.C).

To reconstruct femur and tibia positions and orientations for each biplanar x-ray, custom MATLAB (The Mathworks Inc., Natick, MA, USA) code manually transformed the 3D MRI-based bone geometry until its projected contours roughly overlay the bi-plane segmented contours. Hereafter, an iterative closest point optimization method minimized the least-square difference between the bi-planar contours and the 3D geometry generated contour. Subsequently, the positions and orientations were read into AnyBody Modeling System (AMS v 6.1, Aalborg Denmark) to compute the clinical translations and rotations based on ISB standards (Grood and Suntay, 1983). The femur and tibia STL surfaces obtained from the 0 and 90 EOS reconstructions (**Error! Reference source not found.**.D) were used in s ubject-specific moving-axis tibiofemoral joint development.

1.4 Tibiofemoral coordinate systems kinematic measurement

Identical anatomical coordinate systems (Figure 2-2) were created for the EOS reconstructions and models following ISB standards (Grood and Suntay, 1983; Wu and Cavanagh, 1995). Anatomical landmarks were defined by averaging clusters of triangles on the STL surfaces at the medial and lateral: femoral epicondyles, tibia edges, and intercondylar tibial eminences. The hip joint center was defined by fitting a sphere to the femoral head surface. The ankle (talocrural) joint axis was defined as

a vector joining the centers of two spheres fit to the medial and lateral halves of the talus trochlea, with origin midway between these centers (Parra et al., 2012). The displacements were calculated at the femur origin relative to tibia. The rotations between femur and tibia were measured in the sequence of flexion/extension, abduction/adduction and internal/external rotation going from the femoral to the tibial coordinate system.

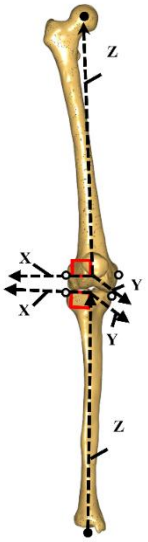

Figure 2-2. Right leg anatomical axes definitions. Femur: Z-axis (longitudinal axis) was defined from hip joint center to midpoint between medial and lateral epicondyles. X-axis (medial-lateral axis) was defined to be orthogonal to the Z-axis axis and pointing towards the medial epicondyle. Y-axis was orthogonal to both the Z and X axes and pointing anteriorly. Tibia: Z-axis was defined from the talocrural joint center (Parra et al. 2012) to the midpoint between the medial tibia edge and lateral tibia edge. X-axis (medial-lateral axis) was defined to be orthogonal to the Z-axis and pointing towards the medial tibia edge. Y-axis was orthogonal to both the Z and X axes and pointing anteriorly.

1.5 Tibiofemoral Model Development

Tibiofemoral models were developed in AMS using the femur and tibia STLs segmented from the lower limb MRI (Figure 2-3 3.A *left image*) as rigid body segments. To establish the moving-axis model, transformation matrices were obtained from the EOS 0˚ and 90˚ reconstructions (Figure 2-3.A *right images*) to the MRI bone positions for the femur and tibia (Figure 2-3.B). This was done by using the 3D linear transformation function in AMS, which utilizes a rigid-body least-squares approach based on two sets of landmarks. The tibiofemoral contact areas on the medial and lateral femoral condyles were selected in 3-Matic 11.0 (Materialise, Belgium) for both

the EOS 0° and EOS 90° bone positions (Figure 2-3.C). A least-square cylindrical fitting function in MATLAB was used to determine the medial and lateral extension (EFC) and flexion facet centers (FFC) (Iwaki et al., 2000), shown in Figure 2-3.D. These were found by fitting a cylinder, yielding a longitudinal axis and radius, to each of the four contact surfaces. The respective condyle center was defined as the average point along the cylinder axis. The EFC points and the medial FFC point were transformed to the femur and tibia segments unaffected; whereas the lateral FFC point was separated by a distance equivalent to that between the EFC points, while remaining on the FFC axis. These points were used to define a tibiofemoral model with an axis passing through the EFC points when the flexion angle corresponds to the EOS 0° reconstruction and through the FFC points when the flexion angle corresponds with the EOS 90°reconstruction. In between, the tibiofemoral axis is assumed to move linearly from the EFC to the FFC points as a function of tibiofemoral flexion. When the tibiofemoral flexion is below the EOS 0° or above the EOS 90° angles, the tibiofemoral axis is assumed to remain fixed through the EFC and FFC points, respectively. To model this, two additional rigid segments were introduced, so-called invisible femur and invisible tibia, which were used to move the tibiofemoral flexion axis relative to the femur and tibia according to the relationship above.

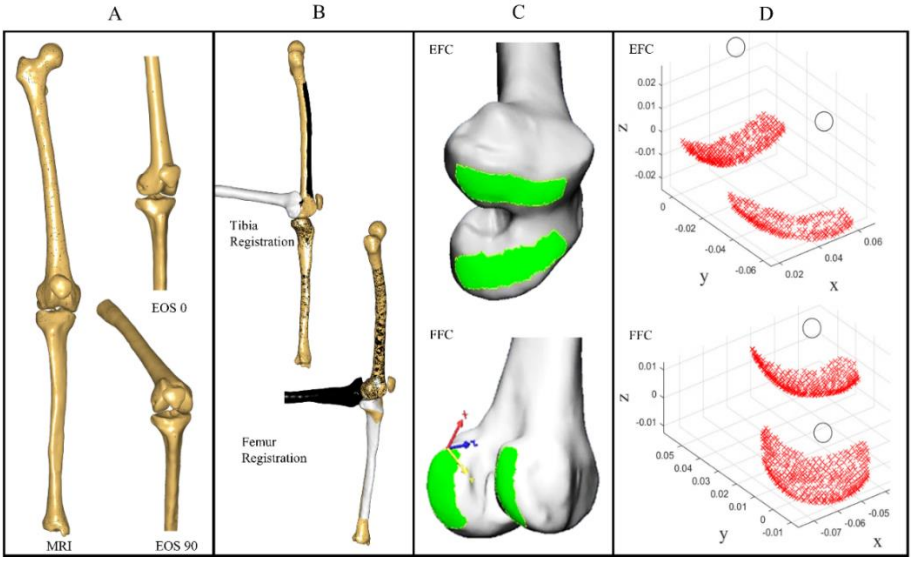

Figure 2-3. Overview of extension (EFC) and flexion facet centers (FFC) axes definition: A, Lower limb MRI segmentation and resulting bone positions from EOS 0 and 90 reconstructions to obtain respective transformation matrices. B, Femur and Tibia Registrations of the EOS 0 and 90 STLs on to MRI STLs. C, Tibiofemoral contact surface selection on EOS 0 and EOS 90 Femur STLs. D, Cylinder fits on medial and lateral femoral condyle surface selections with resulting EFCs and FFCs.

To describe this mathematically, a full Cartesian formulation was applied, in which the position and orientation of each body relative to the global coordinates system was used as the unknowns and collectively denoted, $\mathbf{q}$ (see Figure 2-4). The position vector of each body is denoted ${}_{(i)}\mathbf{r} = \geq \left[{}_{(i)}x \quad {}_{(i)}y \quad {}_{(i)}z \right]^{\mathrm{T}}$ and the orientation is described by four Euler parameters ${}_{(i)}\mathbf{p} = \geq \left[{}_{(i)}e_0 \quad {}_{(i)}e_1 \quad {}_{(i)}e_2 \quad {}_{(i)}e_3 \right]^{\mathrm{T}}$, where the left sub-script denotes the *i*th segment, i.e. $i = \{\mathrm{T}, \mathrm{F}, \mathrm{IT}, \mathrm{IF}\}$ with T for tibia, F for femur, IT for invisible tibia and IF for invisible femur. To formulate the equations, the rotation matrix of each body is required and denoted ${}_{(i)}\mathbf{A} = \left[{}_{(i)}\mathbf{a}_x \quad {}_{(i)}\mathbf{a}_y \quad {}_{(i)}\mathbf{a}_z \right]$, where ${}_{(i)}\mathbf{a}_x$, ${}_{(i)}\mathbf{a}_y$ and ${}_{(i)}\mathbf{a}_z$ are the first, second and third columns, respectively.

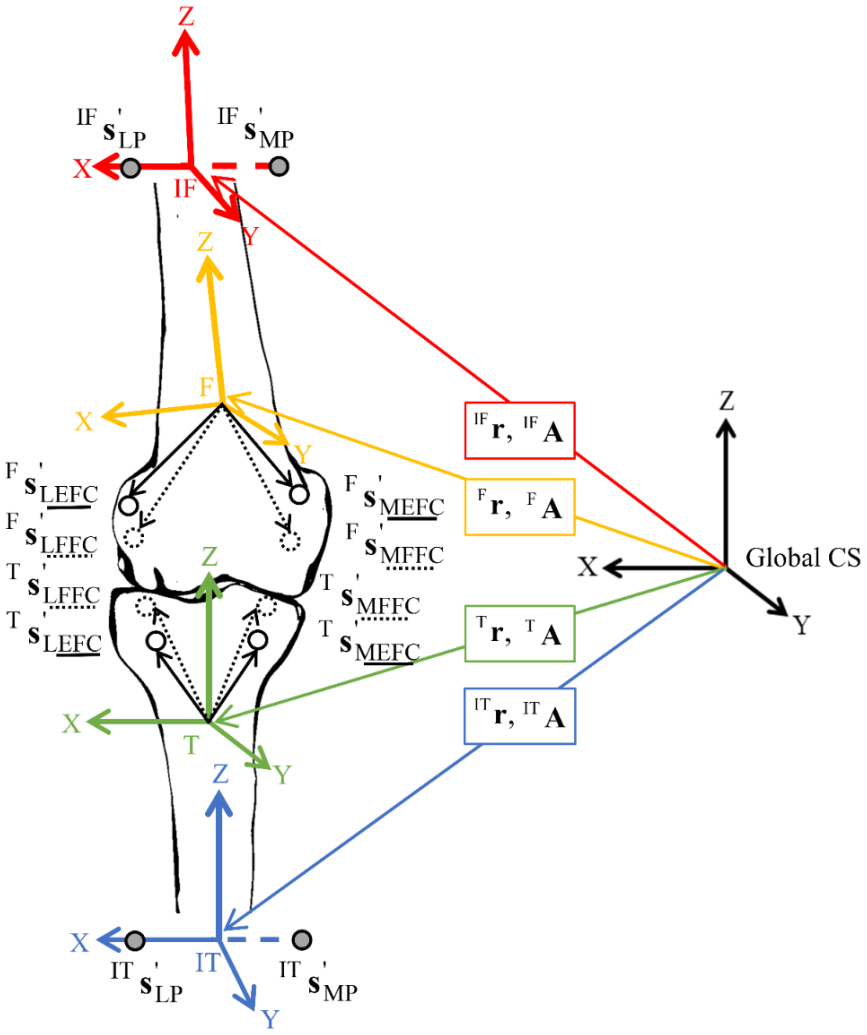

Figure 2-4. Schematic of position vectors and rotation matrices of the femur, tibia, invisible femur, and invisible tibia rigid body segments with respect to the global coordinate system. The black coordinate system refers to the global, yellow: femur, red: invisible femur, green: tibia, and blue: invisible tibia. Solid colored arrows represent position vector and rotation matrices between global coordinate systems and respective rigid body segment coordinate systems. Solid black lines represent position vectors of EFC points in femoral/tibial coordinate systems while dotted lines depict position vectors of FFC points in femoral/tibia coordinate systems.

Although the rotation matrix is a function of Euler parameters, the function argument is omitted to keep the equations concise. For each segment, coordinates systems are defined and the required points for the tibiofemoral model are transformed into these coordinate systems. For the invisible tibia and invisible femur, medial and lateral points were defined along the x-axis separated by a distance equivalent to that between the EFC points. The orientation of the y- and z-axis are irrelevant for axis movement, but defined such that the z-axis of each invisible segment was orthogonal to the x-axis (pointing towards the hip center and away from the ankle joint center respectively), and the y-axis orthogonal to the x- and z- axis. The points on all the segments are systematically named ${}_{(i)}\mathbf{s}'_j$ where *j* is denoting the point name, e.g. ${}_{(\mathrm{T})}\mathbf{s}'_{\mathrm{LFFC}}$ is the position vector of the lateral FFC point in the tibial coordinate system. With this, the holonomic constraint equations to describe the tibiofemoral model can be expressed as:

$$\mathbf{\Phi}(\mathbf{q}) = \begin{bmatrix} {}_{(\mathrm{F})}\mathbf{f}_{\mathrm{MP}} - {}_{(\mathrm{IF})}\mathbf{r} - {}_{(\mathrm{IF})}\mathrm{A}_{(\mathrm{IF})}\mathbf{s}'_{\mathrm{MP}} \\ {}_{(\mathrm{T})}\mathbf{f}_{\mathrm{MP}} - {}_{(\mathrm{IT})}\mathbf{r} - {}_{(\mathrm{IT})}\mathrm{A}_{(\mathrm{IT})}\mathbf{s}'_{\mathrm{MP}} \\ \left({}_{(\mathrm{IF})}\mathrm{A}^{\mathrm{T}}\left({}_{(\mathrm{F})}\mathbf{f}_{\mathrm{LP}} - {}_{(\mathrm{IF})}\mathbf{r} - {}_{(\mathrm{IF})}\mathrm{A}_{(\mathrm{IF})}\mathbf{s}'_{\mathrm{LP}}\right)\right)_{yz} \\ \left({}_{(\mathrm{IT})}\mathrm{A}^{\mathrm{T}}\left({}_{(\mathrm{T})}\mathbf{f}_{\mathrm{LP}} - {}_{(\mathrm{IT})}\mathbf{r} - {}_{(\mathrm{IT})}\mathrm{A}_{(\mathrm{IT})}\mathbf{s}'_{\mathrm{LP}}\right)\right)_{yz} \\ {}_{(\mathrm{IF})}\theta_x \\ {}_{(\mathrm{IT})}\theta_x \\ {}_{(\mathrm{IF})}\mathbf{r} - {}_{(\mathrm{IT})}\mathbf{r} \\ {}_{(\mathrm{IF})}\mathbf{a}_x^T \, {}_{(\mathrm{IT})}\mathbf{a}_y \\ {}_{(\mathrm{IF})}\mathbf{a}_x^T \, {}_{(\mathrm{IT})}\mathbf{a}_z \\ {}_{(\mathrm{F})}\mathbf{p}^T \, {}_{(\mathrm{F})}\mathbf{p} - 1 \\ {}_{(\mathrm{IF})}\mathbf{p}^T \, {}_{(\mathrm{IF})}\mathbf{p} - 1 \\ {}_{(\mathrm{T})}\mathbf{p}^T \, {}_{(\mathrm{T})}\mathbf{p} - 1 \\ {}_{(\mathrm{IT})}\mathbf{p}^T \, {}_{(\mathrm{IT})}\mathbf{p} - 1 \end{bmatrix} = \mathbf{0} \qquad [2\text{-}1]$$

where

$$ {}_{(F)}\mathbf{f}_{MP} = \begin{cases} {}_{(T)}\mathbf{r}_{MEFC} & \theta_{TF} < \theta^{0}_{EOS} \\ {}_{(T)}\mathbf{r}_{MEFC}(1-\nu)+{}_{(T)}\mathbf{r}_{MFFC}\nu & \theta^{0}_{EOS} \le \theta_{TF} \le \theta^{90}_{EOS} \\ {}_{(T)}\mathbf{r}_{MFFC} & \theta^{90}_{EOS} < \theta_{TF} \end{cases} \qquad [2\text{-}2] $$

and

$$ \nu = \frac{\theta_{TF}}{\theta^{90}_{EOS} - \theta^{0}_{EOS}} - \frac{\theta^{0}_{EOS}}{\theta^{90}_{EOS} - \theta^{0}_{EOS}} \qquad [2\text{-}3] $$

${}_{(F)}\mathbf{f}_{LP}$, ${}_{(T)}\mathbf{f}_{MP}$ and ${}_{(T)}\mathbf{f}_{LP}$ are defined in the same manner using instead the lateral points of femur, and the medial and lateral points of tibia respectively. θ_{TF} is the tibiofemoral flexion angle measured between the femur and tibia anatomical coordinate systems; θ^{0}_{EOS} and θ^{90}_{EOS} are the tibiofemoral flexion angles corresponding to the EOS 0˚ and EOS 90˚ scans. ${}_{(IF)}\theta_x$ and ${}_{(IT)}\theta_x$ are Euler angles around the x-axis of the invisible femur and invisible tibia relative to the femur and tibia anatomical frames respectively, measured with a rotation sequence of x-y-z. The top two equations in Equation [2-1] constrain the medial point of the invisible segments to a position in between the EFC and FFC depending on the tibiofemoral flexion. Similarly, the third and fourth equations constrain the y and z coordinates of the lateral point of each invisible segment to a position between the EFC and FFC. The fifth and sixth equation ensure zero rotation about the x-axis relative to the anatomical frames for the invisible segments. Equations seven to nine enforce a revolute joint between the invisible segments by constraining their origins to be at the same position in the global coordinate system and ensuring that only relative rotation around the x-axis is allowed. The last four equations ensure the Euler parameters have unity length.

Equation (2-1) provides 21 constraint equations, however the total system has 28 coordinates, i.e. seven for each rigid body. Therefore, seven equations are still required to perform a kinematically determinate analysis. These are specified as:

$$\mathbf{\Phi}^{(\mathrm{d})}(\mathbf{q},t)=\begin{bmatrix} {}_{(\mathrm{T})}\mathbf{r} \\ {}_{(\mathrm{T})}\theta_x \\ {}_{(\mathrm{T})}\theta_y \\ {}_{(\mathrm{T})}\theta_z \\ \theta_{\mathrm{TF}}-at-b \end{bmatrix}=\mathbf{0} \qquad (4)$$

where ${}_{(\mathrm{T})}\theta_x$, ${}_{(\mathrm{T})}\theta_y$ and ${}_{(\mathrm{T})}\theta_z$ are the Euler angles of tibia relative to the global coordinate system measured in the sequence x-y-z. These equations enforce tibia to align with the global coordinate system and control the tibiofemoral flexion angle, θ_{TF}, to flex with a constant velocity, *a*, and with a flexion angle of *b* at time $t=0$. *b* was specified as the tibiofemoral flexion angle during the EOS 0˚ and, as the knee kinematics is independent of flexion velocity, *a* was set to 110˚s^{-1}. The constraint equations in [2-1] and [2-4] were simultaneously solved in the AMS using a Newton-Raphson-based nonlinear equation solver with time intervals set to ensure that knee flexion angles both before and after the EOS 0˚ and EOS 90˚ were included.

In addition, a subject-specific hinge model was created for each subject to investigate how well the moving-axis model performs against a commonly used tibiofemoral joint in the musculoskeletal community. The hinge joint was defined by a line passing through the medial and lateral femoral epicondyles (Churchill et al., 1998) and driven from 0 to 110 degrees flexion.

1.6 Model Evaluation and Statistics

Tibiofemoral kinematics were extracted from EOS scans at five conditions of varying tibiofemoral flexion. Model predicted results were extracted at these five corresponding conditions per subject (n = 10). Since the 0 and 90 EOS reconstructions were used for the moving-axis model calibrations, these did not provide any model prediction capabilities and were excluded when evaluating the moving-axis model. The model (hinge and moving-axis) predictions were then evaluated against EOS experimental measurements and each other, in terms of mean difference and coefficient of determination (R2). Fifteen one-way repeated measures ANOVAs (5 clinical measures at 3 lunge conditions) were performed with post-hoc tests using Bonferroni adjustments ($\alpha = 0.01$) for multiple comparisons. The data was tested for normality using a Shapiro-Wilk tests and adjusted for small sample size (n = 10) using the Greenhouse-Geisser estimates of sphericity (Maxwell et al., 2013).

2.3 RESULTS

The tibiofemoral secondary joint kinematics of each subject (n = 10) were extracted from the EOS reconstructions (circles), hinge (left column), and moving-axis (right column) models, shown in Figure 2-5. More subject deviation existed in the rotational measures compared to translational. The experimental abduction and internal rotations increased as the tibiofemoral joint flexes from 0 to 90 degrees; the moving-axis models agreed, while the hinge models opposed with this trend. Due to the nature of a hinge joint, the compression/distraction (CD) remained constant during the entire flexion/extension (FE) cycle which is not consistent with the in vivo experimental (EOS) results. Most EOS subject data decreased in CD as the tibiofemoral joint is flexed from 0 to 90 degrees, similarly to how the moving-axis model responded. The EOS data showed clear anterior/posterior (AP) displacement amongst subjects, which is captured by the moving-axis model but not by the hinge model.

The mean kinematic parameters (n = 10) for each quasi-static lunge position were calculated for experimental EOS data (Table 2-1), moving-axis model output (Table 2-2) and hinge model output (Table 2-3). In addition, minimum, maximum, and range of motion values (mean ± standard deviation) were extracted. Overall, the moving-axis model better captured the in vivo ROM data which was often underestimated by the hinge model.

Mean differences (MD) and standard error (SE) between models and experimental data were recorded (Table 2-4) and R^2 values are presented (Table 2-5) to compare model predictive capabilities. Almost exclusively, the moving-axis model has lower mean differences and higher R^2 values when compared to the hinge model. However, at low angles of flexion (20 and 45 degrees) the moving-axis ML translations are significantly different (MD ± SE: -2.43 ± 0.35 mm and -2.31 ± 0.44 mm) than the experimental data (p-value $\leq$ 0.01). In addition, moving-axis and hinge models significantly underestimated experimental AP translations (average MD ± SE: 6.50 ± 0.82mm and 10.11 ± 0.88mm respectively) for all lunge angles. The hinge model varied significantly from the experimental data in abduction/adduction (AA) and internal/external (IE) rotations (average MD ± SE: -3.17 ± 0.86^0 and 11.60 ± 1.51^0). While no significant differences were found between the moving-axis model and experimental data with respect to rotational measures (see Supplementary Table for p-values and confidence intervals).

Table 2-1. Experimental EOS data: Tibiofemoral secondary joint kinematics (mean ± standard deviation) at quasi-static lunge angles. Averaged kinematic means with and without moving-axis calibration angles (0 and 90). Range of motion (ROM), minimum, and maximum values (mean ± SD) during knee flexion of 3.48 ± 5.62^0 to 86.59 ± 8.54^0.

Condition	EOS				
	ML (mm)	**AP (mm)**	***CD (mm)***	**AA (^{0})**	***IE (^{0})***
EOS_0	4.80 ± 1.87	-3.39 ± 3.42	34.63 ± 3.48	0.05 ± 2.68	5.06 ± 7.59
EOS_20	2.88 ± 1.35	0.61 ± 2.70	35.62 ± 4.13	-1.14 ± 3.22	8.26 ± 6.64
EOS_45	2.68 ± 1.60	4.81 ± 3.89	35.49 ± 3.26	-2.30 ± 2.50	9.61 ± 4.88
EOS_60	2.90 ± 1.19	6.88 ± 5.06	35.01 ± 3.51	-2.59 ± 2.81	10.16 ± 4.08
EOS_90	2.58 ± 2.10	10.58 ± 4.41	33.48 ± 3.32	-2.62 ± 2.49	11.29 ± 5.86
Average (0-90)	**3.17 ± 1.62**	**3.90 ± 3.90**	**34.84 ± 3.54**	**-1.72 ± 2.74**	**8.87 ± 5.81**
Average (20-60)	**2.82 ± 1.38**	**4.10 ± 3.88**	**35.37 ± 3.63**	**-2.01 ± 2.84**	**9.34 ± 5.20**
min	1.77 ± 1.33	-3.51 ± 3.35	33.07 ± 3.35	-3.57 ± 2.50	2.48 ± 5.15
max	5.02 ± 1.98	10.58 ± 4.41	36.21 ± 3.66	0.35 ± 2.47	14.31 ± 4.84
ROM	3.25 ± 1.48	14.09 ± 5.09	3.14 ± 1.69	3.92 ± 2.11	11.84 ± 5.23

Table 2-2. Moving-axis model output: Tibiofemoral secondary joint kinematics (mean ± standard deviation) at quasi-static lunge angles. Averaged kinematic means with and without moving-axis calibration angles (0 and 90). Range of motion (ROM), minimum, and maximum values (mean ± SD) during knee flexion of 3.48 ± 5.62^0 to 86.59 ± 8.54^0.

Condition	Moving-Axis				
	ML (mm)	**AP (mm)**	***CD (mm)***	**AA (^{0})**	***IE (^{0})***
EOS_0	4.80 ± 1.87	-3.39 ± 3.42	34.64 ± 3.48	0.05 ± 2.68	5.06 ± 7.59
EOS_20	5.30 ± 1.35	-5.58 ± 3.52	34.63 ± 3.30	-1.89 ± 2.71	6.32 ± 5.33
EOS_45	4.99 ± 1.42	-2.98 ± 4.16	35.60 ± 3.52	-2.96 ± 2.29	7.66 ± 4.27
EOS_60	4.11 ± 1.70	1.35 ± 5.63	35.75 ± 3.44	-2.94 ± 2.25	8.36 ± 4.12
EOS_90	2.58 ± 2.10	10.57 ± 4.41	33.48 ± 3.32	-2.62 ± 2.49	11.29 ± 5.86
Average (0-90)	**4.35 ± 1.69**	**-0.00 ± 4.23**	**34.82 ± 3.41**	**-2.07 ± 2.48**	**7.74 ± 5.43**
Average (20-60)	**4.80 ± 1.49**	**-2.40 ± 4.44**	**35.33 ± 3.42**	**-2.60 ± 2.42**	**7.45 ± 4.57**
min	2.35 ± 1.67	-5.95 ± 3.58	32.83 ± 3.24	-3.41 ± 2.37	2.56 ± 5.20
max	5.72 ± 1.42	10.59 ± 4.41	36.32 ± 3.21	0.06 ± 2.68	13.79 ± 4.04
ROM	3.37 ± 1.39	16.55 ± 4.25	3.48 ± 1.48	3.47 ± 2.19	11.23 ± 5.56

Table 2-3. Hinge model output: Tibiofemoral secondary joint kinematics (mean ± standard deviation) at quasi-static lunge angles. Averaged kinematic means with and without moving-axis calibration angles (0 and 90). Range of motion (ROM), minimum, and maximum values (mean ± SD) during knee flexion of 3.48 ± 5.62^0 to 86.59 ± 8.54^0. Hinge knee model has fixed CD of 34.72 ± 3.54 mm.

Condition	Hinge			
	ML (mm)	**AP (mm)**	**AA (^{0})**	***IE (^{0})***
EOS_0	4.60 ± 1.66	-5.91 ± 1.86	-0.26 ± 2.17	-0.91 ± 5.84
EOS_20	4.08 ± 1.59	-5.96 ± 1.86	0.53 ± 1.93	-1.66 ± 5.94
EOS_45	3.67 ± 1.71	-6.00 ± 1.85	1.15 ± 2.11	-2.24 ± 6.08
EOS_60	3.23 ± 1.88	-6.05 ± 1.83	1.81 ± 2.35	-2.87 ± 6.38
EOS_90	2.75 ± 1.95	-6.10 ± 1.83	2.52 ± 2.55	-3.58 ± 6.72
Average (0-90)	**3.67 ± 1.76**	**-6.00 ± 1.84**	**1.15 ± 2.22**	**-2.25 ± 6.19**
Average (20-60)	**3.66 ± 1.73**	**-6.00 ± 1.84**	**1.16 ± 2.13**	**-2.25 ± 6.13**
min	2.54 ± 1.91	-6.08 ± 1.83	-0.01 ± 2.00	-3.34 ± 6.49
max	4.52 ± 1.60	-5.88 ± 1.87	2.90 ± 2.54	-0.49 ± 5.85
ROM	1.98 ± 1.29	0.20 ± 0.12	2.91 ± 2.18	2.85 ± 1.84

Table 2-4. Mean differences ± standard error between experimental data (EOS) and moving-axis model, EOS and hinge model, and moving-axis and hinge models for quasi-static lunge conditions. Average (± SD) are calculated for each clinical measure. *denotes that the clinical measure was statistically significantly different for the given lunge condition.

	Translations (mm)			Rotations (°)	
	ML	**AP**	**CD**	**AA**	**IE**
EOS - Moving-Axis Model					
20 Flexion	-2.43 ± 0.35*	6.19 ± 0.73*	0.96 ± 0.32	0.75 ± 0.40	1.94 ± 0.88
45 Flexion	-2.31 ± 0.44*	7.79 ± 1.02*	-0.11 ± 0.26	0.66 ± 0.48	1.95 ± 1.10
60 Flexion	-1.21 ± 0.43	5.53 ± 0.86*	-0.74 ± 0.20	0.35 ± 0.41	1.80 ± 0.97
Average	**-1.98 ± 0.37**	**6.50 ± 0.82**	**0.05 ± 0.20**	**0.59 ± 0.36**	**1.90 ± 0.79**
EOS - Hinge Model					
20 Flexion	-1.20 ± 0.35	6.57 ± 0.51*	0.90 ± 0.60	-1.66 ± 0.84	9.92 ± 1.40*
45 Flexion	-0.99 ± 0.61	10.82 ± 1.09*	0.78 ± 0.67	-3.46 ± 0.93	11.84 ± 1.59*
60 Flexion	-0.32 ± 0.47	12.93 ± 1.36*	0.29 ± 0.68	-4.40 ± 0.97*	13.03 ± 2.15*
Average	**-0.84 ± 0.45**	**10.11 ± 0.88**	**0.66 ± 0.62**	**-3.17 ± 0.86**	**11.60 ± 1.51**
Moving-Axis Model – Hinge Model					
20 Flexion	1.23 ± 0.37	0.38 ± 0.83	-0.08 ± 0.63	-2.41 ± 0.72	7.98 ± 1.14*
45 Flexion	1.32 ± 0.50	3.03 ± 1.13	0.88 ± 0.84	-4.11 ± 0.87*	9.90 ± 1.09*
60 Flexion	0.88 ± 0.57	7.40 ± 1.59*	1.03 ± 0.78	-4.75 ± 0.93*	11.23 ± 1.58*
Average	**1.14 ± 0.47**	**3.60 ± 1.06**	**0.61 ± 0.74**	**-3.76 ± 0.82**	**9.70 ± 1.10**

Table 2-5. Model predictive capabilities: Coefficient of determination (R2) and adjusted R2 values calculated from model (hinge and moving-axis) and experimental data (EOS) for quasi-static 20-60 lunge angles combined.

	Model	Translations (mm)			Rotations (^{0})	
		ML	**AP**	***CD***	**AA**	***IE***
R^2	MA	0.31	0.71	0.91	0.79	0.67
	Hinge	0.26	0.21	0.70	0.08	0.27
Adj. R^2	MA	0.29	0.70	0.90	0.78	0.65
	Hinge	0.23	0.18	0.68	0.05	0.25

When comparing the models themselves, significant differences more often arise in the rotational measures than translations. The AP translation significantly differs in the hinge joint model (MD ± SE: 7.40 ± 1.59^0) compared to the moving-axis model in deeper tibiofemoral flexion (60^0 lunge). While the AA and IE rotations significantly differ in the hinge model (average MD ± SE: -3.76 ± 0.82^0 and 9.70 ± 1.10^0) when compared to the moving-axis model for all lunge conditions except AA rotation at 20^0 tibiofemoral flexion.

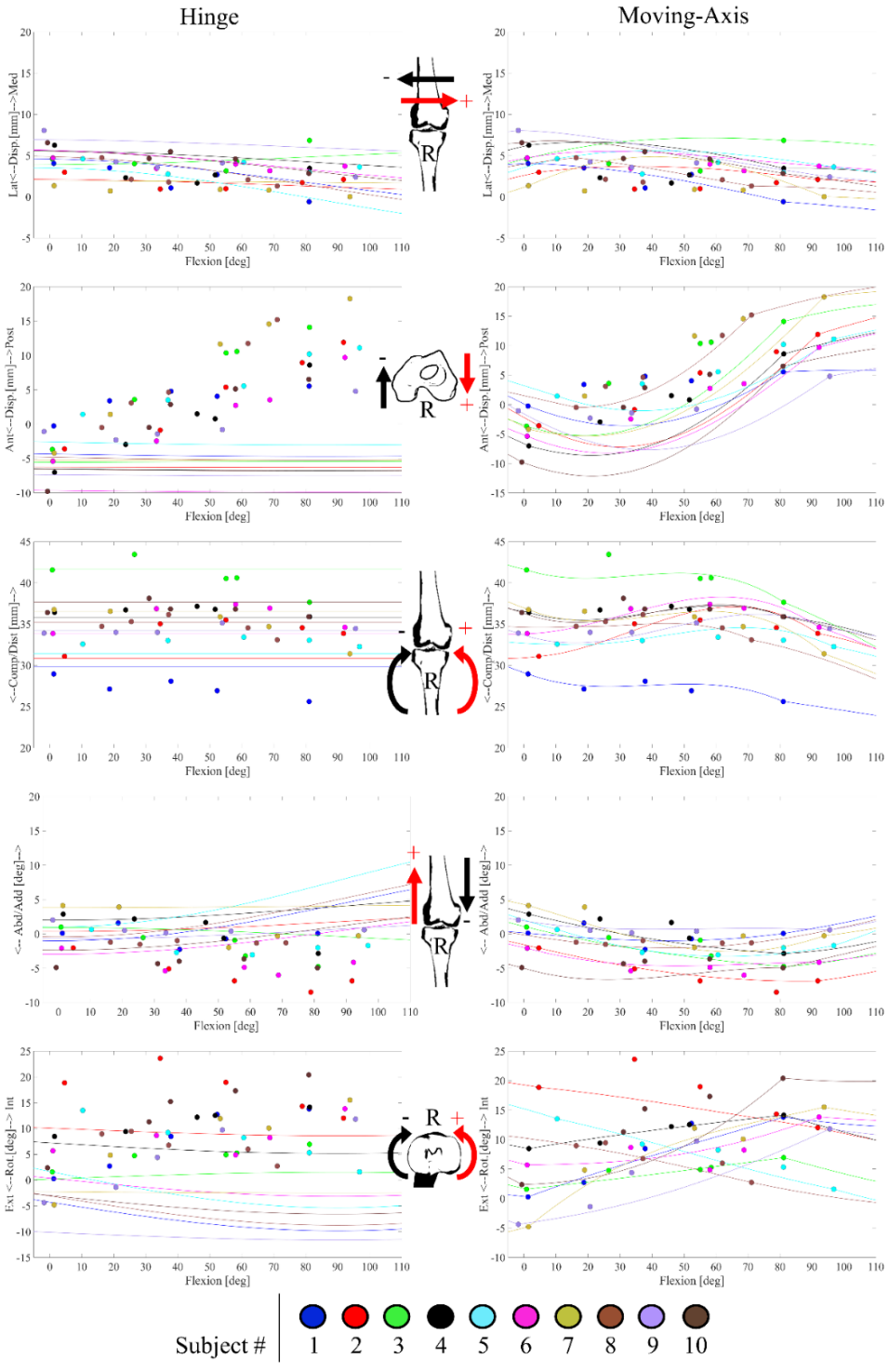
Hinge
Moving-Axis
Lat<--Disp.[mm]-->Med
Ant<--Disp.[mm]-->Post
<--Comp/Dist [mm]-->
<-- Abd/Add [deg]-->
Ext <--Rot.[deg]--> Int
Flexion [deg]
R
Subject #
1 2 3 4 5 6 7 8 9 10

Figure 2-5. Secondary joint kinematic data for hinge and moving-axis models (lines) compared to experimental EOS data (circles) for each subject (n = 10). Clinical translations (ML: medial/lateral displacement, AP: anterior/posterior displacement, and CD: compression/distraction) are measured from femur origin relative to tibia. Rotations are measured in the order FE: flexion/extension, AA: abduction/adduction and IE: internal/external rotation from the femoral to the tibial coordinate system.

2.4 DISCUSSION

In this study, we introduced a novel moving-axis tibiofemoral model and validated it against experimental EOS data. Our results showed that the moving-axis tibiofemoral model better represents the in vivo secondary kinematics during a quasi-static lunge as compared to a hinge model. The in vivo EOS data we recorded agrees with healthy tibiofemoral kinematics found in the literature (Al Hares et al., 2015; Dennis et al., 2005; Hamai et al., 2013; Komistek and Dennis, 2003; Qi et al., 2013; Yue et al., 2011; Zeighami et al., 2017), and furthermore the resulting secondary joint kinematics from the moving-axis model better captures these literature trends. The moving-axis model seems to overestimate the tibiofemoral joint medial-lateral displacement, but by about 2 mm. While the hinge model underestimates joint dislocation due to its 1 DOF nature.

In another EOS study (Zeighami et al., 2017), subjects performed a quasi-static lunge from 0 to 70^0 flexion. The secondary joint kinematics of healthy subjects consisted of a 1.7 ± 2.5 mm femur medial displacement until 15^0 flexion, afterwards the femur moved laterally 2.3 ± 1.4 mm. Researchers found an AP of 9.6 ± 4. 8 mm, IE of 11.8 ± 5.5^0, and AA of 2.4 ± 2.8^0 which agrees nicely with our findings. A bi-planar fluoroscopy study (Yue et al., 2011) found that healthy subjects exhibited AP of 18.1 ± 2.5 mm, for flexion up until 105^0, with a consistent medially positioned femur relative to tibia. The study also documented IE of 10.8 ± 4.6^0 and AA of 3 ± 2^0, also corresponding well with our findings. While a similar biplanar fluoroscopy study of a single legged lunge showed AP:11.5 ± 4 mm, ML: 2.5 ± 2.5 mm, AA: 2.75 ± 1.5^0, and IE: 6 ± 6^0 movement from full extension to 90 tibiofemoral flexion (Qi et al., 2013). In single plane fluoroscopy studies recording tibiofemoral flexion from 0-90 to 0-140, researchers have found an AP ranging from roughly 10 ± 5 mm to 21.07 ± 9.30 mm (Dennis et al., 2005; Komistek and Dennis, 2003; Moro-oka et al., 2008) and an IE ranging from 16.8 ± 9.5^0 to 23.9 ± 6^0 (Dennis et al., 2005; Komistek and Dennis, 2003; Moro-oka et al., 2008; Tanifuji et al., 2011).

Why does the research community need another simple subject-specific tibiofemoral model? It has been shown, when using multibody optimization (Lu and O'Connor, 1999) secondary joint kinematics can be improved by employing more advanced (compared to hinge) and subject-specific tibiofemoral models (Clément et al., 2015). The moving-axis tibiofemoral model is simply calibrated from two poses, which avoids having to obtain full range of motion data which is required in models using coupling constraints. In addition, no additional tuning is required to run the moving-

axis model, which is often needed to avoid singularities in parallel mechanism or sphere-on-plane models (Brito da Luz et al., 2017; Habachi et al., 2015). The moving-axis tibiofemoral model has its limitations. Specifically, the kinematics will remain the same independent of external load, which for some applications may play a role. Complex multibody contact models (Guess et al., 2014; Marra et al., 2017, 2015; Smith et al., 2017; Thelen et al., 2014) have been established to avoid these limitations, however these models are much more computationally expensive and have therefore been applied on small cohorts.

Although large improvements were achieved by modeling the TF joint on a moving-axis, creating a linear relationship between EFC and FFC axes may not be capturing the entire trend. The moving-axis model presented in this study is calibrated off two poses (0-degree and 90-degree). Conceivably, an infinite number of poses could be used to calibrate this model; however, this will increase the radiation the subject is exposed to and eliminate the EOS means of validation. Additionally, we did not use a positioning jig to keep quasi-static flexion angles consistent amongst subjects. Although the original goal of this study was to obtain two extreme angles to drive the moving-axis model and three intermediate angles to show how well the model performs; it would have been beneficial to ensure lunge consistency to more effectively compare secondary joint kinematics between subjects. Furthermore, the images were captured quasi-statically for one movement type so the results cannot be generalized to other activities.

In conclusion, we have developed a new approach in constructing the tibiofemoral joint in musculoskeletal modeling. This method allows for a computational fast model with subject-specific geometries and kinematics. The results indicate that a piecewise linear model constructed from two active tibiofemoral positions, acquired from EOS imaging technology, can accurately represent secondary kinematics. Furthermore, the moving-axis joint can better predict the experimentally observed rotations tibiofemoral joint rotations when compared to the commonly used subject-specific hinge model.

2.5 SUPPLEMENTARY MATERIALS

SUPPLEMENTARY TABLE. Post hoc pairwise comparisons for 15 one-way repeated measures ANOVAs (five clinical measures at three lunge angle conditions) with Bonferroni adjustments due to multiple comparisons ($\alpha = 0.01$). Results include: mean differences (model I-J), standard error, p-value, and confidence intervals.

Clinical Measure	Lunge Angle (°)	(I) model	(J) model	Mean Difference (I-J)	Std. Error	p-value	Confidence Interval	
							Lower Bound	*Upper Bound*
Medial-Lateral Displacement (*mm*)	20	EOS	MA	-2.425	0.352	***0.000***	-3.817	-1.034
		EOS	Hinge	-1.201	0.354	0.024	-2.600	0.199
		MA	Hinge	1.225	0.369	0.027	-0.236	2.686

		EOS	MA	-2.311	0.438	***0.002***	-4.044	-0.578
	45	EOS	Hinge	-0.991	0.610	0.416	-3.404	1.421
		MA	Hinge	1.320	0.497	0.079	-0.647	3.286
		EOS	MA	-1.206	0.429	0.061	-2.900	0.489
	60	EOS	Hinge	-0.324	0.472	1.000	-2.190	1.541
		MA	Hinge	0.881	0.570	0.470	-1.373	3.136
		EOS	MA	6.189	0.729	***0.000***	3.308	9.071
	20	EOS	Hinge	6.57	0.508	***0.000***	4.560	8.580
		MA	Hinge	0.381	0.831	1.000	-2.906	3.668
		EOS	MA	7.792	1.016	***0.000***	3.775	11.809
Anterior-Posterior Displacement (*mm*)	45	EOS	Hinge	10.817	1.085	***0.000***	6.525	15.108
		MA	Hinge	3.025	1.127	0.075	-1.433	7.482
		EOS	MA	5.53	0.855	***0.000***	2.148	8.912
	60	EOS	Hinge	12.93	1.362	***0.000***	7.545	18.314
		MA	Hinge	7.4	1.588	***0.004***	1.122	13.677
		EOS	MA	0.985	0.317	0.038	-0.268	2.238
	20	EOS	Hinge	0.903	0.604	0.507	-1.485	3.292
		MA	Hinge	-0.081	0.625	1.000	-2.552	2.389
		EOS	MA	-0.105	0.259	1.000	-1.130	0.920
Superior-Inferior Displacement (*mm*)	45	EOS	Hinge	0.778	0.672	0.831	-1.879	3.434
		MA	Hinge	0.883	0.843	0.967	-2.450	4.216
		EOS	MA	-0.738	0.203	0.016	-1.539	0.064
	60	EOS	Hinge	0.293	0.678	1.000	-2.389	2.975
		MA	Hinge	1.031	0.777	0.652	-2.041	4.103
		EOS	MA	0.750	0.396	0.273	-0.817	2.317
	20	EOS	Hinge	-1.664	0.841	0.238	-4.991	1.663
		MA	Hinge	-2.414	0.719	0.025	-5.256	0.428
		EOS	MA	0.656	0.475	0.601	-1.222	2.534
Abduction-Adduction Rotation (^{g})	45	EOS	Hinge	-3.455	0.925	0.014	-7.112	0.201
		MA	Hinge	-4.111	0.870	***0.003***	-7.550	-0.673
		EOS	MA	0.349	0.406	1.000	-1.256	1.954
	60	EOS	Hinge	-4.4	0.968	***0.004***	-8.227	-0.573
		MA	Hinge	-4.749	0.934	***0.002***	-8.441	-1.056
		EOS	MA	1.939	0.879	0.164	-1.536	5.415
	20	EOS	Hinge	9.916	1.403	***0.000***	4.368	15.463
		MA	Hinge	7.976	1.137	***0.000***	3.480	12.472
		EOS	MA	1.945	1.097	0.330	-2.392	6.283
Internal-External Rotation (^{g})	45	EOS	Hinge	11.841	1.590	***0.000***	5.554	18.129
		MA	Hinge	9.896	1.086	***0.000***	5.603	14.189
		EOS	MA	1.801	0.971	0.290	-2.038	5.639
	60	EOS	Hinge	13.029	2.154	***0.001***	4.511	21.546
		MA	Hinge	11.228	1.576	***0.000***	4.998	17.458

CHAPTER 3. PAPER II

Evaluation of predicted patellofemoral joint kinematics with a moving-axis joint model

Dzialo, C.M., Pedersen, P.H., Krogh, K., de Zee, M., Andersen, M.S.

Submitted to Medical Engineering and Physics

CHAPTER 4. PAPER III

Workflow assessing the effect of gait alterations on stresses in the medial tibial cartilage – combined musculoskeletal modelling and finite element analysis

K. S. Halonen, C. M. Dzialo, M. Mannisi, M. S. Venäläinen, M. de Zee & M. S. Andersen. *Scientific Reports 7, Article number: 17396 (2017). https://doi.org/10.1038/s41598-017-17228-x*

SCIENTIFIC REPORTS

Workflow assessing the effect of gait alterations on stresses in the medial tibial cartilage - combined musculoskeletal modelling and finite element analysis

K. S. Halonen[1], C. M. Dzialo[2], M. Mannisi[3], M. S. Venäläinen[4], M. de Zee[1] & M. S. Andersen[2]

Knee osteoarthritis (KOA) is most common in the medial tibial compartment. We present a novel method to study the effect of gait modifications and lateral wedge insoles (LWIs) on the stresses in the medial tibial cartilage by combining musculoskeletal (MS) modelling with finite element (FE) analysis. Subject's gait was recorded in a gait laboratory, walking normally, with 5° and 10° LWIs, toes inward ('Toe in'), and toes outward ('Toe out wide'). A full lower extremity MRI and a detailed knee MRI were taken. Bones and most soft tissues were segmented from images, and the generic bone architecture of the MS model was morphed into the segmented bones. The output forces from the MS model were then used as an input in the FE model of the subject's knee. During stance, LWIs failed to reduce medial peak pressures apart from Insole 10° during the second peak. Toe in reduced peak pressures by −11% during the first peak but increased them by 12% during the second. Toe out wide reduced peak pressures by −15% during the first and increased them by 7% during the second. The results show that the work flow can assess the effect of interventions on an individual level. In the future, this method can be applied to patients with KOA.

With an incidence of 240 per 100 000 person-years[1], knee osteoarthritis (KOA) is one of the largest burdens to healthcare. It is estimated that over half of adults in the US diagnosed with KOA undergo total knee replacement surgery[2]. Invasive treatment options such as osteochondral graft transplantation and total knee arthroplasty are costly procedures that are resorted to when non-invasive options such as non-pharmacological or pharmacological therapy have already been exhausted[3,4]. Currently, repairing the degenerated articular cartilage is not deemed possible, which is why alternative ways to preserve the cartilage are sought.

Knee osteoarthritis (KOA) has been shown to develop most often in the medial tibial plateau[5–7]. As excessive loading is believed to be a major contributor to the development and progression of KOA, several methods to reduce loading in the medial tibial plateau have been proposed. Gait modifications, such as toe in, toe out wide, medial knees, wide stance, and trunk sway are non-invasive techniques aimed to reduce the adduction moment in the knee, resulting in decreased medial tibial plateau loads[8–10]. However, studies have showed that a reduction in knee adduction moment (KAM) does not directly reduce stresses in medial tibial compartment[11,12]. Walter *et al.*[11] speculate that the focus of KAM might not give a complete picture of medial knee loading. Lateral wedge insoles (LWIs) introduce a wedge in the hopes of shifting the weight from medial tibial compartment to the lateral side. The effect of lateral wedge insoles is debatable. Some studies showed a 5–7% reduction in knee adduction moment[13–15], while a meta-analysis concluded that despite a statistically significant association between the use of

[1]Department of Health Science and Technology, Aalborg University, Fredrik Bajers Vej 7D, DK-9220, Aalborg, Denmark. [2]Department of Mechanical and Manufacturing Engineering, Aalborg University, Fibigerstræde 16, DK-9220, Aalborg, Denmark. [3]School of Health and Life Science, Glasgow Caledonian University, Cowcaddens Rd, G4 0BA, Glasgow, United Kingdom. [4]Department of Applied Physics, University of Eastern Finland, POB 1627, FI-70211, Kuopio, Finland. M. Mannisi, M. S. Venäläinen and M. de Zee contributed equally to this work. Correspondence and requests for materials should be addressed to K.S.H. (email: ksh@hst.aau.dk)

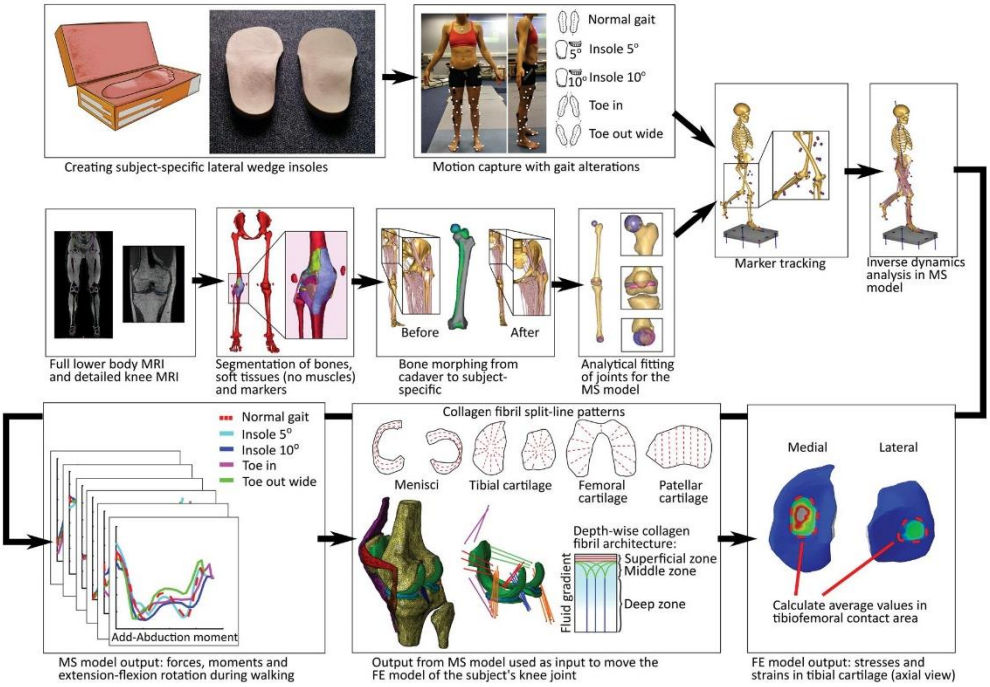

Figure 1. Study workflow.

insoles and reduced pain in medial KOA, the findings did not support the use of LWIs as a conservative treatment option[16].

Direct measurement of stresses in the subject's knee is not ethically viable, therefore computational modelling, such as *musculoskeletal* (MS), *finite element* (FE) or discrete element (DE)[17] modelling are needed. MS models are used to investigate how the human body internally reacts to external forces and movements by providing methods to quantify forces in muscles, ligaments, and joint contact while avoiding invasive procedures. KOA patients tend to adjust their gait to alleviate pain and, in turn, alter their lower limb kinematics, kinetics, and muscle activities[18]. Since KOA patients deviate from the generalized MS model, there is a great need for individualization with regard to gait and patient's anatomy. The Twente Lower Extremity Model 2.0 (TLEM 2.0) was implemented in the MS software package the AnyBody Modeling System (AMS) to use in combination with novel image-based morphing techniques[19]. In order for a MS model to obtain subject-specific architecture, geometric morphing techniques are applied to the TLEM 2.0 cadaver-based model to scale the bones, joints, and muscle attachments relative to the subject. Advancements in these techniques are explained in greater detail in the literature[20–24]. MS models have shown their potential at studying gait modification techniques to find the best modification for the individual[25–32].

While MS models can estimate cartilage pressure patterns, they do not provide detailed information about the inner stresses, changes in fluid pressures, or fibril strains of cartilage. For that purpose, finite element analysis (FEA) is needed. In FEA, tissues are divided into small ('*finite*'), discrete elements that are then assigned specific material properties, respective to the tissues they describe. Material models of the cartilage have been developed and validated against experimental results in laboratory conditions[33–35]. By implementing the forces, moments, rotations and/or translations provided by MS models as boundary conditions, FEA enables the non-invasive estimation of stresses and strains present in the cartilage during daily activities, such as gait[36].

A multiscale model combining the use of subject-specific MS modelling and FEA of the subject's knee joint, reflecting bones, menisci, ligaments, and tendons has yet to be created. Studies that have combined MS and FEA have either excluded patient-specific muscle attachments[37–40], are done with cadavers only[40], have not used subject-specific MS output data[9,38,17], or have excluded soft tissue structures[41].

The present study presents a method that allows scientists to simultaneously estimate net joint loads (resulting from subject-specific knee joint kinematics, external loads and ligament/muscle forces) and stresses in soft tissues of the knee during normal and modified gait. We postulated that promising techniques, such as the toe-in modification, would reduce forces in the medial compartment of the knee and furthermore reduce stresses in the medial tibial cartilage.

Methods

Workflow of the study is presented in Fig. 1.

Experimental data. All experiments were approved by the West of Scotland Research Ethics Service ethical committee of the NHS-Greater Glasgow and Clyde. The study was carried out in accordance with the relevant guidelines and regulations, and an informed consent was obtained from the subject. Impressions of the subject's (27 year-old female, 172 cm, m = 61.2 kg) feet were obtained using Podotech Foot Impression Boxes (A. Algeo Ltd, Liverpool, United Kingdom). The impressions were scanned using Sense 3D Scanner (3D Systems, Rock Hill, SC, US) and transferred to Rhinoceros 3D V5 software (Robert McNeel & Associate, Barcelona, Spain) which was used for designing two sets of LWIs with 5° and 10° inclines. The orthotics were fabricated using an Airwolf 3D HDX 3D printing system (Airwolf 3D printers, Costa Mesa, USA), utilizing a soft polylactide thermoplastic to achieve necessary flexibility for LWI.

Various gait modifications were recorded at the Human Performance Lab of Glasgow Caledonian University (GCU, Glasgow, UK) using Qualisys Oqus (Qualisys Motion Capture System, Gothenburg, Sweden) camera system. 54 reflective skin markers were applied to the subject's lower limbs at key anatomical landmarks to track lower limb motion. In addition, six markers were placed on the pelvis region and six on the torso and head to track upper body motion. A static trial of the subject standing on the force platform (Kistler 9286BA, Kistler Group, Winterhur, Switzerland) was also recorded. The subject walked with self-selected speed having their right foot come in contact with the force plate for each trial. Five trials were completed for each of the following gait styles: Normal walking ('*Normal gait*'), toes turned slightly inward ('*Toe in*'), toes slightly outward and a widened stance ('*Toe out wide*'), walking with 5° lateral wedge insole ('*Insole 5°*'), and with 10° wedge ('*Insole 10°*'). The subject wore neutral walking shoes during all trials. The force data were synchronized with the motion capture trajectories and exported as a C3D files to be utilized by AMS.

The subject's right knee was imaged on a 1.5 T General Electric Discovery MRI scanner using a quad knee coil. A modified Osteoarthritis Initiative (OAI) protocol[42] based on GE scanner recommendations[43] was applied (SAG FSPGR 3D FS and COR SPGR 3D acquisitions, slice thickness = 1 mm) to clearly distinguish between bone, articular cartilage, menisci, and ligament attachment regions. This acquisition series was labeled *Detailed Knee*. Subsequently, the subject's lower extremities were imaged in three parts using a 3 T Siemens Prisma MRI (COR T1W-Vibe-Dixon, slice thickness = 1.4 mm) and Peripheral Angio 36 coil. During the scans, the feet were positioned in 0 degrees dorsiflexion. Prior to the scan, non-magnetic markers were applied to the subject's pelvis and lower limbs at key anatomical landmarks coinciding with the motion capture marker locations. These three acquisitions were then stitched together by the radiologist using custom Siemens software and exported as Digital Imaging and Communications in Medicine (DICOM) files. This series of images was labeled *Lower Limbs*.

Musculoskeletal model. The subject-specific MS model was created in the AnyBody Modeling System (AMS v 6.1 beta, AnyBody Technology, Aalborg, Denmark) using the generic human body model, excluding arms, within the AnyBody Managed Model Repository (AMMR) version 1.6. The lower extremities were updated to incorporate the TLEM 2.0 dataset.

Various anatomical structures (bone, articular cartilage, menisci, and ligaments) were required for both MS and FE models. Segmentation of these 3D geometrical surfaces from two stacks (*Detailed Knee* and *Lower Limbs*) of MRI images was completed in Mimics Research 18.0 (Materialise, Leuven, Belgium) and exported as stereolithography files (STLs). The femur, tibia, and patella were segmented from both image series (bilaterally for *Lower Limbs*). While in the *Detailed Knee*, the menisci, articular cartilage, and ligament origin and insertions were additionally segmented. In the *Lower Limbs* series, the non-magnetic markers, pelvis, fibula, talus, and foot bones on both limbs were segmented. Using functions in Mimics' Align toolbox, the STLs from the *Lower Limb* series were registered onto the *Detailed Knee* scan to obtain a common coordinate system (MRI CS).

The hip joint was modelled as a spherical joint and the joint center estimated by fitting a sphere to the articular surface. The talocrural and subtalar joints were modelled as revolute joints and defined by fitting spheres to the articulating surfaces from the *Lower Limb* STLs[44]. Two types of joint models were implemented for the tibiofemoral (TF) and patellofemoral (PF) joints:

1. Hinge joints for both the TF and PF with one degree of freedom each (DOF)[45].
2. Force-dependent kinematics (FDK) model with 11 DOF (6 in the TF joint and 5 DOF in the PF joint)[45].

In both models the patella tendon was assumed rigid and its length estimated from the *Detailed Knee* MRI. For the hinge joint, the TF joint was defined with an origin at the midpoint between the centers of two circles fitted in the sagittal plane of the medial and lateral condylar articular surfaces[24]. A similar process was employed for the PF joint, selecting contact areas from the trochlear articular surface.

The FDK model was defined similarly to[45] with an elastic foundation contact model (with a pressure modulus of 9.3 GNm^{-3}) between the articular cartilages of the femur and tibia for the TF joint and the femur and patella for the PF model, respectively. The ligaments were modelled as nonlinear elastic elements with slack, toe and linear elastic regions. The toe region was set to 3% similar to[45] and the pre-strains and ligament stiffness were defined to be identical to the FEA model (see the section about ligaments below).

Due to its lower computational cost, the hinge knee model was used for two analysis: selecting the most representative gait trials out of a total of 30 trials (Please see supplementary figure A), and investigation of the effect of weakened knee flexion and extensor muscle strength on the predicted knee reaction forces. The evaluation of gait alterations was conducted with the FDK model.

Geometric morphing and scaling. In order to morph the femur, tibia, patella, and talus of each leg and the pelvis, we ensured the subject-specific bones had the same number of vertices as the TLEM bones (*source bones*). This was accomplished by registering a duplicated source bone to the SS bone's coordinate system, which is defined based on the moment of inertia. The shape of vertices of the registered *source bone* were then morphed

using an advanced morphing function developed by Materialise to best represent the geometry of the SS bone[46]. This morphed bone was then labelled as the *target bone* for use in AMS to scale muscle attachment sites[19]. For each bone, a modified interpolation scheme, outlined in Marra *et al.*[45], was followed: First, an affine transformation was performed to roughly scale and register the *source bone* vertices to the respective *target bone* vertices, secondly, a tri-harmonic radial basis function (RBF) interpolation based upon the vertices of the affine-transformed *source bone* and *target bone* was performed, and third, a reverse rigid-body transformation based upon the points of the affine-transformed and RBF scaled points and the unscaled (pre affine transformation) *source bone* to bring the morphed bone back from the MRI CS to the AMS CS. The remaining 25 bones of each TLEM 2.0 foot were morphed as one rigid body using an affine transformation based on 36 anatomical landmarks capturing the shape and size of the subject-specific foot (For details, see Supplementary figure B).

To determine the location of the cluster markers relative to the morphed TLEM 2.0 model, the standing reference trial was used. A nonlinear least-square optimization problem was defined to compute the pose of the model segments based on the non-magnetic MRI markers and the corresponding markers in the motion capture data[47]. Subsequently, the local coordinates of the cluster markers were computed in the TLEM 2.0 bone coordinate systems and saved for later use.

Muscle modelling. The muscles were modelled with a Hill-type muscle model based on the TLEM data set and scaled using a length-mass-fat scaling law[48]. The muscle recruitment problem we solved was a 3rd order polynomial cost function (G) with the muscle volume, v_i, as the normalization factor and subject to the dynamic equilibrium equations and an inequality constraint ensuring that muscles can only pull and not push. Except the addition of the muscle volume normalization factor, the muscle recruitment was formulated as described by Damsgaard[49].

$$\begin{aligned} \underset{\mathbf{f}}{\text{minimize}} \quad & G(\mathbf{f}^{(M)}) = \sum_{i=1}^{n^{(M)}} v_i \left(\frac{f_i^{(M)}}{N_i^{(M)}} \right)^3 \\ \text{subject to} \quad & \mathbf{Cf} = \mathbf{d} \\ & 0 \le \mathbf{f}_i^{(M)}, \quad i = 1, \cdots, n^{(M)} \end{aligned} \tag{1}$$

where $\mathbf{f}^{(M)}$ is a vector consisting of $n^{(M)}$ unknown muscle forces, $\mathbf{C}$ is the coefficient matrix for the dynamic equilibrium equations, $\mathbf{f}$ is made up of all unknown forces in the problem, which depends on whether the knee is modelled as a hinge or with FDK (see the section below). $f_i^{(M)}$ denotes the *i th* muscle force, and $N_i N_i$ is the muscle strength of the *i th* muscle. $\mathbf{d} = [\mathbf{d}_1 T \ldots \mathbf{d}_n] T\, \mathrm{d} = [\mathrm{d}_1 T \ldots \mathrm{d}] T n$contains the external loads and inertia forces:

$$\mathbf{d}_j = \mathbf{g}_j^{(\mathrm{app})} - \begin{bmatrix} m_j \mathbf{I} & \mathbf{0} \\ \mathbf{0} & \mathbf{J}_j' \end{bmatrix} \dot{\mathbf{v}}_j - \begin{bmatrix} \mathbf{0} \\ \tilde{\omega}_j' \mathbf{J}_j' \omega_j' \end{bmatrix} \tag{2}$$

$\mathbf{g}_j^{(app)}$ contain the forces and moments applied around the center of mass of the *j th* segment in body-fixed coordinates. m_j, $\mathbf{J}'j$, $\dot{\mathbf{v}}_j$ and ω_j' are the mass, mass moment of inertia in body-fixed coordinates, and the linear and angular velocity of the *j th* segment. The tilde indicates the skew-symmetric matrix.

Within the TLEM 2.0 data set, muscles are sub-divided to account for wide origin/insertion areas. Without a normalization factor, this sub-division affects the estimated muscle and joint reaction forces as shown by Holmberg and Klarbring[50]. Therefore, a normalization factor based on muscle volume was introduced as similarly done in previous studies[45,51].

Marker kinematics, inverse dynamics, Force-dependent Kinematics and output for FE model. The subject-specific model was run using an inverse kinematic technique[47], tracking the motion capture marker trajectories for each of gait trials. In this process, the TF and PF joints were modelled as hinges. The resulting translation and rotation of pelvis and the joint angles, angular velocities, angular accelerations and the measured ground reaction forces and moments (GRF & Ms) were then used as input for the inverse dynamic analysis or FDK simulations similar to Marra *et al.*[45] depending on whether the hinge or FDK knee model was applied.

In these two cases, the vector of unknown forces, $\mathbf{f}$, and corresponding coefficient matrix, $\mathbf{C}$, in equation (1) were set up differently. When a hinge knee was applied, $\mathbf{f} = [\mathbf{f}^{(M)T} \quad \mathbf{f}^{(R)T}]^T$, where $\mathbf{f}^{(R)}$ are the unknown joint reaction forces. The coefficient matrix $\mathbf{C} = [\mathbf{C}^{(M)}\, \mathbf{C}^{(R)}]$ is made up of the coefficient matrix for the muscles, $\mathbf{C}^{(M)}$, and for the reaction forces $\mathbf{C}^{(R)}$. These coefficient matrices can be determined by the derivative of the origin to insertion length and the joint constraint equations with respect to a set of coordinates that correspond to the linear and angular velocity of the segments as shown by Damsgaard *et al.*[49].

When performing FDK analysis, specific DOFs of the model are identified, where the movement is computed for each time step based on an assumption of quasi-static force equilibrium (see Andersen.. and Marra *et al.*[45]). In the FDK knee model, these are all the DOFs of the knee except TF and PF flexion. All other joint angles and the TF flexion angle obtained from the inverse kinematic analysis and the PF flexion is controlled by an assumption of a rigid patellar tendon. To accomplish this type of analysis, an iterative algorithm is applied to determine the position and orientation at each time step of these FDK DOFs such that static equilibrium along these is obtained. To this end, residual forces along these FDK DOFs are introduced among the unknown forces, $\mathbf{f} = [\mathbf{f}^{(M)\mathrm{T}}\, \mathbf{f}^{(R)\mathrm{T}}\, \mathbf{f}^{(FDK)\mathrm{T}}]^{\mathrm{T}}$ and with coefficient matrix $\mathbf{C} = [\mathbf{C}^{(M)}\, \mathbf{C}^{(R}\, \mathbf{C}^{(FDK)}]$ and the numerical solver searches for the positions of the FDK DOFs until the residual forces are below a specified tolerance of 0.3 N (Nm) similarly to Marra *et al.*[45]. For full details of FDK analysis, we refer the reader to Andersen *et al.*[52].

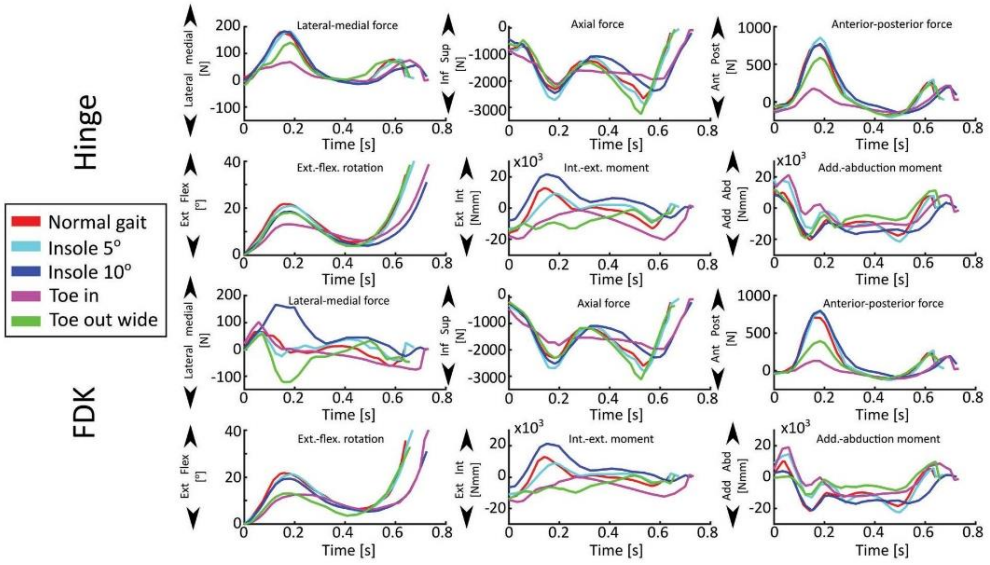

Figure 2. Musculoskeletal model outputs for femur (**top**: Hinge knee model, **bottom**: FDK knee model), used as the input for the finite element model of subject's knee joint. Note: patellar inputs omitted for clarity.

To transfer the TF extension-flexion knee movement and estimated forces and moments affecting on the patella and femur of the MS model to the FEA model, identical reference frames were defined in both models based on the MRI scans. For the right femur, tibia and patella, a coordinate system was defined with the x-axis pointing from the lateral to the medial epicondyle, the y-axis orthogonal to the x-axis and pointing towards the hip joint center and the z-axis the cross product of the two. The origin was located midway between the epicondyles. This coordinate system was transformed to the morphed TLEM2.0 right femur, tibia, and patella bones and moved rigidly with the respective bone. These we denote the *FEA coordinate systems*. The origins of the FEA coordinate systems of femur and patella, we denote the *femoral reference point* and the *patellar reference point*, respectively.

The extension-flexion angle was measured as the first angle (abduction-adduction and internal-external rotation were second and third respectively) in a Cardan angle representation from the femur to the tibia. A free body diagram was set up for the right femur which sums up all forces and moments from the muscle forces, hip joint reaction forces, gravity, and inertia forces but with the reaction forces of the tibiofemoral joint and the patellofemoral joint omitted. The equivalent force and moment of these were computed around the *femoral reference point* but represented in the basis of the tibia *FEA coordinate system* as this is used as the global reference frame in the FEA model as shall be clear later. A similar procedure was applied to compute the equivalent force and moment for patella, where the reaction forces of the patellofemoral joint and the reaction forces in the rigid patellar tendon were excluded. These forces and moments were computed around the *femoral reference point* and given in the basis of the tibia *FEA coordinate system*.

The MS model provided five inputs for the FE model (Fig. 2) of each walking technique (*Normal gait*, *Toe in*, *Toe out wide*, *Medial knees*, *Insole 5°*, and *Insole 10°*), so 30 in total. Out of each technique, three trials with a stance phase time most comparable with normal walking (for this subject, approximately 0.65 s) were selected (*i.e.* total of 18). This was done because slowing the walking pace reduces the impact loads on cartilage, and would, therefore, possibly show artificially decreased stresses in the cartilage. For the same reason, all trials of the medial knees technique had to be excluded due to a 35% longer stance phase compared with normal walking, leaving a total of 15. For the remaining techniques, each with three trials, the trial with the most average trend was selected as the final input for the FE model, resulting in a total of 5 inputs. Please see Supplementary figure B for a plot of internal-external and adduction-abduction moments for all trials.

Finite element model. The soft tissues were segmented from the *Detailed Knee* MRI acquisition, exported as STL files and then transformed into solid geometry form using a custom Matlab R2015b script (Mathworks Inc., Natick, MA, United States). The solid geometries were imported into Abaqus (v. 6.13–3, Dassault Systémes Simulia, Vélizy-Villacoublay, France). Tibial cartilage was kept at the MRI position, while all other tissue geometries were moved respective to tibia, from their MRI positions into the position at the beginning of stance phase. The cartilages and menisci were meshed using 8-node porous elements (element type = C3D8P). The total number of elements for femoral, tibial and patellar cartilages was 7245, 7830 and 3075, respectively. For the lateral and medial meniscus, the number of elements was 8160 and 5250, respectively.

Material properties	Femoral cartilage	Tibial cartilage	Patellar cartilage	Menisci
E_m (MPa)	0.215[33]	0.106[33]	0.505[33]	0.5[89]
ν_m	0.15[34]	0.15[34]	0.15[34]	0.36[89]
E_0 (MPa)	0.92[33]	0.18[33]	1.88[33]	28[89]
E_ε (MPa)	150[33]	23.6[33]	597[33]	—
$k0$ ($\times 10^{15}$m^4/Ns))	6[33]	18[33]	1.9[33]	1.25[90]
M	5.09[33]	15.64[33]	15.93[33]	5.09[33]
η (MPa s)	1062[33]	1062[33]	1062[34]	—
n_f	0.8–0.15$_Z$[91]	0.8–0.15 z[91]	0.8–0.15$_z$[91]	0.72[90]
D	12.16[33]	12.16[33]	12.16[33]	12.16[33]

Table 1. Material parameters implemented for cartilages and menisci. E_m = Non-fibrillar matrix modulus, ν_m = Poisson's ratio, E_0 = initial fibril network modulus, E_ε = strain-dependent fibril network modulus, k_0 = initial permeability, M = exponential term for the strain-dependent permeability, η = damper coefficient, n_f = fluid fraction as a function of the cartilage depth (z), D = ratio of primary collagen fibrils to secondary fibrils.

Material model. A fibril-reinforced poroviscoelastic (FRPVE) material model[33–35], was used for all cartilages and menisci, while bones were defined rigid. In the FRPVE material model, the cartilage is considered a biphasic material consisting of a fluid phase and a solid matrix. The solid matrix consists of a fibrillar part, mimicking the collagen fibril network of articular cartilage, and a Neo-Hookean poro-hyperelastic part, mimicking the proteoglycans, chondrocytes and smaller constituents. The total stress ρ^{tot} is given as

$$\rho^{tot} = \rho^{f} + \rho^{nf} - \mathbf{I}\mathbf{p} \tag{3}$$

where ρ^f is the fibrillar stress, ρ^{nf} non-fibrillar stress, $\mathbf{p}$ fluid pressure and $\mathbf{I}$ unity tensor. Further, the fibrillar stress ρ^f is defined as a sum of stresses in each individual collagen fibril:

$$\rho^{f} = \sum_{i=1}^{N} \rho_i^{f} \tag{4}$$

where ρ_i^f is the stress of one fibril and N the total number of fibrils. The viscoelastic behaviour of collagen fibrils is modelled using a linear spring (spring coefficient E_0) in parallel with a set of a non-linear spring (spring coefficient E_ε) in series with a damper (damping coefficient η). The collagen fibrils consist of primary and secondary fibrils, with their relative density denoted by D. Primary fibrils are oriented parallel to the cartilage surface in the superficial zone, randomly oriented in the middle zone and perpendicular to the surface in the deep zone. In addition, the macro-pattern of primary collagen fibrils in the superficial zone follows the split-line pattern of cartilages[53–55]. The secondary fibrils are randomly oriented. Similarly to the cartilages, the menisci were also modelled as biphasic material using the FRPVE material model. However, in the menisci, the primary collagen fibrils are oriented circumferentially. The full list of material parameters in cartilages and menisci are given in Table 1. For more detailed description of the implementation of the material model, please see these previous studies[56–59].

Ligaments. The ligaments were defined as linear spring elements (SPRINGA). The ligament stiffnesses, defined as spring coefficients, were obtained from Marra *et al.*[45]: anterior cruciate ligament (ACL) 306 Nmm^{-1}, posterior cruciate ligament (PCL) 406 Nmm^{-1}, lateral collateral ligament (LCL) 99 Nmm^{-1}, medial collateral ligament (MCL) 168 Nmm^{-1}, lateral patellofemoral ligament (LPFL) 68 Nmm^{-1}, and medial patellofemoral ligament (MPFL) 49 Nmm^{-1}. Pre-strains for ACL, PCL, MCL, LCL, MPFL, and LPFL, were defined as 3%, 3%, 2%, 3%, 5% and 5%, respectively, by modelling tests from radiographic knee laxity studies[60,61]. The patellar tendon was also defined as a linear spring element with a spring coefficient of 545 Nmm^{-1} without prestrain[62]. No quadriceps tendon was defined as an explicit structure as the forces and moments that were obtained from the MS model account for the forces in the quadriceps.

Contact definitions and boundary conditions. In the FE model, the tibial cartilage was fixed at the cartilage-bone interface. During simulations, all forces, moments and extension-flexion rotation were applied to femur and patella with respect to the tibia *FEA coordinate system*. Surface-to-surface contact was used for all contacting surfaces, the master surface being a surface and the slave surface a node surface. Patellar cartilage was defined as a master to femoral cartilage, femoral cartilage master to tibial cartilage and menisci, and tibial cartilage master to the menisci. Bottom elements of the menisci were subdivided into smaller elements and tied to the upper meniscal elements using a constraint in order to improve convergence in the tibia-meniscus contact.

In the simulations, first the cartilages and menisci were brought into light contact with each other and ligament pre-strains were applied. Next, the forces and moments present at the start of stance phase of gait were applied. Finally, the stance phase of gait was simulated by applying translational forces (anterior-posterior, axial, and medial-lateral), moments (internal-external, varus-valgus) and a rotation (extension-flexion) to the *femoral reference point*. This point was tied to the cartilage-bone-interface of femoral cartilage as well as all the femoral ligament attachments[63]. Similarly, patellar forces and moments were applied through the *patellar reference point*.

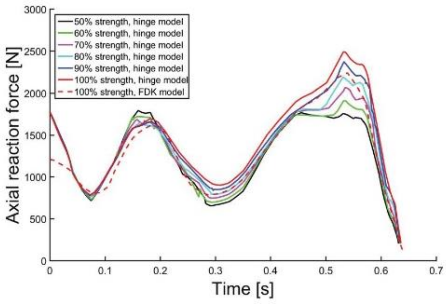

Figure 3. Effect of flexor and extensor strength on tibial reaction forces. Hinge knee (in the MS model) extensor strength scaled from 50% to 100% (normal). Force-dependent kinematics (FDK) model with normal gait in dashed red line.

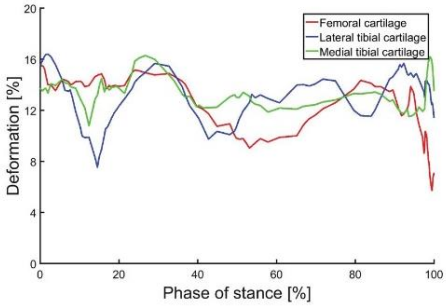

Figure 4. Maximum cartilage deformations during the stance phase of gait, compared with resting cartilage from MRI.

The *patellar reference point* was tied to the cartilage-bone interface of patellar cartilage and was initially located at the same place as *femoral reference point*, up until the application of femoral and patellar forces and moments. During gait, all forces and moments acting on the patella were applied through the *patellar reference point*.

Analysis of results. First, the effect of knee flexor and extensor strength on tibial reaction forces was studied with the hinge MS model. After this, all results were obtained using the FDK knee joint. Peak contact pressures were determined in the tibial cartilage surface. In addition, average contact pressures, maximum principal stresses, maximum principal strains, fibril strains, and fluid pressures were analysed at the tibial cartilage surface. Tibiofemoral contact area was defined by choosing tibial surface nodes with a contact pressure exceeding 0.01 MPa. Additionally, the sum of reaction forces at the bottom of medial and lateral tibial cartilages were calculated.

Results

Knee flexor and extensor muscle strength. When varying the knee flexor and extensor muscle strength in the hinge knee joint model from 100% (normal strength) to 50% (severely weakened), a difference of 720 N was seen during the second axial peak force (Fig. 3). Normal gait with the FDK knee decreased peak reaction forces compared with the hinge model (2239 N vs. 2492 N, respectively).

Cartilage deformation. In the tibiofemoral contact, maximum cartilage deformation (compared with resting cartilage thickness from MRI) for femoral cartilage was 16% during the stance phase of gait (Fig. 4). The maximum medial and tibial cartilage deformations was also 16% and 16%, respectively.

Peak contact pressures. Figure 5 shows the peak contact pressures during the first and second axial peak forces (20% and 80% of stance) during gait. During the first peak, Insole 5° and Insole 10° increased pressures in the medial tibial cartilage by 17% and 14%, respectively (Table 2), while Toe in and Toe out wide reduced them by −11% and −15%, respectively.

During the second axial peak force, Insole 5° increased peak contact pressures by 8%, while Insole 10° reduced them by −11%. Toe in and Toe out wide methods increased peak contact pressures by 12% and 7%, respectively.

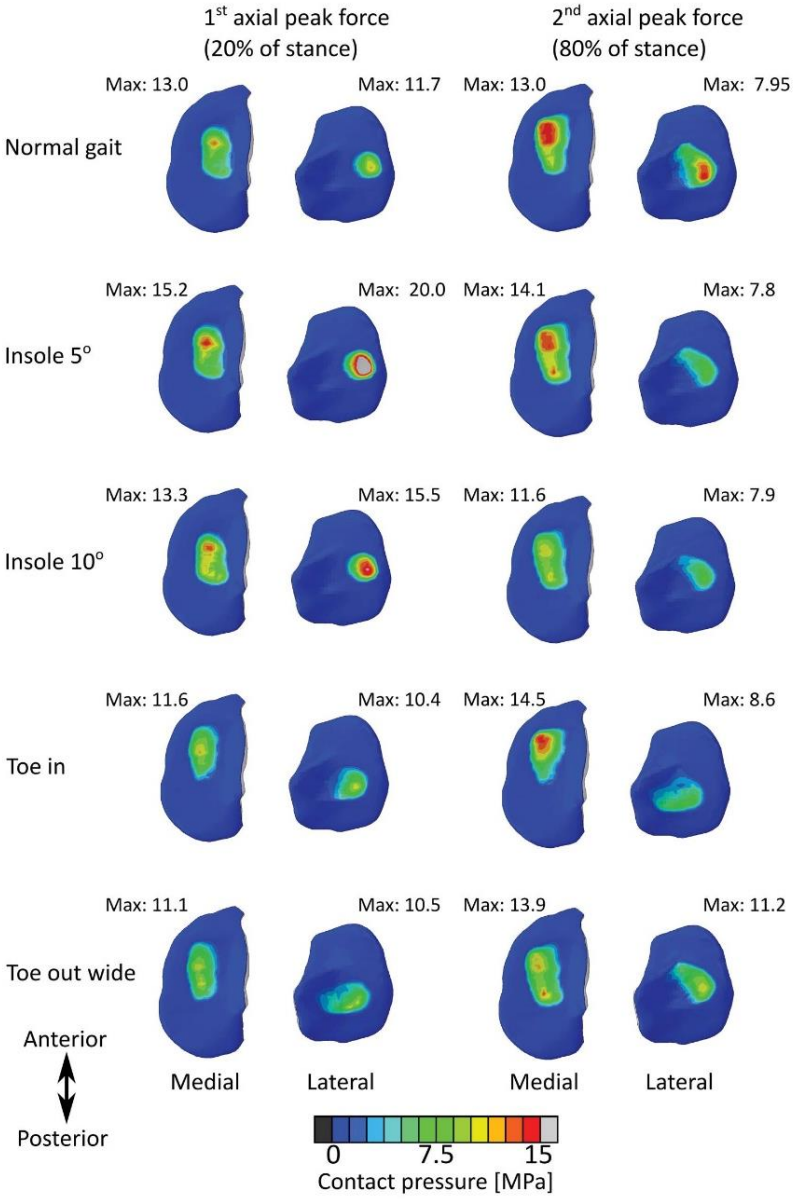

Figure 5. Results of FE analysis: Contact pressures in the tibial cartilage surface during the first and second axial peak forces (20% and 80% of stance). FDK model.

During the first axial peak force, increased lateral peak pressures were observed in Insole 5° and Insole 10° (71% and 33%, respectively). Toe in and Toe out wide decreased lateral peak pressures by −11% and −10%, respectively.

During the second axial peak force, similar lateral contact pressures were seen in Insole 5° and Insole 10° models, compared with the normal gait. Toe in and Toe out wide increased pressures by 8% and 41%, respectively.

Mean stresses and strains. In the medial tibial cartilage, mean contact pressures were elevated in all gait alteration models compared with the normal gait, during both axial peak forces (Fig. 6). Highest medial tibial

	Gait alteration				
	Normal gait	Insole 5°	Insole 10°	Toe in	Toe out wide
1st peak, medial	13.0 MPa	15.2 MPa (+17%)	13.3 MPa (+14%)	11.6 MPa (−11%)	11.1 MPa (−15%)
1st peak, lateral	11.7 MPa	20.0 Mpa (+71%)	15.5 Mpa (+33%)	10.4 Mpa (−11%)	10.5 Mpa (−10%)
2nd peak, medial	13.0 MPa	14.1 MPa (+8%)	11.6 MPa (−11%)	14.5 MPa (+12%)	13.9 MPa (+7%)
2nd peak, lateral	7.95 MPa	7.8 MPa (−2%)	7.9 MPa (−1%)	8.6 MPa (8%)	11.2 MPa (+41%)

Table 2. Peak contact pressures in tibial cartilage surface during first and second peak axial reaction forces of stance, as observed in the FE model.

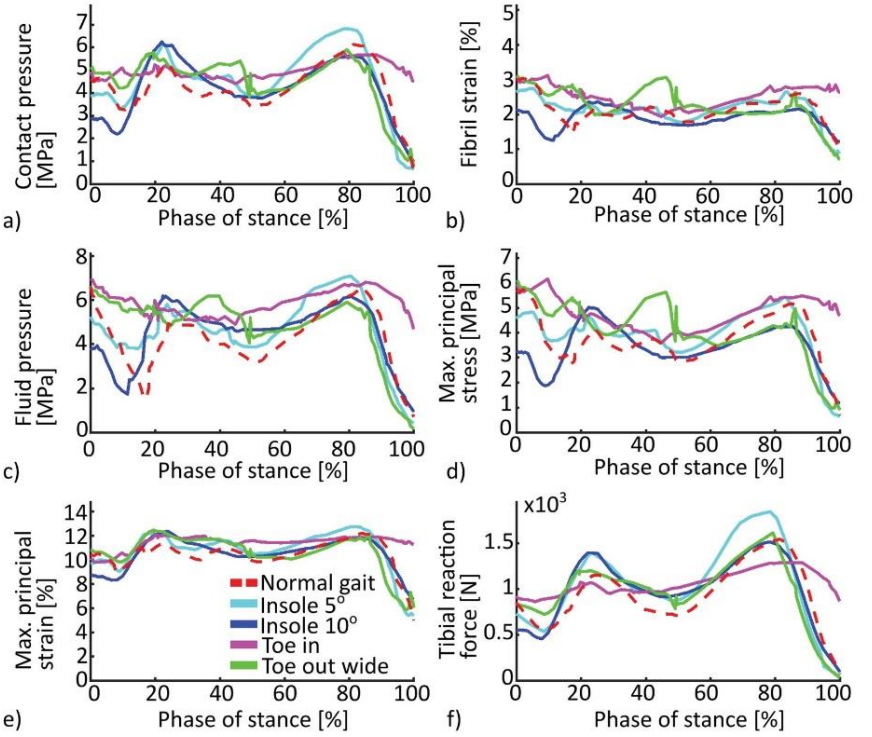

Figure 6. Mean values in the medial tibial cartilage surface **(a)**–**(e)** and summed axial reaction forces in the medial tibial cartilage-bone interface **(f)**.

reaction forces occurred in the Insole 5° and Insole 10° models. All models deviated from the Normal gait model most during the heel strike, especially in fluid pressure. Toe out wide showed an increase in all stresses and strains during midstance.

In the lateral tibial cartilage, Insole 5° and Insole 10° substantially increased mean stresses and strains during the first axial peak force of stance (Fig. 7). Toe in showed a similar trend to normal gait, showing decreased values during the first axial peak.

Discussion

We have combined MS and FE modelling with a highly subject-specific model creation in order to establish a workflow to investigate whether gait alteration techniques reduce medial tibial cartilage stresses and strains on an individual basis. The subject's lower extremities were imaged using a lower-limb MRI and a detailed knee MRI. Subsequently, a bone-morphing technique was applied in order to anatomically scale the generic bone architecture of the MS model to the subject, including muscle attachment sites. A hinge-joint and a FDK joint model were implemented to the knee and the subject's gait trial data were processed into force and moment outputs. Finally, the outputs were used in the FE model to evaluate stresses and strains in the tibial cartilage surface. This method

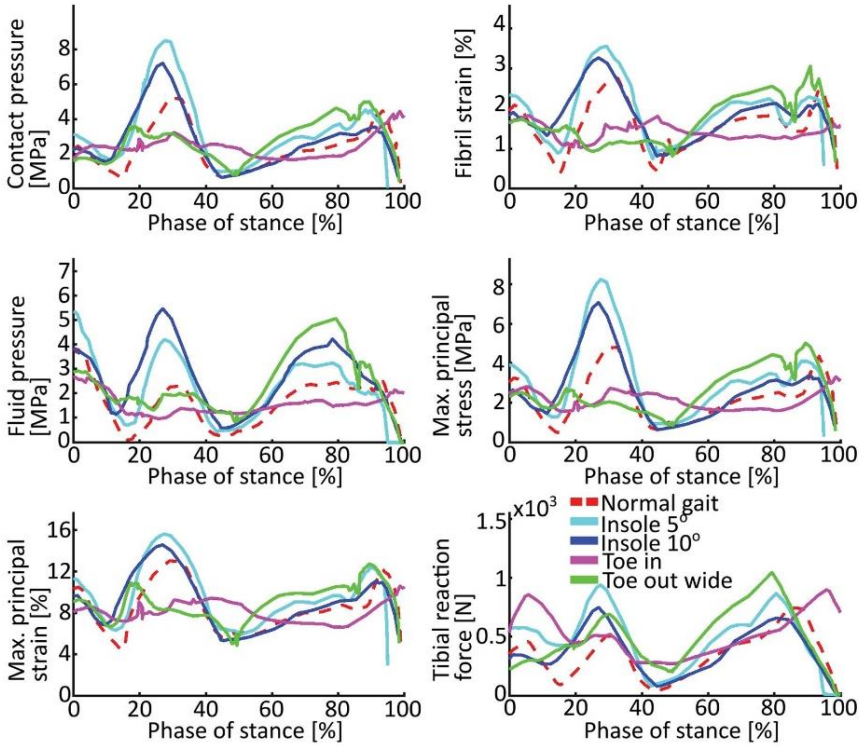

Figure 7. Mean values in the lateral tibial cartilage surface **(a)**–**(e)** and summed axial reaction forces in the lateral tibial cartilage-bone interface **(f)**.

allows non-invasive evaluation of the effectiveness of gait modification techniques in terms of actual stresses in the tibial cartilage, not just the knee adduction moment.

Peak reaction forces of 3.6xBW were observed, which is higher than the 2.5–3.2xBW reported in literature[64–66]. However, we argue that because the contract force data is obtained from TKR joint implants, the forces are lower than those of a healthy person, like the subject of this study. It is known that the quadriceps and hamstring strength of OA patients is weakened[67,68]. When the normal gait was simulated with 50% of the extensor strength, compared with the normal gait, peak reaction forces of 2.8xBW were observed. This falls right into the reported range and supports our argument. Furthermore, the present MS model has shown an RMS error of <0.3 BW for the tibiofemoral contact forces during gait, when tested against *in vivo* measured tibiofemoral joint forces, courtesy of the fifth grand challenge for the 7th World Congress of Biomechanics[45]. The data was gathered from a tibial implant with force-measuring six load components transferred through the prosthesis[12,69,70].

Peak contact pressures of 13 MPa were observed during normal gait, which is in the reported range of 12–15 MPa[71,72]. In addition, the maximum cartilage deformations were within 6–16% of resting cartilage thickness in the tibiofemoral contact, which is in the reported range of deformation during gait[73] and below reported strain threshold of 30% for human chondrocyte apoptosis[74].

Both the Insole 5° and Insole 10° increased peak contact pressures in the lateral side during the first axial peak reaction force, but failed to reduce medial contact pressures. This is likely due to the elevated reaction forces the subject's medial tibia underwent when walking with insoles. This is supported by the fact that during the second axial peak force, when the medial reaction forces were similar in Insole 10° and Normal gait, medial contact pressures did indeed decrease. Furthermore, the peak lateral contact pressures were dangerously high[75] in the Insole 5°. Many studies suggest that LWIs do not reduce KAM[76–78], or medial tibial contact pressures[79]. On the other hand, many studies have reported a significant change in KAM[13–15,80]. Crenshaw *et al.*[80] reported a −7% reduction in KAM, caused by LWI, and suspected the results might depend on the type of insole used. None of the studies above criticizing LWIs mention having used subject-specific, tailored insoles. In the present study, the LWIs used were tailored to the subject using 3D printing technique, yet the results still do not support the use of LWIs for this subject as an intervention.

The MS model predicted reduced axial forces in the medial tibial cartilage for Toe in method, which resulted in decreased medial tibial reaction forces. Toe in reduced KAM during the first peak force, which is in agreement with previous studies[8,81]. However, while the peak medial contact pressures decreased during the first axial peak

force, they actually increased during the second peak. This result is likely due to a change in the size and location of the tibiofemoral contact area. The results suggest that for this subject, the Toe in method might not be optimal.

Toe out wide reduced KAM the most, especially during the second axial peak force, which is in accordance with previous studies suggesting that walking with toes out reduces KAM by up to 40%[82–84]. Previous studies[82–84], indicate that the method has little effect on the first peak force during stance. In this study, the greatest reduction was actually observed during the first peak, while the peak contact pressures were slightly increased during the second peak. For this subject, the Toe out wide method yielded best results out of all methods.

All gait alteration techniques managed to reduce KAM during the stance apart from the second axial peak force, when Insole 5° slightly increased the KAM. The correlation between KAM and mean medial contact pressures varied from 0.25 to 0.80 (see Supplementary figure C), best correlation being in Insole 10° and worst in Toe in method. Normal gait had a correlation of 0.45.

It needs to be noted that the stance phase of Insole 10° and Toe in was approximately 10% longer than in the normal gait, which may have reduced the stresses. For the subject, it was difficult to maintain a consistent walking speed during the gait alterations, which is why we used a criterion of maximum 10% deviation in stance time in the trials. Stance time was chosen instead of walking speed, because the highest forces on the knee occur during the stance phase.

Due to the methodological nature of this study, the largest limitation is the use of only one subject. We want to emphasize that the focus of this study is to establish a method to study the effect of gait alterations, not provide prove or disprove a particular method. Therefore, before establishing any generalized findings, the workflow needs to be applied to extended patient cohorts. For this purpose, several OA patients with medial tibial cartilage wear will be investigated in the future.

Within the MS model, we applied revolute joint models for the tibiofemoral and patellofemoral joints when processing the 30 gait trials as well as the flexor and extensor knee muscle strength testing due to the computational requirements of a full FDK model. As the knee is a complex joint and does demonstrate significant movements besides flexion/extension[85], this will result in some uncertainty in the muscle strength study. It should be noted, however, that we observed only minor differences when comparing the predicted knee contact forces with an FDK-based model and a hinge.

One of the advantages of applying FDK or other similar algorithms to predict secondary joint kinematics (see Brandon *et al.*[86] for a review of methods) is that these are estimated based on joint mechanics and the dynamics of the musculoskeletal system rather than pure kinematic constraint equations. As shown by Marra *et al.*[45] and Lenhart *et al.*[87], these types of models are capable of predicting secondary joint kinematics that generally agree with *in vivo* measurements.

A limitation of all skin marker-based movement analysis is soft tissue artefacts[85]. As shown by Benoit *et al.*[85], only knee extension-flexion can be accurately estimated from the skin markers. Due to the ethical and technical issues of obtaining accurate full lower extremity kinematics, no data set exists which we can use to fully validate the kinematics of our models. However, because the FDK model only relies on the estimated gross joint kinematics and predicts the secondary knee joint kinematics based on the forces, the knee kinematics and kinetics are likely better estimated than if a kinematic constraint-based model was applied. Future studies should investigate this further.

While we have implemented subject-specific geometry based on MRI, subject-specific movements based on skin markers, and subject-specific insoles, there are still parameters in the models that were obtained from literature and for which subject-specific parameters should be included in future studies. First of all, generic ligament parameters were applied in the FEA models due to the lack of experimental setups to estimate the full 3D joint laxities of the tibiofemoral and patellofemoral joints from which the ligament stiffness and slack lengths can be identified. Secondly, due to ethical reasons subject-specific material parameters cannot be currently obtained for the cartilage material model, but from cadaver studies and bovine samples. Thirdly, generic muscle-tendon parameters were applied in the models. Ideally, this should be personalized e.g. based on isometric and isokinetic measurements for instance using optimization-based approaches[88]. While these strength measurements can be performed, there is the issue of whether the subject is producing maximal forces especially in a patient population. Future work should investigate methodologies for obtaining these parameters with as few measurements as possible.

In conclusion, we propose a workflow to investigate the effect of gait alterations on cartilage stresses by combining motion capture, ground reaction forces, MR images, bone morphing, multibody dynamics, and finite element analysis. This method enables subject-specific and non-invasive evaluation of low-cost clinical interventions, aiming to unload the medial tibial cartilage. Currently, creating the models is time-consuming, especially tissue segmentation. In order to bring the method to clinical practice, improvements in automatic tissue segmentation are needed. The cartilage material may in fact be overly complex for the present study, but its features are required when implementing the method to KOA patients in order to simulate changes in the structure of OA cartilage. The presented workflow provides groundwork to develop patient-specific models and optimised treatments on a more individualised basis.

References

1. Bijlsma, J. W. J., Berenbaum, F. & Lafeber, F. P. J. G. Osteoarthritis: An update with relevance for clinical practice. *Lancet* **377**, 2115–2126 (2011).
2. Weinstein, A. M. *et al.* Estimating the burden of total knee replacement in the United States. *J. Bone Joint Surg. Am.* **95**, 385–92 (2013).
3. Murawski, C. D. & Kennedy, J. G. Operative treatment of osteochondral lesions of the talus. *J. Bone Joint Surg. Am.* **95**, 1045–1054 (2013).
4. Bruyère, O. *et al.* An algorithm recommendation for the management of knee osteoarthritis in Europe and internationally: A report from a task force of the European Society for Clinical and Economic Aspects of Osteoporosis and Osteoarthritis (ESCEO). *Semin. Arthritis Rheum.* **44**, 253–263 (2014).

5. Bruns, J., Volkmer, M. & Luessenhop, S. Pressure distribution at the knee joint. Influence of varus and valgus deviation without and with ligament dissection. *Arch. Orthop. Trauma Surg.* **113**, 12–19 (1993).
6. Eckstein, F. *et al.* Trajectory of cartilage loss within 4 years of knee replacement–a nested case-control study from the osteoarthritis initiative. *Osteoarthritis Cartilage* **22**, 1542–1549 (2014).
7. Mills, K., Hunt, M. A. & Ferber, R. Biomechanical deviations during level walking associated with knee osteoarthritis: A systematic review and meta-analysis. *Arthritis Care Res* **65**, 1643–1665 (2013).
8. Shull, P. B. *et al.* Toe-in gait reduces the first peak knee adduction moment in patients with medial compartment knee osteoarthritis. *J. Biomech.* **46**, 122–128 (2013).
9. Ardestani, M. M., Moazen, M. & Jin, Z. Gait modification and optimization using neural network-genetic algorithm approach: Application to knee rehabilitation. *Expert Syst. Appl.* **41**, 7466–7477 (2014).
10. van den Noort, J. C., Schaffers, I., Snijders, J. & Harlaar, J. The effectiveness of voluntary modifications of gait pattern to reduce the knee adduction moment. *Human Movement Sci.* **32**, 412–424 (2013).
11. Walter, J. P., D'Lima, D. D., Colwell, C. W. & Fregly, B. J. Decreased knee adduction moment does not guarantee decreased medial contact force during gait. *J. Orthop. Res.* **28**, 1348–1354 (2010).
12. Kirking, B., Krevolin, J., Townsend, C., Colwell, C. W. & D'Lima, D. D. A multiaxial force-sensing implantable tibial prosthesis. *J. Biomech.* **39**, 1744–1751 (2006).
13. Kakihana, W. *et al.* Effects of laterally wedged insoles on knee and subtalar joint moments. *Arch. Phys. Med. Rehabil.* **86**, 1465–1471 (2005).
14. Hinman, R. S., Bowles, K. A., Metcalf, B. B., Wrigley, T. V. & Bennell, K. L. Lateral wedge insoles for medial knee osteoarthritis: Effects on lower limb frontal plane biomechanics. *Clin. Biomech.* **27**, 27–33 (2012).
15. Butler, R. J., Marchesi, S., Royer, T. & Davis, I. S. The effect of a subject-specific amount of lateral wedge on knee. *J. Orthop. Res.* **25**, 1121–1127 (2007).
16. Parkes, M. J. *et al.* Lateral wedge insoles as a conservative treatment for pain in patients with medial knee osteoarthritis: a meta-analysis. *JAMA* **310**, 722–730 (2013).
17. Guess, T. M., Thiagarajan, G., Kia, M. & Mishra, M. A subject specific multibody model of the knee with menisci. *Med. Eng. Phys.* **32**, 505–515 (2010).
18. Heiden, T. L., Lloyd, D. G. & Ackland, T. R. Knee joint kinematics, kinetics and muscle co-contraction in knee osteoarthritis patient gait. *Clin. Biomech.* **24**, 833–841 (2009).
19. Carbone, V. *et al.* TLEM 2.0 – A comprehensive musculoskeletal geometry dataset for subject-specific modeling of lower extremity. *J. Biomech.* **48**, 734–741 (2015).
20. Reinbolt, J. A. *et al.* Determination of patient-specific multi-joint kinematic models through two-level optimization. *J. Biomech.* **38**, 621–626 (2005).
21. Andersen, M. S. M., Damsgaard, M., MacWilliams, B. & Rasmussen, J. A computationally efficient optimisation-based method for parameter identification of kinematically determinate and over-determinate biomechanical systems. *Comput. Methods Biomech. Biomed. Eng.* **13**, 171–183 (2010).
22. Pellikaan, P. *et al.* Evaluation of a morphing based method to estimate muscle attachment sites of the lower extremity. *J. Biomech.* **47**, 1144–1150 (2014).
23. Lund, M. E., Andersen, M. S., de Zee, M. & Rasmussen, J. Scaling of musculoskeletal models from static and dynamic trials. *Int. Biomech.* **2**, 1–11 (2015).
24. Dzialo, C. M. *et al.* A subject-specific analysis framework to investigate gait alterations. *OA Cartilage* **24**, 126 (2016).
25. Anderson, F. C. & Pandy, M. G. Dynamic optimization of human walking. *J. Biomech.* **123**, 381–390 (2001).
26. Ackermann, M. & van den Bogert, A. J. Optimality principles for model-based prediction of human gait. *J. Biomech.* **43**, 1055–1060 (2010).
27. Barrios, J. A., Crossley, K. M. & Davis, I. S. Gait retraining to reduce the knee adduction moment through real-time visual feedback of dynamic knee alignment. *J. Biomech.* **43**, 2208–2213 (2010).
28. Fregly, B. J., Reinbolt, J. A., Rooney, K. L., Mitchell, K. H. & Chmielewski, T. L. Design of patient-specific gait modifications for knee osteoarthritis rehabilitation. *IEEE Trans. Biomed. Eng.* **54**, 1687–1695 (2007).
29. Fregly, B. J., D'Lima, D. D. & Colwell, C. W. Effective gait patterns for offloading the medial compartment of the knee. *J. Orthop. Res.* **27**, 1016–1021 (2009).
30. Mündermann, A., Asay, J. L., Mündermann, L. & Andriacchi, T. P. Implications of increased medio-lateral trunk sway for ambulatory mechanics. *J. Biomech.* **41**, 165–170 (2008).
31. Hunt, M. *et al.* Lateral trunk lean explains variation in dynamic knee joint load in patients with medial compartment knee osteoarthritis. *Osteoarthritis Cartilage* **16**, 591–599 (2008).
32. Willson, J., Torry, M. R., Decker, M. J., Kernozek, T. & Steadman, J. R. Effects of walking poles on lower extremity gait mechanics. *Med. Sci. Sports Exerc.* **33**, 142–147 (2001).
33. Julkunen, P., Kiviranta, P., Wilson, W., Jurvelin, J. S. & Korhonen, R. K. Characterization of articular cartilage by combining microscopic analysis with a fibril-reinforced finite-element model. *J. Biomech.* **40**, 1862–1870 (2007).
34. Wilson, W., van Donkelaar, C., van Rietbergen, B., Ito, K. & Huiskes, R. Stresses in the local collagen network of articular cartilage: a poroviscoelastic fibril-reinforced finite element study. *J. Biomech.* **37**, 357–366 (2004).
35. Wilson, W., van Donkelaar, C., van Rietbergen, B., Ito, K. & Huiskes, R. Erratum to "Stresses in the local collagen network of articular cartilage: a poroviscoelastic fibril-reinforced finite element study" [J. Biomech. 37 (2004) 357–366] and "A fibril-reinforced poroviscoelastic swelling model for articular cartil. *J. Biomech.* **38**, 2138–2140 (2005).
36. Adouni, M. & Shirazi-Adl, A. Evaluation of knee joint muscle forces and tissue stresses-strains during gait in severe OA versus normal subjects. *J. Orthop. Res.* **32**, 69–78 (2014).
37. Tanska, P., Mononen, M. E. & Korhonen, R. K. A multi-scale finite element model for investigation of chondrocyte mechanics in normal and medial meniscectomy human knee joint during walking. *J. Biomech.* **48**, 1397–1406 (2015).
38. Mononen, M. E., Jurvelin, J. S. & Korhonen, R. K. Effects of radial tears and partial meniscectomy of lateral meniscus on the knee joint mechanics during the stance phase of the gait cycle - A 3D finite element study. *J. Orthop. Res.* **31**, 1208–1217 (2013).
39. Peña, E., Calvo, B., Martínez, M. & Doblaré, M. A three-dimensional finite element analysis of the combined behavior of ligaments and menisci in the healthy human knee joint. *J. Biomech.* **39**, 1686–1701 (2006).
40. Godest, A. C., Beaugonin, M., Haug, E., Taylor, M. & Gregson, P. J. Simulation of a knee joint replacement during a gait cycle using explicit finite element analysis. *J. Biomech.* **35**, 267–275 (2002).
41. Seo, J.-W., Kang, D.-W., Kim, J.-Y., Yang, S.-T. & Kim, D.-H. Finite element analysis of the femur during stance phase of gait based on musculoskeletal model simulation. *Bio-Med. Mat. Eng.* **24**, 2485–2493 (2014).
42. Peterfy, C. G., Schneider, E. & Nevitt, M. The osteoarthritis initiative: report on the design rationale for the magnetic resonance imaging protocol for the knee. *Osteoarthritis Cartilage* **16**, 1433–1441 (2008).
43. Balamoody, S. *et al.* Comparison of 3T MR scanners in regional cartilage-thickness analysis in osteoarthritis: a cross-sectional multicenter, multivendor study. *Arthritis Res. Ther.* **12**, 1–9 (2010).
44. Parra, W. C. H., Chatterjee, H. J. & Soligo, C. Calculating the axes of rotation for the subtalar and talocrural joints using 3D bone reconstructions. *J. Biomech.* **45**, 1103–1107 (2012).

45. Marra, M. A. *et al.* A subject-specific musculoskeletal modeling framework to predict *in vivo* mechanics of total knee arthroplasty. *J. Biomech. Eng.* **137**, 1–12 (2015).
46. Wretenberg, P., Ramsey, D. K. & Németh, G. Tibiofemoral contact points relative to flexion angle measured with MRI. *Clin. Biomech.* **17**, 477–485 (2002).
47. Andersen, M. S., Damsgaard, M. & Rasmussen, J. Kinematic analysis of over-determinate biomechanical systems. *Comput. Methods Biomech. Biomed. Eng.* **12**, 371–384 (2009).
48. Rasmussen, J. *et al.* A general method for scaling musculoskeletal models. In *2005 Int. Symp. Comp. Sim. Biomech.*, 3 (2005).
49. Damsgaard, M., Rasmussen, J., Christensen, S., Surma, E. & de Zee, M. Analysis of musculoskeletal systems in the AnyBody Modeling System. *Sim. Model. Pr. Theory* **14**, 1100–1111 (2006).
50. Holmberg, A. & Klarbring, A. Muscle decomposition and recruitment criteria influence muscle force estimates. *Multibody Syst. Dyn.* **28**, 283–289 (2012).
51. Happee, R. & Van Der Helm, F. C. T. The control of shoulder muscles during goal directed movements, an inverse dynamic analysis. *Journal of Biomechanics* **28**, 1179–1191 (1995).
52. Andersen, M. S., de Zee, M., Damsgaard, M., Nolte, D. & Rasmussen, J. Introduction to Force-dependent Kinematics: Theory and Application to Mandible Modeling. *J. Biomech. Eng.* **139**, 1–14 (2017).
53. Böttcher, P., Zeissler, M., Maierl, J., Grevel, V. & Oechtering, G. Mapping of split-line pattern and cartilage thickness of selected donor and recipient sites for autologous osteochondral transplantation in the canine stifle joint. *Vet. Surg.* **38**, 696–704 (2009).
54. Below, S., Arnoczky, S. P., Dodds, J., Kooima, C. & Walter, N. The split-line pattern of the distal femur. *Arthroscopy* **18**, 613–617 (2002).
55. Bullough, P. & Goodfellow, J. The significance of the fine structure of articular cartilage. *J. Bone Joint Surg.* **50**, 852–857 (1968).
56. Halonen, K. S., Mononen, M. E., Jurvelin, J. S., Töyräs, J. & Korhonen, R. K. Importance of depth-wise distribution of collagen and proteoglycans in articular cartilage – A 3D finite element study of stresses and strains in human knee joint. *J. Biomech.* **46**, 1184–1192 (2013).
57. Halonen, K. *et al.* Deformation of articular cartilage during static loading of a knee joint – Experimental and finite element analysis. *J. Biomech.* **47**, 2467–2474 (2014).
58. Halonen, K. *et al.* Optimal graft stiffness and pre-strain restore normal joint motion and cartilage responses in ACL reconstructed knee. *J. Biomech.* 1–11 (2016).
59. Halonen, K. *et al.* Importance of patella, quadriceps forces and depth-wise cartilage structure on knee joint motion and cartilage response during gait. *J. Biomech.* **138**, 1–11 (2016).
60. Jakobsen, K. Stress radiographical measurement of the anteroposterior, medial and lateral stability of the knee joint. *Acta Orth. Scand.* **47**, 335–344 (1976).
61. Brandsson, S., Karlsson, J. & Eriksson, B. & KÃ¤rrholm, J. Kinematics after tear in the anterior cruciate ligament. *Acta Orth. Scand.* **72**, 372–378 (2001).
62. Schatzmann, L., Brunner, P. & Stäubli, H. U. Effect of cyclic preconditioning on the tensile properties of human quadriceps tendons and patellar ligaments. *Knee Surg. Sports Traumatol. Arthrosc.* **6**(Suppl 1), 56–61 (1998).
63. Mononen, M. E., Jurvelin, J. S. & Korhonen, R. K. Implementation of a gait cycle loading into healthy and meniscectomised knee joint models with fibril-reinforced articular cartilage. *Comput. Methods Biomech. Biomed. Eng.* **18**, 141–152 (2013).
64. Shelburne, K. B., Torry, M. R. & Pandy, M. G. Muscle, ligament, and joint-contact forces at the knee during walking. *Med. Sci. Sports. Exerc.* **37**, 1948–1956 (2005).
65. Kutzner, I. *et al.* Loading of the knee joint during activities of daily living measured *in vivo* in five subjects. *J. Biomech.* **43**, 2164–2173 (2010).
66. Bergmann, G. *et al.* Standardized loads acting in knee implants. *PLoS ONE* **9**, 1–12 (2014).
67. Brandsson, S., Karlsson, J., Eriksson, B. & Kärrholm, J. Quadriceps weakness and osteoarthritis of the knee. *Ann. Intern. Med.* **127**, 372–378 (1997).
68. Litwic, A., Edwards, M., Dennison, E. & Cooper, C. *Br. Med. Bull.*
69. D'Lima, D. D., Townsend, C. P., Arms, S. W., Morris, B. A. & Colwell, C. W. An implantable telemetry device to measure intra-articular tibial forces. *J. Biomech.* **38**, 299–304 (2005).
70. Silva, M. *et al.* Knee Strength After Total Knee Arthroplasty. *J. Arthroplasty* **18**, 605–611 (2003).
71. Brandsson, S., Karlsson, J., Eriksson, B. & Kärrholm, J. Contact stresses in the knee joint in deep flexion. *Med. Eng. Phys.* **27**, 329–335 (2005).
72. Thambyah, A., Goh, J. & Das De, S. Contact stresses in both compartments of the tibiofemoral joint are similar even when larger forces are applied to the medial compartment. *The Knee* **14**, 336–338 (2007).
73. Liu, F. *et al. In vivo* tibiofemoral cartilage deformation during the stance phase of gait. *Journal of Biomechanics* **43**, 658–665 (2010).
74. D'Lima, D., Hashimoto, S., Chen, P., Colwell, C. & Lotz, M. Human chondrocyte apoptosis in response to mechanical injury. *OA Cartilage* **9**, 712–719 (2001).
75. Loening, A. M. *et al.* Injurious mechanical compression of bovine articular cartilage induces chondrocyte apoptosis. *Arch. Biochem. Biophys.* **381**, 205–212 (2000).
76. Abdallah, A. A. & Radwan, A. Y. Biomechanical changes accompanying unilateral and bilateral use of laterally wedged insoles with medial arch supports in patients with medial knee osteoarthritis. *Clin. Biomech.* **26**, 783–789 (2011).
77. Nester, C. J., Hutchins, S. & Bowker, P. Effect of foot orthoses on rearfoot complex kinematics during walking gait. *Foot Ankle Int.* **22**, 133–139 (2001).
78. Schmalz, T., Blumentritt, S., Drewitz, H. & Freslier, M. The influence of sole wedges on frontal plane knee kinetics, in isolation and in combination with representative rigid and semi-rigid ankle-foot-orthoses. *Clin. Biomech.* **21**, 631–639 (2006).
79. Kutzner, I. *et al.* The effect of laterally wedged shoes on the loading of the medial knee compartment-*in vivo* measurements with instrumented knee implants. *J. Orthop. Res.* **29**, 1910–1915 (2011).
80. Crenshaw, S. J., Pollo, F. E. & Calton, E. F. Effects of lateral-wedged insoles on kinetics at the knee. *Clin. Orthop. Relat. Res.* **375**, 185–192 (2000).
81. Lynn, S. K. & Costigan, P. A. Effect of foot rotation on knee kinetics and hamstring activation in older adults with and without signs of knee osteoarthritis. *Clin. Biomech.* **23**, 779–786 (2008).
82. Guo, M., Axe, M. J. & Manal, K. The influence of foot progression angle on the knee adduction moment during walking and stair climbing in pain free individuals with knee osteoarthritis. *Gait Posture* **26**, 436–441 (2007).
83. Andrews, M., Noyes, F. R., Hewett, T. E. & Andriacchi, T. P. Lower limb alignment and foot angle are related to stance phase knee adduction in normal subjects: A critical analysis of the reliability of gait analysis data. *J. Orthop. Res.* **14**, 289–295 (1996).
84. Hurwitz, D. E., Ryals, A. B., Case, J. P., Block, J. A. & Andriacchi, T. P. The knee adduction moment during gait in subjects with knee osteoarthritis is more closely correlated with static alignment than radiographic disease severity, toe out angle and pain. *J. Orthop. Res.* **20**, 101–107 (2002).
85. Benoit, D. *et al.* Effect of skin movement artifact on knee kinematics during gait and cutting motions measured *in vivo*. *Gait Posture* **24**, 152–164 (2006).
86. Brandon, S., Smith, C. & Thelen, D. *Handbook of human motion*, chap.Simulation of soft tissue loading from observed movement dynamics, 1–34 (2017).

87. Lenhart, R., Kaiser, J., Smith, C. & Thelen, D. Prediction and validation of load-dependent behavior of the tibiofemoral and patellofemoral joints during movement. *Ann. Biomed. Eng.* **43**, 2675–85 (2015).
88. Heinen, F., Lund, M., Rasmussen, J. & de Zee, M. Muscle-tendon unit scaling methods of Hill-type musculoskeletal models: an overview. *J. Eng. Med.* **230**, 976–984 (2016).
89. Dabiri, Y. & Li, L. Influences of the depth-dependent material inhomogeneity of articular cartilage on the fluid pressurization in the human knee. *Med. Eng. Phys.* **35**, 1591–1598 (2013).
90. Makris, E. A., Hadidi, P. & Athanasiou, K. A. The knee meniscus: Structureâ€"function, pathophysiology, current repair techniques, and prospects for regeneration. *Biomaterials* **32**, 7411–7431 (2011).
91. Mow, V. C. & Guo, X. E. Mechano-electrochemical properties of articular cartilage: their inhomogeneities and anisotropies. *Annu. Rev. Biomed. Eng.* **4**, 175–209 (2002).

Acknowledgements

The research leading to these results has received funding from the European Union Seventh Framework Programme (FP7-PEOPLE-2013-ITN; KNEEMO) under grant agreement n. 607510.

Author Contributions

K.S.H. created the FE models, extracted and analysed FE results, C.M.D. and M.S.A. created the MS models, extracted and analysed MS results, M.M. gathered gait data, M.V. created the custom scripts used in the material model, and M.d.Z. and M.S.A. conceived the study. All authors reviewed the manuscript.

Additional Information

Supplementary information accompanies this paper at https://doi.org/10.1038/s41598-017-17228-x.

Competing Interests: The authors declare that they have no competing interests.

Publisher's note: Springer Nature remains neutral with regard to jurisdictional claims in published maps and institutional affiliations.

Workflow assessing the effect of gait alterations on stresses in the medial tibial cartilage – combined musculoskeletal modelling and finite element analysis

K S Halonen[1,*], C M Dzialo[2], M Mannisi[3], M S Venäläinen[4], M de Zee[1], and M S Andersen[2]

[1]Department of Health Science and Technology, Aalborg University, Fredrik Bajers Vej 7D, DK-9220 Aalborg, Denmark

[2]Department of Mechanical and Manufacturing Engineering, Aalborg University, Fibigerstræde 16, DK-9220 Aalborg, Denmark

[3]School of Health and Life Science, Glasgow Caledonian University, Cowcaddens Rd, G4 0BA, Glasgow, United Kingdom

[4]Department of Applied Physics, University of Eastern Finland, POB 1627, FI-70211 Kuopio, Finland

*ksh@hst.aau.dk

Supplementary Info

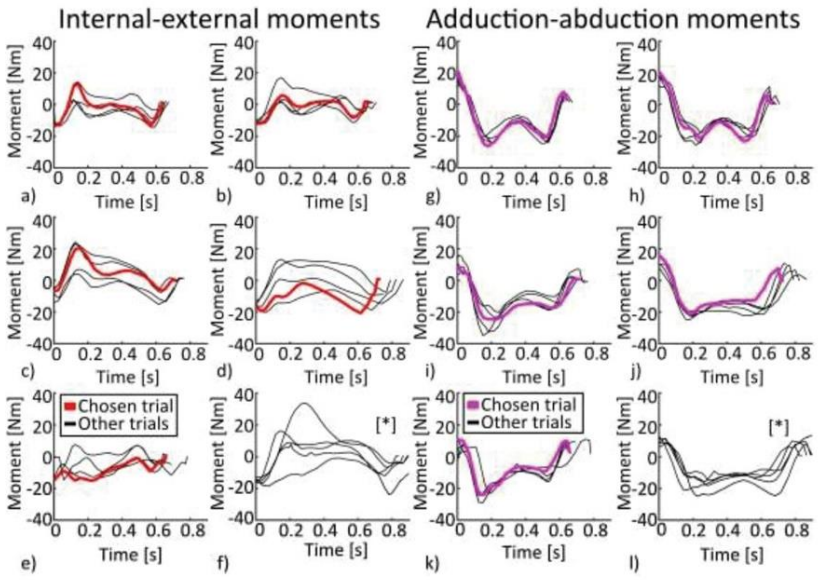

Supplementary Figure A. Left: Internal-external moments in **(a)** normal gait, **(b)** Insole 5°, **(c)** Insole 10°, **(d)** Toe in, **(e)** Toe out wide, and **(f)** Medial knees. **Right:** Adduction-abduction moments in (g) normal gait, (h) Insole 5°, **(i)** Insole 10°, **(j)** Toe in, **(k)** Toe out wide, and **(l)** Medial knees. The chosen trial for the FE input is highlighted in color. [*]: Medial knees were excluded from the analysis due to large difference in stance duration compared with normal gait.

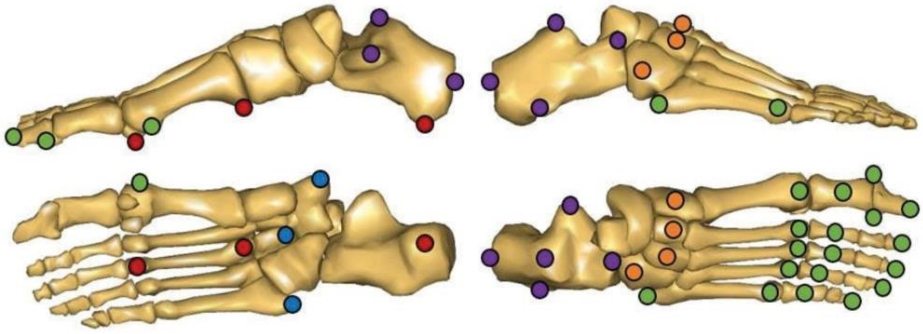

Supplementary Figure B. Anatomical landmarks on right foot: (**Red circles**) Longitudinal arch selection 1, 2, 3 (**Blue circles**) Transverse arch selection 1, 2, 3 (**Green circles**) $2^{nd} - 5^{th}$ distal and $1^{st} - 5^{th}$ proximal phallanges, $1^{st} - 5^{th}$ metatarsal heads, 5^{th} proximal metatarsal, Hallux: distal, lateral, and medial, tuberosity navicular, (**Orange circles**) Cuboid and Cuneiform: lateral, intermediate, medial (**Purple circles**) Calcaneous: superior, anterior, posterior, lateral, and medial.

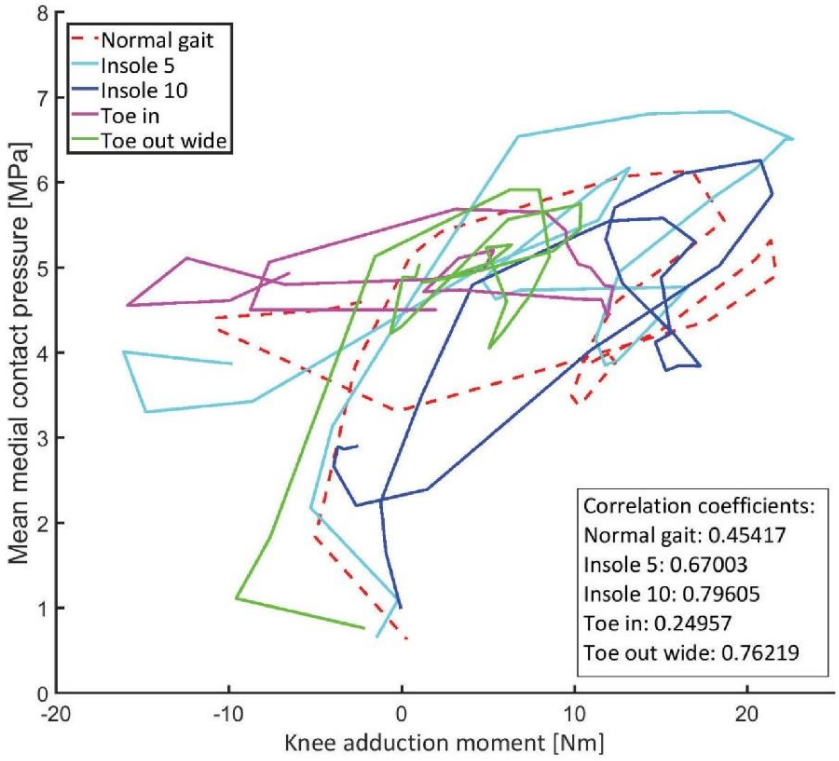

Supplementary Figure C. Mean medial contact pressures in the tibiofemoral contact area vs. knee adduction moment during the stance phase of gait.

CHAPTER 5. PAPER IV

Gait alteration strategies for knee osteoarthritis: a comparison of joint loading via generic and patient-specific musculoskeletal model scaling techniques

Dzialo, C.M., Mannisi, M., Halonen, K. S., de Zee, M., Woodburn, J., Andersen, M.S.

Submitted to International Biomechanics

CHAPTER 6. DISCUSSION

6.1. SUMMARY OF KEY RESULTS

This final chapter contains summaries of the key results from each publication. Paper I and II focus on the development and validation of a novel moving-axis joint model applied to the tibiofemoral and patellofemoral joints. While Paper III introduces a workflow to create a multi-scale (MS and FEA) subject-specific model with the potential application of investigating the effect of gait alteration techniques on the soft tissue structures of the knee. Lastly, Paper IV examines the influence of gait alteration techniques on knee loading on a small patient group diagnosed with medial knee osteoarthritis. The main aims of Paper IV are to investigate if model scaling technique (linear scaling vs MRI-based morphing) has an effect on which gait alteration has the greatest reduction in medial contact force, considering the patients as a group on average vs the patients individually. In addition, an overview of the contributions and the expected impact of this dissertation on the musculoskeletal modeling community is presented. Finally, the limitations of this work are addressed and recommendations for future work outlined in hopes of better validating personalized knee joint models and directing patient-specific musculoskeletal modeling into to the clinical setting.

Paper I: Development and validation of a subject-specific moving-axis tibiofemoral joint model using MRI and EOS imaging during a quasi-static lunge

This paper introduces and validates a novel computationally-efficient subject-specific tibiofemoral joint model. In the literature, musculoskeletal tibiofemoral joint models can range from simple generic (hinge) to complex subject-specific (multi-body contact models) depending on their generic qualities and computational time. The novelty of this study introduces a subject-specific tibiofemoral model that avoids time-consuming procedures (avoiding singularities through means of tuning (Brito da Luz et al., 2017) and/or collecting full range of motion joint data (Tsai and Lung, 2014)), is computationally efficient, and can recreate anatomically accurate secondary joint kinematics. Additionally, the study compares the model against a commonly used subject-specific hinge model in attempt to show the advantages and advancements of the proposed model. In this study, a full lower limb MRI acquisition was taken of each subject and the bone geometries segmented in order to create the models and find necessary joint centers and axis. Each subject also performed a quasi-static lunge while micro-dose radiation, bi-planar x-rays (EOS Imaging, Paris, France) were captured at roughly 0, 20, 45, 60, and 90 degrees of tibiofemoral flexion. In order to establish the model from two active tibiofemoral positions, and have experimental data to validate the model against, joint translations and rotations were extracted from this experimental data through 2D-to-3D bone reconstructions. This process is completed using an iterative closest point optimization technique. The models were developed and run in AMS with (1) the tibiofemoral axis of the hinge model

established between the femoral epicondyles. (2) The moving-axis was defined as a piecewise linear model constructed from two tibiofemoral flexion positions, roughly 0° and 90°, with the articulation of the tibiofemoral joint axis moving linearly between these two positions as a function of the tibiofemoral flexion. Outside this range, the joint axis remained stationary rotating about its current position. The resulting secondary joint kinematics proved to be better predicted when employing a moving-axis tibiofemoral model, which achieved an average mean difference and standard error of (translations: 2.84 ± 0.31 mm, rotations: 1.25 ± 0.43^0) and higher coefficients of determination (R^2) for each clinical measure. The commonly used hinge model had an average mean difference and standard error of (3.87 ± 0.39 mm, 7.39 ± 0.87^0). No significant differences were found between the moving-axis model and the experimentally observed tibiofemoral joint rotations from the EOS data, while this was not the case for the hinge model. Overall, Paper I presents a new approach in constructing the tibiofemoral joint in musculoskeletal modeling, allowing for a computationally fast model with subject-specific geometries and kinematics. It was concluded that the moving-axis joint can better predict experimentally observed rotations and translations when compared to the commonly used subject-specific hinge model. It should be noted that although the model is computationally fast once it is created, the process of establishing the model takes a considerable amount of time and money due to the imaging (MRI & EOS) and segmentation needed. With the progression of automatic segmentation this will decrease the processing time and cost.

Paper II: Evaluation of predicted patellofemoral joint kinematics with a moving-axis joint model

Paper II expanded on Paper I by applying the moving-axis concept to the patellofemoral joint and evaluates patellar motion derived from different configurations of the tibiofemoral and patellofemoral joints against experimental patellofemoral kinematic data. The same 2D-to-3D bone reconstruction process was followed as in Paper I, now for the patellofemoral joint. The six knee model variations were developed in AMS using subject-specific bone geometries and joint centers obtained through MRI segmentation. The six configurations were made up from combinations of tibiofemoral (hinge, moving-axis, and interpolated) and patellofemoral (hinge and moving-axis) joint types. In addition to the novel moving-axis patellofemoral joint, this paper introduces an interpolated tibiofemoral joint calibrated from the five EOS quasi-static lunge positions. This model only permits error from the patellofemoral model when comparing against the EOS experimental data, which is important due to the relationship between patellar and femoral kinematics during weighted knee flexion (Li et al., 2007), and thus the potential error arising from the TF model. The hinge axis was modeled as a line connecting the centers of cylinder surface fits of the medial and lateral patellofemoral contact area. While the moving-axis articulated linearly as a function of tibiofemoral flexion from an axis defined at 0° tibiofemoral flexion, established by connecting the centers of cylinder surface fits of the medial and lateral contact areas, to the same construction

at 90° tibiofemoral flexion. Outside these angles, the axis remained fixed about with the extension (0°) or flexion (90°) facet center axes. The results from this paper showed that a moving-axis tibiofemoral joint in combination with a hinge patellofemoral joint offers (-5.12 ± 1.23 mm, 5.81 ± 0.97 mm, 14.98 ± 2.30°, -4.35 ± 1.95°) mean differences when compared to the experimental EOS data in terms of lateral-shift, superior translation, patellofemoral-flexion, and patellar-rotation respectively. While when using a moving-axis patellofemoral joint in exchange for the hinge provides (-2.69 ± 1.04 mm, 1.13 ± 0.80 mm, 12.63 ± 2.03°, 1.74 ± 1.46°). This displays that a piecewise linear model can provide accurate estimates of patellofemoral joint kinematics when investigating patellar motion between two active TF-flexion positions. Furthermore, the commonly used hinge model resulted in the most significantly different patellofemoral measures when compared to the experimental EOS data in particularly in deep TF-flexion. The paper concludes that the model predictive capabilities increase as a direct result of adding more calibrated positions to the tibiofemoral model (hinge-1, moving-axis-2, and interpolated-5) for most of the patellofemoral kinematic measures. Overall, the aim of establishing a novel subject-specific moving-axis patellofemoral model was established; that produces realistic patellar motion and is computationally efficient enough for clinical applications.

Paper III: Workflow assessing the effect of gait alterations on stresses in the medial tibial cartilage - combined musculoskeletal modelling and finite element analysis

A workflow is presented in Paper III that combines motion capture, ground reaction forces, MRI, bone morphing, multibody dynamics, and finite element analysis to investigate the effect of gait alterations on cartilage stresses and strains. Potential applications of the multi-scale model are explored in the form of how gait modifications (toe-in and toe-out) and lateral wedge insoles (LWI) influence medial tibial cartilage stresses. This is made possible by combining musculoskeletal (MS) modeling with finite element (FE) analysis. Due to the methodological nature of this study and the focus of establishing a method to study the effect of gait alterations effects (not aimed at proving or disproving the benefits of a particular technique), we only modeled and analyzed one subject. MRI of the subject's lower limbs and detailed knee scans were obtained and then the bones and most soft tissues were manually segmented. Generic bone architectures were then morphed into the segmented bones to obtain a subject-specific musculoskeletal model. The subject's normal walking and various alterations were recorded in a gait laboratory and processed through the subject-specific musculoskeletal model in the AMS. The output forces and moments achieved from the musculoskeletal model were used as boundary conditions for the FE model of the detailed knee joint. The study showed that for this particular individual during the stance phase, the LWI failed to reduce medial peak pressures apart from the insole-10° during the second loading peak. The toe-in modification achieved reduced peak pressures of -11% during the first peak, however had the

opposite effect during the second peak increasing the pressures by nearly 12%. When the subject walked with toe-out gait, the peak pressures showed the same trend, reducing by -15% during the first peak and increasing by 7% during the second peak. Paper III establishes a method that will allow researchers to simultaneously investigate the loads individual structures, estimate net joint loads (resulting from subject-specific knee joint kinematics, external loads, and ligament/muscle forces), and examine stresses in soft tissues of the knee during normal and modified gait. Furthermore, the proposed method allows for a non-invasive subject-specific (and hopefully in the future patient-specific) evaluation of low-cost clinical interventions, aimed at reducing loads in the medial tibial cartilage.

Paper IV: Gait alteration strategies for knee osteoarthritis: a comparison of joint loading via generic and patient-specific musculoskeletal model scaling techniques

In Paper IV, non-invasive approaches (gait modifications and lateral wedged insoles) aimed at reducing medial compartment knee loading are further examined, however this time with respect to a patient cohort. Gait alterations are a controversial topic, with the success of these interventions not always exclusive. This study explores what might contribute to the inconsistencies, whether how the population is analyzed plays a role (on a group or individual level) or perhaps if the type musculoskeletal model scaling approach may influence the outcomes. More specifically, this paper looks at how common gait alteration techniques may have varying effects on individual patients as opposed to a patient group; and furthermore, the way musculoskeletal models are scaled to estimate medial contact force may influence knee loading conditions. In this study, 3D motion capture was taken of five patients with clinical evidence of medial knee osteoarthritis during normal walking, walking with patient-specific lateral wedged insoles (0°, 5°, and 10°), walking with a gait modification (toe-in, toe-out, wide stance). Patient-specific musculoskeletal models were constructed from manually segmented MRI images of the patients that were used to morph a generic model to the patient-specific bone geometries. A different scaling technique, simple linear scaling (LS), was also used to create an additional five patient-specific models for comparison. The medial contact force (MCF) was examined in terms of peak and impulse values during stance phase of walking. The results of this paper conclude that a ‘one-size-fits-all’ gait alteration aimed at minimizing medial contact loading does not exist for these five patients, suggesting the importance of individually assigned interventions. Of course, the small sample size was a limitation and although beyond the scope of this study, restricting detection of meaningful clinical results. Interestingly, the different scaling and morphing techniques used on the musculoskeletal models lead to differences in medial contact forces. This highlights the importance of further investigation of scaling approaches prior to being able to use such models in the clinical setting to assist in prescribing gait alterations.

6.2. CONTRIBUTIONS AND IMPACT

Whether estimated knee kinematics will be used exclusively with musculoskeletal modeling for estimating knee contact forces, or as boundary conditions for FEA models, the importunate of achieving realistic joint kinematics depends on the research question being asked. The novelty behind the established moving-axis is that it not only provides realistic joint kinematics, but also allows for a computationally fast model with subject-specific geometries, which may make it more accessible for clinical applications than a more advanced multi-body contact model. In particular, it is common for x-rays of the lower limb to be taken of patients with KOA, substituting these for bi-planar fluoroscopy, ultrasound, or lower radiation biplanar EOS imaging at roughly 0 and 90 degrees may be a viable option, given the technology that is available. In addition, comparing the 3D bone reconstructions obtained through statistical shape modeling to that achieved through manual (or semi-automatic) MRI/CT segmentations (Baldwin et al., 2010; Heimann and Meinzer, 2009; Li et al., 2013; Nolte et al., 2016; Quijano et al., 2013) would prove to be beneficial to see if the MRI/CT segmentations make a significant difference. In cases where biplanar imaging is available, this potentially eliminates the need for MRI/CT acquisition and segmentation, when bone is solely required for the model.

The development of a workflow for creating, processing, and analyzing multi-scale (musculoskeletal & finite element analysis) personalized models has been achieved; and when further validated, a patient-specific multi-scale knee model will enable studies of how interventions influence the detailed joint mechanics and can be used as a tool to tailor treatments to the given patient. This allows for an advancement in knowledge pertaining to personalized mechanical load distribution and its effect on cartilage and bone integrity in the knee joint (or other lower limb joint of interest). Currently, longitudinal studies are required to understand how interventions influence KOA progression. Nevertheless, possibilities exist to create more in-depth multi-scale models by integrating mathematical models of articular cartilage damage and degeneration that simulate KOA progression (Hosseini et al., 2014; Landinez-Parra et al., 2011; Liukkonen et al., 2017). Once thoroughly validated, these models may have the clinical potential of investigating how personalized gait alterations effect KOA progression, on a soft tissue level, in a more time-efficient manner. Furthermore, diving into the musculoskeletal modeling side of this workflow allowed us to take into consideration the potential sensitivities that (1) model scaling method and (2) how the data is interpreted (with respect to the individual patient or to the entire patient group) may have on the outcome of gait alteration technique that results in the greatest decrease in medial knee loading. With the increase in knowledge regarding phenotyping in patients with KOA (Dell'Isola et al., 2016; Deveza et al., 2017), and the hope of utilizing this knowledge in clinics when allocating treatment methods (Bierma-Zeinstra and van Middelkoop, 2017) it may be important to consider the individual beyond their assigned patient group.

Lastly, it should be noted that although MRI imaging is used in many studies investigating KOA, it is currently not the standard in KOA care due to the fact that it is a lengthy and expensive procedure. The most common imaging modality for OA is radiography due to its simplicity and low cost (Hayashi et al., 2016). However, without MRI imaging, this puts a limitation on musculoskeletal and finite element modeling. If we are able to demonstrate that MRI-based models can identify individualized interventions that will actually make a difference in terms of OA treatment, spending the money upfront could save money in the future. Identification of an individualized interventions aimed to slow down OA disease progression, may keep individuals active for longer (exercise & working), improve the quality of their lives, and ultimately decrease surgical intervention costs if individuals only need one (or none at all) total knee replacement in their lifetime. However, if we are unable to identify these interventions correctly, it is not worth the money no matter how accurate the models turn out to be.

6.3. LIMITATIONS AND RECOMMENDATIONS FOR FUTURE WORK

With research advancements come the inevitable limitations. These limitations have the benefit of proposing new directions for future research, by refocusing the question at hand in an attempt to fill knowledge gaps.

For instance, in the moving-axis tibiofemoral and patellofemoral models that were established in Paper I and II, have major limitations in the anterior-posterior translation and internal-external rotation measures.

- An idea for improvement is to introduce ligaments and contact (in 2 DOF), giving the model a force response along the directions where the major external influences are expected to be. The remaining directions are more clearly given by the shape of the bones.

Although large improvements were made by introducing the moving-axis model, it is currently only based on a linear relationship, calibrate from two positions, which may not best represent realistic joint movements. Additionally, the images were only captured quasi-statically for one movement type, so the results cannot be generalized to other activities. Finally, using more frames available to compare against will allow for a better evaluation of model predictive capabilities.

- The investigation of other relationships for the moving-axis model, quadradic or polynomial (avoiding overfitting the model), to determine which best mimics the reality of knee joint kinematics. This would require a more comprehensive validation data set, perhaps utilizing dynamic imaging techniques, such as biplanar fluoroscopy, dynamics MRI, ultrasound, or radiostereometric analysis (RSA). Additionally, recording of various activities of daily living would be of interest to see if the relationships hold true for different movements. However, with some of these imaging techniques, more imaging means more costs and radiation exposure which is important to consider when developing a study.
- If a dynamic data set of several movements is obtained, a further recommendation is to make a larger comparison against a variety of knee

models including, but not limited to, the FDK, moving-axis, and hinge models.

Patella instability most often occurs between 0° and 30° flexion, where the patella may not be fully engaged with the trochlear groove, and flexion beyond this point may cause the patella not to track smoothly (Amis, 2007; Waryasz and McDermott, 2008). With this in mind, applying a moving-axis to particular subjects and or patients may not be appropriate. For instance, if the patella is not sitting correctly in the trochlear groove when the initial EOS-0 scan was taken, a linear piecewise linear relationship would not result in a realistic patellar motion. This furthers the need for moving-axis models of the knee joint to be calibrating off of more than two poses and investigating different relationships between the poses.

Currently, the most commonly used knee joint in many musculoskeletal modeling systems is a hinge. This is mostly due to the fact that other models require personalized bone geometries and or ligament attachment regions. It is recommended that these musculoskeletal modeling programs adopt the moving-axis knee joint, so researchers can utilize it and potentially find improvements for the model in the future. Additionally, this should be expanded to include a moving-axis joint that can be scaled or morphed from a generic model to individualized parameters depending on the input data available to the user.

The methodological nature of Paper III comes with a large limitation of only modeling one subject. We would like to reiterate that the focus of the study was not to find out the best gait alteration for reducing medial knee stresses, but rather to establish such a workflow that could be used in the future on other subjects and patient groups. Large advancements of this research include the implementation of subject-specific geometry based on MRI, motion capture data, personalized insoles, and combining this with a subject-specific FE model. However, many of the model parameters were not personalized and obtained from the literature in the final multi-scale model (generic muscle-tendon parameters, ligament laxity, and finite element model material properties). Future work should investigate the how to best obtain such parameters with as few measurements and as ethically as possible, to investigate their influence on the outcomes of various gait alterations on the stresses and strains in the knee joint.

- The addition of subject-specific strength measurements, which could be based on isometric and isokinetic measurements and applied using optimization-based approaches (Heinen et al., 2016).
- Measuring 3D joint laxities of the tibiofemoral and patellofemoral joints using the new and improved laxity machine developed by (Pedersen et al., 2018) in order to better estimate the ligament stiffnesses and slack lengths.
- Observe personalized cartilage strains and meniscal movement during static loading trial utilizing conical bean CT-scanner, or equivalent, to better estimate properties for the cartilage material model and meniscal movement patterns for finite element model (K.S. Halonen et al., 2014).

Similarly, an obvious limitation of Paper IV was the limited sample size, which restricted detection of meaningful clinical results, however this was beyond the scope of the study.

These patient-specific musculoskeletal models use generic muscle-tendon parameters because during the data collection one of the patients was unable to perform the maximum isometric strength measurements.

- Investigate the difference, if any, of analyzing the models with patient-specific muscle-tendon parameters for the four patients that were able to perform maximum isometric strength measurements.

The use of skin marker-based movement analysis in this study, in addition to modeling the knee as a hinge joint, is a clear limitation due to the presence of soft tissue artefacts (Andersen et al., 2010a; Benoit et al., 2006).

- Comparing lower limb kinematics and resulting medial contact knee forces obtained through (1) skin marker-based motion capture system and (2) bi-planar fluoroscopy from patients with KOA when examining various gait alterations.
- Exchange the hinge joint in the patellofemoral and tibiofemoral joints with moving-axis or FDK joints and compare the output to what the hinge joint achieved.

Only the immediate effects of gait alteration techniques on knee contact force were investigated in Paper IV. Moreover, these gait modifications were taught to the patients in a single session. What is needed in order to determine if the model designated gait alterations (and how these are obtained) actually result in better clinical outcomes, i.e. in terms of cartilage health and patient satisfaction is a longitudinal study. A study randomly assigning the resulting optimal gait alteration obtained based on a combination of the following:

- model type (LS vs MRI, etc.)
- The parameter we are interested in reducing (peak MCF, MCF impulse, etc.)
- If data is processed with respect to the individual or the patient group
- How the alterations are introduced to the patients. Gradual introduction of LWI and multiple training sessions for gait modification techniques (may include at home practicing and biofeedback), have been known to change the results (Hunt and Takacs, 2014; Lewinson and Stefanyshyn, 2016; Richards et al., 2017; Shull et al., 2013b).

Finally, the initial aim of the last study for this dissertation was to follow the same workflow established in paper III for patients with medial compartment knee osteoarthritis. However, the intriguing question of whether musculoskeletal model scaling technique swayed us from this objective leaving it to future researchers to explore.

- Use patient-specific musculoskeletal outputs as boundary conditions for corresponding patient-specific finite element knee models (already established) to estimate tissue stresses and strains. Then researchers can better understand whether parameters that closer represent the tissue

response, can better identify the true patient response to the selected treatment and how that may relate to long-term outcomes.

6.4. CONCLUDING REMARKS

The objective behind this dissertation was to advance the field of personalized musculoskeletal models through means of knee joint modeling, bone morphing, and the application of established models. Novel moving-axis joint models utilizing subject-specific bone geometries were first established, applied to two joints (tibiofemoral and patellofemoral), and evaluated against experimental kinematic data (Papers I and II) resulting in more realistic secondary joint kinematics than commonly used hinge joints. In addition, the process of developing and combining musculoskeletal modeling and finite analysis was presented as a workflow in Paper III providing groundwork for clinical applications (along with Paper IV) to develop patient-specific models and furthermore optimize non-invasive treatment methods based on a more individualized approach. Finally, concerns regarding personalized musculoskeletal scaling techniques and the selection of optimal (providing greatest reduction in medial compartment loading) gait alterations with respect to a patient group vs individual patient were addressed in Paper IV. Overall, the work presented in Papers III and IV did not aim at providing clinical recommendations; but rather to establish methodological groundwork for future researchers.

LITERATURE LIST

Ackermann, M., van den Bogert, A.J., 2010. Optimality principles for model-based prediction of human gait. J. Biomech. 43, 1055–1060. https://doi.org/10.1016/j.jbiomech.2009.12.012

Adouni, M., Shirazi-Adl, A., 2014. Evaluation of knee joint muscle forces and tissue stresses-strains during gait in severe OA versus normal subjects. J. Orthop. Res. 32, 69–78. https://doi.org/10.1002/jor.22472

Al Hares, G., Eschweiler, J., Radermacher, K., 2015. Combined magnetic resonance imaging approach for the assessment of in vivo knee joint kinematics under full weight-bearing conditions. Proc. Inst. Mech. Eng. H. 229, 439–51. https://doi.org/10.1177/0954411915585863

Altman, R.D., Gold, G.E., 2007. Atlas of individual radiographic features in osteoarthritis, revised, Osteoarthritis and Cartilage. https://doi.org/10.1016/j.joca.2006.06.017

Amis, A.., 2007. Current concept on anatomy and biomechanics of patellar stability. Sport Med. Arthrosc. Rev. 15, 48–56.

Andersen, M.S., Benoit, D.L., Damsgaard, M., Ramsey, D.K., Rasmussen, J., 2010a. Do kinematic models reduce the effects of soft tissue artefacts in skin marker-based motion analysis? An in vivo study of knee kinematics. J. Biomech. 43, 268–273. https://doi.org/10.1016/j.jbiomech.2009.08.034

Andersen, M.S., Damsgaard, M., MacWilliams, B., Rasmussen, J., 2010b. A computationally efficient optimisation-based method for parameter identification of kinematically determinate and over-determinate biomechanical systems. Comput. Methods Biomech. Biomed. Engin. 13, 171–183. https://doi.org/10.1080/10255840903067080

Andersen, M.S., de Zee, M., Damsgaard, M., Nolte, D., Rasmussen, J., 2017. Introduction to Force-Dependent Kinematics: Theory and Application to Mandible Modeling. J. Biomech. Eng. 139, 091001. https://doi.org/10.1115/1.4037100

Anderson, A.E., Ellis, B.J., Maas, S.A., Peters, C.L., Weiss, J.A., 2008. Validation of Finite Element Predictions of Cartilage Contact Pressure in the Human Hip Joint. J. Biomech. Eng. 130, 051008. https://doi.org/10.1115/1.2953472

Anderson, F.C., Pandy, M.G., 2001. Dynamic optimization of human walking. J.

Biomech. Eng. 123, 381–390. https://doi.org/10.1115/1.1392310

Ardestani, M.M., Chen, Z., Wang, L., Lian, Q., Liu, Y., He, J., Li, D., Jin, Z., 2014a. A neural network approach for determining gait modifications to reduce the contact force in knee joint implant. Med. Eng. Phys. 36, 1253–1265. https://doi.org/10.1016/j.medengphy.2014.06.016

Ardestani, M.M., Moazen, M., Jin, Z., 2014b. Gait modification and optimization using neural network-genetic algorithm approach: Application to knee rehabilitation. Expert Syst. Appl. https://doi.org/10.1016/j.eswa.2014.06.034

Arnold, A.S., Asakawa, D.J., Delp, S.L., 2000. Do the hamstrings and adductors contribute to excessive internal rotation of the hip in persons with cerebral palsy ? 11, 181–190.

Arnold, A.S., Salinas, S., Asakawa, D.J., Delp, S.L., 2000. Accuracy of muscle moment arms estimated from MRI-based musculoskeletal models of the lower extremity. Comput. Aided Surg. 5, 108–119. https://doi.org/10.1002/1097-0150(2000)5:2<108::AID-IGS5>3.0.CO;2-2

Arnold, J.B., 2016. Lateral wedge insoles for people with medial knee osteoarthritis: One size fits all, some or none? Osteoarthr. Cartil. 24, 193–195. https://doi.org/10.1016/j.joca.2015.09.016

Azmy, C., Guérard, S., Bonnet, X., Gabrielli, F., Skalli, W., 2010. EOS® orthopaedic imaging system to study patellofemoral kinematics: Assessment of uncertainty. Orthop. Traumatol. Surg. Res. 96, 28–36. https://doi.org/10.1016/j.otsr.2009.10.013

Balamoody, S., Williams, T.G., Waterton, J.C., Bowes, M., Hodgson, R., Taylor, C.J., Hutchinson, C.E., 2010. Comparison of 3T MR scanners in regional cartilage-thickness analysis in osteoarthritis: a cross-sectional multicenter, multivendor study. Arthritis Res. Ther. 12, R202. https://doi.org/10.1186/ar3174

Baldwin, M. a., Langenderfer, J.E., Rullkoetter, P.J., Laz, P.J., 2010. Development of subject-specific and statistical shape models of the knee using an efficient segmentation and mesh-morphing approach. Comput. Methods Programs Biomed. 97, 232–240. https://doi.org/10.1016/j.cmpb.2009.07.005

Barrios, J.A., Crossley, K.M., Davis, I.S., 2010. Gait retraining to reduce the knee adduction moment through real-time visual feedback of dynamic knee alignment. J. Biomech. 43, 2208–2213. https://doi.org/10.1016/j.jbiomech.2010.03.040

Bayliss, L.E., Culliford, D., Monk, A.P., Glyn-Jones, S., Prieto-Alhambra, D., Judge, A., Cooper, C., Carr, A.J., Arden, N.K., Beard, D.J., Price, A.J., 2017. The effect of patient age at intervention on risk of implant revision after total replacement of the hip or knee: a population-based cohort study. Lancet 389, 1424–1430. https://doi.org/10.1016/S0140-6736(17)30059-4

Bedson, J., Croft, P.R., 2008. The discordance between clinical and radiographic knee osteoarthritis: A systematic search and summary of the literature. BMC Musculoskelet. Disord. 9, 1–11. https://doi.org/10.1186/1471-2474-9-116

Bellamy, N., Bell, M.J., Goldsmith, C.H., Pericak, D., Walker, V., Raynauld, J.P., Torrance, G.W., Tugwell, P., Polisson, R., 2005. Evaluation of WOMAC 20, 50, 70 response criteria in patients treated with hylan G-F 20 for knee osteoarthritis 881–885. https://doi.org/10.1136/ard.2004.026443

Bendjaballah, M., Shirazi-Adl, a, Zukor, D., 1995. Biomechanics of the human knee joint in compression: reconstruction, mesh generation and finite element analysis. Knee 2, 69–79. https://doi.org/10.1016/0968-0160(95)00018-K

Bennell, K.L., Bowles, K.A., Payne, C., Cicuttini, F., Williamson, E., Forbes, A., Hanna, F., Davies-Tuck, M., Harris, A., Hinman, R.S., 2011. Lateral wedge insoles for medial knee osteoarthritis: 12 Month randomised controlled trial. Bmj 342. https://doi.org/10.1136/bmj.d2912

Benoit, D.L., Ramsey, D.K., Lamontagne, M., Xu, L., Wretenberg, P., Renström, P., 2006. Effect of skin movement artifact on knee kinematics during gait and cutting motions measured in vivo. Gait Posture 24, 152–164. https://doi.org/10.1016/j.gaitpost.2005.04.012

Bergmann, G., 2008. OrthoLoad.com [WWW Document]. Charite – Univ. Berlin. URL http://www.orthoload.com/

Bergmann, G., Bender, A., Graichen, F., Dymke, J., Rohlmann, A., Trepczynski, A., Heller, M.O., Kutzner, I., 2014. Standardized loads acting in knee implants. PLoS One 9. https://doi.org/10.1371/journal.pone.0086035

Bierma-Zeinstra, S.M., van Middelkoop, M., 2017. Osteoarthritis: In search of phenotypes. Nat. Rev. Rheumatol. 13, 705–706. https://doi.org/10.1038/nrrheum.2017.181

Bijlsma, J.W.J., Berenbaum, F., Lafeber, F.P.J.G., 2011. Osteoarthritis: An update with relevance for clinical practice. Lancet 377, 2115–2126. https://doi.org/10.1016/S0140-6736(11)60243-2

Blankevoort, L., Kuiper, J.H., Huiskes, R., Grootenboer, H.J., 1991. Articular contact in a three-dimensional model of the knee. J. Biomech. 24, 1019–1031. https://doi.org/10.1016/0021-9290(91)90019-J

Borotikar, B., Lempereur, M., Lelievre, M., Burdin, V., Ben Salem, D., Brochard, S., 2017. Dynamic MRI to quantify musculoskeletal motion: A systematic review of concurrent validity and reliability, and perspectives for evaluation of musculoskeletal disorders. PLoS One 12, e0189587. https://doi.org/10.1371/journal.pone.0189587

Brekelmans, W.A.M., Poort, H.W., Slooff, T.J.J.H., 1972. A new method to analyse the mechanical behaviour of skeletal parts. Acta Orthop. 43, 301–317. https://doi.org/10.3109/17453677208998949

Brito da Luz, S., Modenese, L., Sancisi, N., Mills, P.M., Kennedy, B., Beck, B.R., Lloyd, D.G., 2017. Feasibility of using MRIs to create subject-specific parallel-mechanism joint models. J. Biomech. 53, 45–55. https://doi.org/10.1016/j.jbiomech.2016.12.018

Bruns, J., Volkmer, M., Luessenhop, S., 1994. Pressure distribution in the knee joint - Influence of flexion with and without ligament dissection. Arch. Orthop. Trauma Surg. 113, 204–209. https://doi.org/10.1007/BF00441833

Bruyère, O., Cooper, C., Pelletier, J.P., Branco, J., Luisa Brandi, M., Guillemin, F., Hochberg, M.C., Kanis, J.A., Kvien, T.K., Martel-Pelletier, J., Rizzoli, R., Silverman, S., Reginster, J.Y., 2014. An algorithm recommendation for the management of knee osteoarthritis in Europe and internationally: A report from a task force of the European Society for Clinical and Economic Aspects of Osteoporosis and Osteoarthritis (ESCEO). Semin. Arthritis Rheum. 44, 253–263. https://doi.org/10.1016/j.semarthrit.2014.05.014

Buchanan, T.S., Lloyd, D.G., Manal, K., Besier, T.F., 2006. Neuromusculoskeletal Modeling: Estimation of Muscle Forces and Joint Moments and Movements From Measurements of Neural Command 20, 367–395.

Burr, D.B., Milgrom, C., Fyhrie, D., Forwood, M., Nyska, M., Finestone, A., Hoshaw, S., Saiag, E., Simkin, A., 1996. In vivo measurement of human tibial strains during vigorous activity. Bone 18, 405–410. https://doi.org/10.1016/8756-3282(96)00028-2

Butler, R.J., Marchesi, S., Royer, T., Davis, I.S., 2007. The Effect of a Subject-Specific Amount of Lateral Wedge on Knee. J. Orthop. Res. Sept. 25, 1121–1127. https://doi.org/10.1002/jor

Caldwell, L.K., Laubach, L.L., Barrios, J.A., 2013. Effect of specific gait modifications on medial knee loading, metabolic cost and perception of task difficulty. Clin. Biomech. 28, 649–654. https://doi.org/10.1016/j.clinbiomech.2013.05.012

Carbone, V., Fluit, R., Pellikaan, P., Krogt, M.M. Van Der, Janssen, D., Damsgaard, M., Vigneron, L., Feilkas, T., Koopman, H.F.J.M., Verdonschot, N., 2015. TLEM 2 . 0 – A comprehensive musculoskeletal geometry dataset for subject-specific modeling of lower extremity.

Carbone, V., van der Krogt, M.M., Koopman, H.F.J.M., Verdonschot, N., 2012. Sensitivity of subject-specific models to errors in musculo-skeletal geometry. J. Biomech. 45, 2476–2480. https://doi.org/10.1016/j.jbiomech.2012.06.026

Carey, R.E., Zheng, L., Aiyangar, A.K., Harner, C.D., Zhang, X., 2014. Subject-Specific Finite Element Modeling of the Tibiofemoral Joint Based on CT, Magnetic Resonance Imaging and Dynamic Stereo-Radiography Data in Vivo. J. Biomech. Eng. 136, 041004. https://doi.org/10.1115/1.4026228

Carr, A.J., Robertsson, O., Graves, S., Price, A.J., Arden, N.K., Judge, A., Beard, D.J., 2012. Knee replacement. Lancet 379, 1331–1340. https://doi.org/10.1016/S0140-6736(11)60752-6

Chawla, H., van der List, J.P., Christ, A.B., Sobrero, M.R., Zuiderbaan, H.A., Pearle, A.D., 2017. Annual revision rates of partial versus total knee arthroplasty: A comparative meta-analysis. Knee 24, 179–190. https://doi.org/10.1016/j.knee.2016.11.006

Chen, A., Gupte, C., Akhtar, K., Smith, P., Cobb, J., 2012. The Global Economic Cost of Osteoarthritis: How the UK Compares. Arthritis 2012, 1–6. https://doi.org/10.1155/2012/698709

Chen, C.H., Li, J.S., Hosseini, A., Gadikota, H.R., Gill, T.J., Li, G., 2012. Anteroposterior stability of the knee during the stance phase of gait after anterior cruciate ligament deficiency. Gait Posture 35, 467–471. https://doi.org/10.1016/j.gaitpost.2011.11.009

Churchill, D.L., Incavo, S.J., Johnson, C.C., Beynnon, B.D., 1998. The transepicondylar axis approximates the optimal flexion axis of the knee. Clin. Orthop. Relat. Res. 111–118.

Clément, J., Dumas, R., Hagemeister, N., de Guise, J.A., 2015. Soft tissue artifact compensation in knee kinematics by multi-body optimization: Performance of subject-specific knee joint models. J. Biomech. 48, 3796–3802.

https://doi.org/10.1016/j.jbiomech.2015.09.040

Clement, J., Hagemeister, N., Aissaoui, R., Guise, J.A. De, 2014. Comparison of quasi-static and dynamic squats : A three-dimensional kinematic , kinetic and electromyographic study of the lower limbs. Gait Posture 40, 94–100. https://doi.org/10.1016/j.gaitpost.2014.02.016

Cohen, B., Lai, W.M., Mow, V.C., 1998. A Transversely Isotropic Biphasic Model for Unconfined Compression of Growth Plate and Chondroepiphysis. J. Biomech. Eng. 120, 491–496.

Cook, R.D., Malkus, D.S., Plesha, M.E., Witt, R.J., 2002. Concepts and Applications of Finite Element Analysis, 4th ed. John Wiley & Sons, Inc., University of Wisconsin-Madison.

Cross, M., Smith, E., Hoy, D., Nolte, S., Ackerman, I., Fransen, M., Bridgett, L., Williams, S., Guillemin, F., Hill, C.L., Laslett, L.L., Jones, G., Cicuttini, F., Osborne, R., Vos, T., Buchbinder, R., Woolf, A., March, L., 2014. The global burden of hip and knee osteoarthritis: Estimates from the Global Burden of Disease 2010 study. Ann. Rheum. Dis. 73, 1323–1330. https://doi.org/10.1136/annrheumdis-2013-204763

Crowninshield, R.D., 1978. Use of Optimization Techniques to Predict Muscle Forces. J. Biomech. Enginering 100, 88–92. https://doi.org/10.1115/1.3426197

Damsgaard, M., Rasmussen, J., Christensen, S.T., Surma, E., de Zee, M., 2006. Analysis of musculoskeletal systems in the AnyBody Modeling System. Simul. Model. Pract. Theory 14, 1100–1111. https://doi.org/10.1016/j.simpat.2006.09.001

de Zee, M., Dalstra, M., Cattaneo, P.M., Rasmussen, J., Svensson, P., Melsen, B., 2007. Validation of a musculo-skeletal model of the mandible and its application to mandibular distraction osteogenesis. J. Biomech. 40, 1192–1201. https://doi.org/10.1016/j.jbiomech.2006.06.024

DeFrate, L.E., 2006. The 6 Degrees of Freedom Kinematics of the Knee After Anterior Cruciate Ligament Deficiency: An In Vivo Imaging Analysis. Am. J. Sports Med. 34, 1240–1246. https://doi.org/10.1177/0363546506287299

Dell'Isola, A., Allan, R., Smith, S.L., Marreiros, S.S.P., Steultjens, M., 2016. Identification of clinical phenotypes in knee osteoarthritis: a systematic review of the literature. BMC Musculoskelet. Disord. 17, 425. https://doi.org/10.1186/s12891-016-1286-2

Delp, S.L., Loan, J.P., 2000. A COMPUTATIONAL FRAMEWORKFOR SIMULATING AND ANALYZING HUMAN AND ANIMAL MOVEMENT. Comput. Sci. Eng. 2, 46.

Delp, S.L., Loan, J.P., Hoy, M.G., Zajac, F.E., Topp, E.L., Rosen, J.M., 1990. An Interactive Graphics-Based Model of the Lower Extremity to Study Orthopaedic Surgical Procedures 37, 757–767.

Demehri, S., Hafezi-nejad, N., Carrino, J.A., 2015. Conventional and novel imaging modalities in osteoarthritis: current state of the evidence 295–303. https://doi.org/10.1097/BOR.0000000000000163

Dennis, D.A., Mahfouz, M.R., Komistek, R.D., Hoff, W., 2005. In vivo determination of normal and anterior cruciate ligament-deficient knee kinematics 38, 241–253. https://doi.org/10.1016/j.jbiomech.2004.02.042

Deveza, L.A., Melo, L., Yamato, T.P., Mills, K., Ravi, V., Hunter, D.J., 2017. Knee osteoarthritis phenotypes and their relevance for outcomes: a systematic review. Osteoarthr. Cartil. 25, 1926–1941. https://doi.org/10.1016/j.joca.2017.08.009

Dillon, C.F., Rasch, E.K., Gu, Q., Hirsch, R., 2006. Prevalence of knee osteoarthritis in the United States: arthritis data from the Third National Health and Nutrition Examination Survey 1991-94. J. Rheumatol. 33, 2271 LP-2279.

Disilvestro, M.R., Suh, J.F., 2001. A cross-validation of the biphasic poroviscoelastic model of articular cartilage in unconfined compression , indentation , and confined compression 34, 519–525.

Donahue, T.L.K., Hull, M.L., Rashid, M.., Jacobs, C.R., 2002. A Finite Element Model of the Human Knee Joint for the Study of Tibio-Femoral Contact. J. Biomech. Eng. 124, 273. https://doi.org/10.1115/1.1470171

Donnelly, C.J., Lloyd, D.G., Elliott, B.C., Reinbolt, J.A., 2012. Optimizing whole-body kinematics to minimize valgus knee loading during sidestepping : Implications for ACL injury risk. J. Biomech. 45, 1491–1497. https://doi.org/10.1016/j.jbiomech.2012.02.010

Duprey, S., Cheze, L., Dumas, R., 2010. Influence of joint constraints on lower limb kinematics estimation from skin markers using global optimization. J. Biomech. 43, 2858–2862. https://doi.org/10.1016/j.jbiomech.2010.06.010

Duprey, S., Chèze, L., Dumas, R., 2009. A constraint-based approach to model the lower limb: preliminary results for running motions. Comput. Methods Biomech. Biomed. Engin. 12, 105–106.

https://doi.org/10.1080/10255840903077352

Eckstein, F., Boudreau, R.M., Wang, Z., Hannon, M.J., Wirth, W., Cotofana, S., Guermazi, A., Roemer, F.W., Nevitt, M., John, M.R., Ladel, C., Sharma, L., Hunter, D.J., Kwoh, C.K., 2014. Trajectory of Cartilage Loss within Four Years of Knee Replacement: A Nested Case-Control Study from the Osteoarthritis Initiative Felix. Osteoarthr. Cartil. 22, 1542–1549. https://doi.org/10.1021/jm4004285.QSAR

Egloff, C., Hügle, T., Valderrabano, V., 2012. Biomechanics and pathomechanisms of osteoarthritis. Swiss Med. Wkly. 142, 1–14. https://doi.org/10.4414/smw.2012.13583

Erdemir, A., Guess, T.M., Halloran, J., Tadepalli, S.C., Morrison, T.M., 2012. Considerations for reporting finite element analysis studies in biomechanics. J. Biomech. 45, 625–633. https://doi.org/10.1016/j.jbiomech.2011.11.038

Erdemir, A., McLean, S., Herzog, W., van den Bogert, A.J., 2007. Model-based estimation of muscle forces exerted during movements. Clin. Biomech. 22, 131–154. https://doi.org/10.1016/j.clinbiomech.2006.09.005

Farrokhi, S., Meholic, B., Chuang, W.N., Gustafson, J.A., Fitzgerald, G.K., Tashman, S., 2015. Altered frontal and transverse plane tibiofemoral kinematics and patellofemoral malalignments during downhill gait in patients with mixed knee osteoarthritis. J. Biomech. 48, 1707–1712. https://doi.org/10.1016/j.jbiomech.2015.05.015

Farrokhi, S., Tashman, S., Gil, A.B., Klatt, B.A., Fitzgerald, G.K., 2012. Are the kinematics of the knee joint altered during the loading response phase of gait in individuals with concurrent knee osteoarthritis and complaints of joint instability? A dynamic stereo X-ray study. Clin. Biomech. 27, 384–389. https://doi.org/10.1016/j.clinbiomech.2011.10.009

Farrokhi, S., Voycheck, C.A., Klatt, B.A., Gustafson, J.A., Tashman, S., Fitzgerald, G.K., 2014. Altered tibiofemoral joint contact mechanics and kinematics in patients with knee osteoarthritis and episodic complaints of joint instability. Clin. Biomech. 29, 629–635. https://doi.org/10.1016/j.clinbiomech.2014.04.014

Favre, J., Erhart-Hledik, J.C., Chehab, E.F., Andriacchi, T.P., 2016. General scheme to reduce the knee adduction moment by modifying a combination of gait variables. J. Orthop. Res. 34, 1547–1556. https://doi.org/10.1002/jor.23151

Feikes, J.D., Connor, J.J., Zavatsky, A.B., 2003. A constraint-based approach to

modelling the mobility of the human knee joint. J. Biomech. 36, 125–129. https://doi.org/10.1016/S0021-9290(02)00276-2

Felson, D.T., 2010. Identifying different osteoarthritis phenotypes through epidemiology. Osteoarthr. Cartil. 18, 601–604. https://doi.org/10.1016/j.joca.2010.01.007

Felson, D.T., 2006. Osteoarthritis of the knee. N. Engl. J. Med. 354, 841–848. https://doi.org/10.1016/s0140-6736(05)62494-4

Felson, D.T., Naimark, A., Anderson, J., Kazis, L., Castelli, W., Meenan, R.F., 1987. The prevalence of knee osteoarthritis in the elderly. Arthritis Rheum. 30, 914–918. https://doi.org/10.1002/art.1780300811

Fernandez-Fernandez, R., Rodriguez-Merchan, E.C., 2015. Better survival of total knee replacement in patients older than 70 years: a prospective study with 8 to 12 years follow-up. Arch. bone Jt. Surg. 3, 22–8.

Finan, P.H., Buenaver, L.F., Bounds, S.C., Hussain, S., Park, R.J., Haque, U.J., Campbell, C.M., Jennifer, A., Edwards, R.R., Smith, M.T., 2013. Discordance Between Pain and Radiographic Severity in Knee Osteoarthritis. Arthritis Rheum. 65. https://doi.org/10.1002/art.34646.Discordance

Folinais, D., Thelen, P., Delin, C., Radier, C., Catonne, Y., Lazennec, J.Y., 2013. Measuring femoral and rotational alignment: EOS system versus computed tomography. Orthop. Traumatol. Surg. Res. https://doi.org/10.1016/j.otsr.2012.12.023

Fregly, B.J., 2007. Design of Patient-Specific Gait Modifications for Knee Osteoarthritis Rehabilitation. IEEE Trans. Med. Imaging 29, 997–1003. https://doi.org/10.1016/j.biotechadv.2011.08.021.Secreted

Fregly, B.J., Besier, T.F., Lloyd, D.G., Delp, S.L., Banks, S.A., Pandy, M.G., D'Lima, D.D., 2012. Grand challenge competition to predict in vivo knee loads. J. Orthop. Res. 30, 503–13. https://doi.org/10.1002/jor.22023

Fregly, B.J., Boninger, M.L., Reinkensmeyer, D.J., 2012. Personalized neuromusculoskeletal modeling to improve treatment of mobility impairments: a perspective from European research sites. J. Neuroeng. Rehabil. 9, 18. https://doi.org/10.1186/1743-0003-9-18

Fregly, B.J., D'Lima, D.D., Colwell, C.W., 2009. Effective Gait Patterns for Offloading the Medial Compartment of the Knee. J. Orthop. Res. 27, 1016–1021. https://doi.org/Doi 10.1002/Jor.20843

Gaspar, M., Welke, B., Seehaus, F., Hurschler, C., Schwarze, M., 2017. Dynamic Time Warping compared to established methods for validation of musculoskeletal models. J. Biomech. 55, 156–161. https://doi.org/10.1016/j.jbiomech.2017.02.025

Gerbrands, T.A., Pisters, M.F., Vanwanseele, B., 2014. Clinical Biomechanics Individual selection of gait retraining strategies is essential to optimally reduce medial knee load during gait. JCLB 29, 828–834. https://doi.org/10.1016/j.clinbiomech.2014.05.005

Gerus, P., Sartori, M., Besier, T.F., Fregly, B.J., Delp, S.L., Banks, S. a., Pandy, M.G., D'Lima, D.D., Lloyd, D.G., 2013. Subject-specific knee joint geometry improves predictions of medial tibiofemoral contact forces. J. Biomech. 46, 2778–2786. https://doi.org/10.1016/j.jbiomech.2013.09.005

Gill, T.J., Velde, S.K. Van de, Wing, D.W., Oh, L.S., Hosseini, A., Li, G., 2009. Tibiofemoral and Patellofemoral Kinematics After Reconstruction of an Isolated Posterior Cruciate Ligament Injury: In Vivo Analysis During Lunge. Am. J. Phys. Anthropol. 37.

Gilles, B., Perrin, R., Magnenat-Thalmann, N., Vallee, J.-P., 2005. Bone motion analysis from dynamic MRI: acquisition and tracking. Acad. Radiol. 12, 1285–1292. https://doi.org/10.1016/j.acra.2005.08.006

Glyn-Jones, S., Palmer, A.J.R., Agricola, R., Price, A.J., Vincent, T.L., Weinans, H., Carr, A.J., 2015. Osteoarthritis. lan 386, 376–387. https://doi.org/10.1016/S0140-6736(14)60802-3

Godest, A.C., Beaugonin, M., Haug, E., Taylor, M., Gregson, P.J., 2002. Simulation of a knee joint replacement during a gait cycle using explicit finite element analysis. J. Biomech. 35, 267–275. https://doi.org/10.1016/S0021-9290(01)00179-8

Gold, G.E., Burstein, D., Dardzinski, B., Lang, P., Boada, F., Mosher, T., 2006. MRI of articular cartilage in OA: novel pulse sequences and compositional/functional markers. Osteoarthr. Cartil. 14, 76–86. https://doi.org/10.1016/j.joca.2006.03.010

Goudie, E.B., Robinson, C., Walmsley, P., Brenkel, I., 2017. Changing trends in total knee replacement. Eur. J. Orthop. Surg. Traumatol. 27, 539–544. https://doi.org/10.1007/s00590-017-1934-8

Grood, E.S., Suntay, W.., 1983. A Joint Coordinate System for the Clinical Description of Three-Dimensional Motions: Application to the Knee. J.

Biomech. Enginering 105, 136–144.

Gu, K.B., Li, L.P., 2011. A human knee joint model considering fluid pressure and fiber orientation in cartilages and menisci. Med. Eng. Phys. 33, 497–503. https://doi.org/10.1016/j.medengphy.2010.12.001

Guenoun, B., Zadegan, F., Aim, F., Hannouche, D., Nizard, R., 2012. Reliability of a new method for lower-extremity measurements based on stereoradiographic three-dimensional reconstruction. Orthop. Traumatol. Surg. Res. https://doi.org/10.1016/j.otsr.2012.03.014

Guermazi, A., Roemer, F.W., Hayashi, D., Crema, M.D., Niu, J., Zhang, Y., Marra, M.D., Katur, A., Lynch, J.A., El-Khoury, G.Y., Baker, K., Hughes, L.B., Nevitt, M.C., Felson, D.T., 2011. Assessment of synovitis with contrast-enhanced MRI using a whole-joint semiquantitative scoring system in people with, or at high risk of, knee osteoarthritis: The MOST study. Ann. Rheum. Dis. 70, 805–811. https://doi.org/10.1136/ard.2010.139618

Guess, T.M., Stylianou, A.P., Kia, M., 2014. Concurrent prediction of muscle and tibiofemoral contact forces during treadmill gait. J. Biomech. Eng. 136, 021032:1-9. https://doi.org/10.1115/1.4026359

Guess, T.M., Thiagarajan, G., Kia, M., Mishra, M., 2010. A subject specific multibody model of the knee with menisci. Med. Eng. Phys. 32, 505–515. https://doi.org/10.1016/j.medengphy.2010.02.020

Gustafson, J.A., Robinson, M.E., Fitzgerald, G.K., Tashman, S., Farrokhi, S., 2015. Knee motion variability in patients with knee osteoarthritis: The effect of self-reported instability. Clin. Biomech. 30, 475–480. https://doi.org/10.1016/j.clinbiomech.2015.03.007

Habachi, A. El, Moissenet, F., Duprey, S., Cheze, L., Dumas, R., 2015. Global sensitivity analysis of the joint kinematics during gait to the parameters of a lower limb multi ‐ body model. Med. Biol. Eng. Comput. 655–667. https://doi.org/10.1007/s11517-015-1269-8

Halonen, K.S., 2015. Validation and application of computational knee joint models Finite element modeling analysis. University of Eastern Finland.

Halonen, K.S., Dzialo, C.M., Mannisi, M., Venäläinen, M.S., Zee, M. De, Andersen, M.S., 2017. Workflow assessing the effect of gait alterations on stresses in the medial tibial cartilage – combined musculoskeletal modelling and finite element analysis. Sci. Rep. 7, 17396. https://doi.org/10.1038/s41598-017-17228-x

Halonen, K.S., Mononen, M.E., Jurvelin, J.S., Korhonen, R.K., 2016. Importance of Patella , Quadriceps Forces , and Depthwise Cartilage Structure on Knee Joint Motion and Cartilage Response During Gait 138, 1–11. https://doi.org/10.1115/1.4033516

Halonen, K.S., Mononen, M.E., Jurvelin, J.S., To, J., 2014. Deformation of articular cartilage during static loading of a knee joint – Experimental and fi nite element analysis 47, 2467–2474. https://doi.org/10.1016/j.jbiomech.2014.04.013

Halonen, K.S., Mononen, M.E., Jurvelin, J.S., Töyräs, J., Korhonen, R.K., 2013. Importance of depth-wise distribution of collagen and proteoglycans in articular cartilage—A 3D finite element study of stresses and strains in human knee joint. J. Biomech. 46, 1184–1192. https://doi.org/10.1016/j.jbiomech.2012.12.025

Halonen, K.S., Mononen, M.E., Jurvelin, J.S., Töyräs, J., Salo, J., Korhonen, R.K., 2014. Deformation of articular cartilage during static loading of a knee joint – Experimental and finite element analysis. J. Biomech. 47, 2467–2474. https://doi.org/10.1016/j.jbiomech.2014.04.013

Halonen, K.S., Mononen, M.E., Töyräs, J., Kröger, H., Joukainen, A., Korhonen, R.K., 2016. Optimal graft stiffness and pre-strain restore normal joint motion and cartilage responses in ACL reconstructed knee. J. Biomech. 1–11. https://doi.org/10.1016/j.jbiomech.2016.05.002

Hamai, S., Dunbar, N.J., Moro-Oka, T.A., Miura, H., Iwamoto, Y., Banks, S.A., 2013. Physiological sagittal plane patellar kinematics during dynamic deep knee flexion. Int. Orthop. 37, 1477–1482. https://doi.org/10.1007/s00264-013-1958-6

Handsfield, G.G., Meyer, C.H., Hart, J.M., Abel, M.F., Blemker, S.S., 2014. Relationships of 35 lower limb muscles to height and body mass quantified using MRI. J. Biomech. 47, 631–638. https://doi.org/10.1016/j.jbiomech.2013.12.002

Hast, M.W., Piazza, S.J., 2013. Dual-joint modeling for estimation of total knee replacement contact forces during locomotion. J. Biomech. Eng. 135, 021013. https://doi.org/10.1115/1.4023320

Hayashi, D., Roemer, F.W., Guermazi, A., 2016. Imaging for osteoarthritis. Ann. Phys. Rehabil. Med. 59, 161–169. https://doi.org/10.1016/j.rehab.2015.12.003

Hayes, W.C., Swenson, L.W., Schurman, D.J., 1978. Axisymmetric finite element analysis of the lateral tibial plateau. J. Biomech. 11, 21–33. https://doi.org/10.1016/0021-9290(78)90040-4

Heidari, B., Hajian-Tilaki, K., Babaei, M., 2016. Determinants of pain in patients with symptomatic knee osteoarthritis. Casp. J. Intern. Med. 7, 153–161.

Heiden, T.L., Lloyd, D.G., Ackland, T.R., 2009. Knee joint kinematics, kinetics and muscle co-contraction in knee osteoarthritis patient gait. Clin. Biomech. (Bristol, Avon) 24, 833–41. https://doi.org/10.1016/j.clinbiomech.2009.08.005

Heimann, T., Meinzer, H.P., 2009. Statistical shape models for 3D medical image segmentation: A review. Med. Image Anal. 13, 543–563. https://doi.org/10.1016/j.media.2009.05.004

Heinen, F., Lund, M.E., Rasmussen, J., De Zee, M., 2016. Muscle-tendon unit scaling methods of Hill-type musculoskeletal models: An overview. Proc. Inst. Mech. Eng. Part H J. Eng. Med. 230, 976–984. https://doi.org/10.1177/0954411916659894

Heinlein, B., Graichen, F., Bender, A., Rohlmann, A., Bergmann, G., 2007. Design, calibration and pre-clinical testing of an instrumented tibial tray. J. Biomech. 40, 4–10. https://doi.org/10.1016/j.jbiomech.2007.02.014

Herzog, B.M.N. and W., 2006. Biomechanics of the Musculo-skeletal System, 3rd Ed. ed. Wiley, Calgary, Canada.

Hicks, J.L., Uchida, T.K., Seth, A., Rajagopal, A., Delp, S., 2015. Is my model good enough? Best practices for verification and validation of musculoskeletal models and simulations of human movement. J. Biomech. Eng. 137. https://doi.org/10.1115/1.4029304

Hinman, R.S., Bowles, K.A., Metcalf, B.B., Wrigley, T. V., Bennell, K.L., 2012. Lateral wedge insoles for medial knee osteoarthritis: Effects on lower limb frontal plane biomechanics. Clin. Biomech. 27, 27–33. https://doi.org/10.1016/j.clinbiomech.2011.07.010

Hoshaw, S.J., Fyhrie, D.P., Takano, Y., Burr, D.B., Milgrom, C., 1997. A method suitable for in vivo measurement of bone strain in humans. J. Biomech. 30, 521–524. https://doi.org/10.1016/S0021-9290(96)00176-5

Hoshi, K., Watanabe, G., Kurose, Y., Tanaka, R., Fujii, J., Gamada, K., 2016. International Journal of Physical Medicine & Rehabilitation New Findings in Six-degrees-of-freedom Kinematics during Stationary Stepping in Patients with Knee Osteoarthritis 4. https://doi.org/10.4172/2329-9096.1000381

Hosseini, S.M., Wilson, W., Ito, K., Van Donkelaar, C.C., 2014. A numerical model to study mechanically induced initiation and progression of damage in articular

cartilage. Osteoarthr. Cartil. 22, 95–103. https://doi.org/10.1016/j.joca.2013.10.010

Hoy, M.., Zajac, F.E., Gordon, M.E., 1990. A MUSCULOSKELETAL MODEL OF THE HUMAN LOWER EXTREMITY : THE EFFECT OF MUSCLE , TENDON , AND MOMENT ARM ON THE MOMENT-ANGLE RELATIONSHIP OF MUSCULOTENDON ACTUATORS AT THE HIP , KNEE , AND ANKLE. J. Biomech. 23, 157–169.

Hug, F., 2011. Can muscle coordination be precisely studied by surface electromyography? J. Electromyogr. Kinesiol. 21, 1–12. https://doi.org/10.1016/j.jelekin.2010.08.009

Hunt, M.A., Birmingham, T.B., Bryant, D., Jones, I., Giffin, J.R., Jenkyn, T.R., Vandervoort, A.A., 2008. Lateral trunk lean explains variation in dynamic knee joint load in patients with medial compartment knee osteoarthritis. Osteoarthr. Cartil. 16, 591–599. https://doi.org/10.1016/j.joca.2007.10.017

Hunt, M.A., Takacs, J., 2014. Effects of a 10-week toe-out gait modification intervention in people with medial knee osteoarthritis: A pilot, feasibility study. Osteoarthr. Cartil. 22, 904–911. https://doi.org/10.1016/j.joca.2014.04.007

Hunter, D.J., Guermazi, A., Lo, G.H., Grainger, A.J., Conaghan, P.G., Boudreau, R.M., Roemer, F.W., 2011. Evolution of semi-quantitative whole joint assessment of knee OA : MOAKS (MRI Osteoarthritis Knee Score) 19. https://doi.org/10.1016/j.joca.2011.05.004

Hunter, D.J., Lo, G.H., Gale, D., Grainger, A.J., Guermazi, A., Conaghan, P.G., 2008. The reliability of a new scoring system for knee osteoarthritis MRI and the validity of bone marrow lesion assessment: BLOKS (Boston-Leeds Osteoarthritis Knee Score). Ann. Rheum. Dis. 67, 206–211. https://doi.org/10.1136/ard.2006.066183

Illés, T., Somoskeöy, S., 2012. The EOS™ imaging system and its uses in daily orthopaedic practice. Int. Orthop. https://doi.org/10.1007/s00264-012-1512-y

Isola, A.D., Steultjens, M., 2018. Classification of patients with knee osteoarthritis in clinical phenotypes : Data from the osteoarthritis initiative 1–18.

Iwaki, H., Pinskerova, V., Freeman, M.A.R., 2000. Tibiofemoral movement 1: the shapes and relative movements of the femur and tibia in the unloaded cadaver knee. J. Bone Joint Surg. Br. 82, 1189–1195. https://doi.org/10.1302/0301-620x.82b8.10717

Javaid, M.K., Lynch, J.A., Tolstykh, I., Guermazi, A., Roemer, F., Aliabadi, P., McCulloch, C., Curtis, J., Felson, D., Lane, N.E., Torner, J., Nevitt, M., 2010. Pre-radiographic MRI findings are associated with onset of knee symptoms: the most study. Osteoarthr. Cartil. 18, 323–328. https://doi.org/10.1016/j.joca.2009.11.002

Jordan, J.M., Helmick, C.G., Renner, J.B., Luta, G., Dragomir, A.D., Woodard, J., Fang, F., Schwartz, T.A., Abbate, L.M., Callahan, L.F., Kalsbeek, W.D., Hochberg, M.C., 2007. Prevalence of knee symptoms and radiographic and symptomatic knee osteoarthritis in African Americans and Caucasians: the Johnston County Osteoarthritis Project. J. Rheumatol. 34, 172 LP-180.

Julkunen, P., Kiviranta, P., Wilson, W., Jurvelin, J.S., Korhonen, R.K., 2007. Characterization of articular cartilage by combining microscopic analysis with a fibril-reinforced finite-element model. J. Biomech. 40, 1862–70. https://doi.org/10.1016/j.jbiomech.2006.07.026

Kakihana, W., Akai, M., Nakazawa, K., Takashima, T., Naito, K., Torii, S., 2005. Effects of laterally wedged insoles on knee and subtalar joint moments. Arch. Phys. Med. Rehabil. 86, 1465–1471. https://doi.org/10.1016/j.apmr.2004.09.033

Kia, M., Stylianou, A.P., Guess, T.M., 2014. Evaluation of a musculoskeletal model with prosthetic knee through six experimental gait trials. Med. Eng. Phys. 36, 335–344. https://doi.org/10.1016/j.medengphy.2013.12.007

Kiadaliri, A.A., Lohmander, L.S., Moradi-Lakeh, M., Petersson, I.F., Englund, M., 2018. High and rising burden of hip and knee osteoarthritis in the Nordic region, 1990–2015: Findings from the Global Burden of Disease Study 2015. Acta Orthop. 89, 177–183. https://doi.org/10.1080/17453674.2017.1404791

Kingsbury, S.R., Gross, H.J., Isherwood, G., Conaghan, P.G., 2014. Osteoarthritis in europe: Impact on health status, work productivity and use of pharmacotherapies in five European countries. Rheumatol. (United Kingdom) 53, 937–947. https://doi.org/10.1093/rheumatology/ket463

Kinney, A.L., Besier, T.F., 2013. Update on Grand Challenge Competition to Predict in Vivo Knee Loads 135, 1–4. https://doi.org/10.1115/1.4023255

Kirking, B., Krevolin, J., Townsend, C., Colwell, C.W., D'Lima, D.D., 2006. A multiaxial force-sensing implantable tibial prosthesis. J. Biomech. 39, 1744–1751. https://doi.org/10.1016/j.jbiomech.2005.05.023

Klein Horsman, M.D., Koopman, H.F.J.M., van der Helm, F.C.T., Prosé, L.P.,

Veeger, H.E.J., 2007. Morphological muscle and joint parameters for musculoskeletal modelling of the lower extremity. Clin. Biomech. 22, 239–247. https://doi.org/10.1016/j.clinbiomech.2006.10.003

KNEEMO: Initial Training Network in Knee Osteoarthritis Research [WWW Document], n.d. . https://www.kneemo.eu/.

Komistek, R.D., Dennis, D.A., 2003. In Vivo Fluoroscopic Analysis of the Normal Human Knee. Clin. Orthop. Relat. Res. 410, 69–81. https://doi.org/10.1097/01.blo.0000062384.79828.3b

Kornaat, P.R., Ceulemans, R.Y.T., Kroon, H.M., Riyazi, N., Kloppenburg, M., Carter, W.O., Woodworth, T.G., Bloem, J.L., 2005. MRI assessment of knee osteoarthritis: Knee Osteoarthritis Scoring System (KOSS) - Inter-observer and intra-observer reproducibility of a compartment-based scoring system. Skeletal Radiol. 34, 95–102. https://doi.org/10.1007/s00256-004-0828-0

Kozanek, M. et. al., 2010. Tibiofemoral Kinematics and Condylar Motion During. Bioengineering 42, 1877–1884. https://doi.org/10.1016/j.jbiomech.2009.05.003.TIBIOFEMORAL

Landinez-Parra, N.S., Garzón-Alvarado, D.A., Vanegas-Acosta, J.C., 2011. A phenomenological mathematical model of the articular cartilage damage. Comput. Methods Programs Biomed. 104, e58–e74. https://doi.org/10.1016/j.cmpb.2011.02.003

Lawrence, J.H.K.J.S., 1957. RADIOLOGICAL ASSESSMENT OF OSTEO-ARTHROSIS. Ann. Rheum. Dis. 16, 494–502.

Lawrence, R.C., Felson, D.T., Helmick, C.G., Arnold, L.M., Choi, H., Deyo, R.A., Gabriel, S., Hirsch, R., Hochberg, M.C., Hunder, G.G., Jordan, J.M., Katz, J.N., Kremers, H.M., Wolfe, F., 2008. Estimates of the prevalence of arthritis and other rheumatic conditions in the United States. Part II. Arthritis Rheum. 58, 26–35. https://doi.org/10.1002/art.23176

Lenhart, R.L., Kaiser, J., Smith, C.R., Thelen, D.G., 2015. Prediction and Validation of Load-Dependent Behavior of the Tibiofemoral and Patellofemoral Joints During Movement. Ann. Biomed. Eng. 43, 2675–2685.

Lerner, Z.F., Demers, M.S., Delp, S.L., Browning, R.C., 2015. How tibiofemoral alignment and contact locations affect predictions of medial and lateral tibiofemoral contact forces. J. Biomech. 48, 644–650. https://doi.org/10.1016/j.jbiomech.2014.12.049

Lewinson, R.T., Stefanyshyn, D.J., 2016. Wedged Insoles and Gait in Patients with Knee Osteoarthritis: A Biomechanical Review. Ann. Biomed. Eng. 44, 3173–3185. https://doi.org/10.1007/s10439-016-1696-1

Li, G., 2004. Feasibility of Using Orthogonal Fluoroscopic Images to Measure In Vivo Joint Kinematics. J. Biomech. Eng. 126, 313. https://doi.org/10.1115/1.1691448

Li, G., Gil, J., Kanamori, A., Woo, S.L.-Y., 1999. A Validated Three-Dimensional Computational Model of a Human Knee Joint. J. Biomech. Eng. 121, 657. https://doi.org/10.1115/1.2800871

Li, G., Kozanek, M., Hosseini, A., Liu, F., Van de Velde, S.K., Rubash, H.E., 2009. New fluoroscopic imaging technique for investigation of 6DOF knee kinematics during treadmill gait. J. Orthop. Surg. Res. 4, 6. https://doi.org/10.1186/1749-799X-4-6

Li, G., Papannagari, R., Nha, K.W., Defrate, L.E., Gill, T.J., Rubash, H.E., 2007. The coupled motion of the femur and patella during in vivo weightbearing knee flexion. J. Biomech. Eng. 129, 937–43. https://doi.org/10.1115/1.2803267

Li, G., Van de Velde, S.K., Bingham, J.T., 2008. Validation of a non-invasive fluoroscopic imaging technique for the measurement of dynamic knee joint motion. J. Biomech. 41, 1616–1622. https://doi.org/10.1016/j.jbiomech.2008.01.034

Li, J., Freiberg, A., Rubash, H.E., 2013. Prediction of In Vivo Knee Joint Kinematics Using a Combined Dual Fluoroscopy Imaging and Statistical Shape Modeling Technique 1–6. https://doi.org/10.1115/1.4028819

Li, L.P., Herzog, W., 2004. The role of viscoelasticity of collagen fibers in articular cartilage : Theory and numerical formulation 41, 181–194.

Litwic, A., Edwards, M., 2013. Europe PMC Funders Group Epidemiology and Burden of Osteoarthritis. Br. Med. Bull. 105, 185–199. https://doi.org/10.1093/bmb/lds038.Epidemiology

Liu, X., Ouyang, J., Fan, Y., Zhang, M., 2016. A Footwear–Foot–Knee Computational Platform for Exploring Footwear Effects on Knee Joint Biomechanics. J. Med. Biol. Eng. 36, 245–256. https://doi.org/10.1007/s40846-016-0126-z

Liukkonen, M.K., Mononen, M.E., Klets, O., Arokoski, J.P., Saarakkala, S., Korhonen, R.K., 2017. Simulation of subject-specific progression of knee

osteoarthritis and comparison to experimental follow-up data: Data from the osteoarthritis initiative. Sci. Rep. 7, 1–14. https://doi.org/10.1038/s41598-017-09013-7

Lloyd, D.G., Besier, T.F., 2003. An EMG-driven musculoskeletal model to estimate muscle forces and knee joint moments in vivo. J. Biomech. 36, 765–776. https://doi.org/10.1016/S0021-9290(03)00010-1

Losina, E., Thornhill, T.S., Rome, B.N., Wright, J., Katz, J.N., 2012. The dramatic increase in total knee replacement utilization rates in the United States cannot be fully explained by growth in population size and the obesity epidemic. J. Bone Joint Surg. Am. 94, 201–7. https://doi.org/10.2106/JBJS.J.01958

Lu, T.W., O'Connor, J.J., 1999. Bone position estimation from skin marker co-ordinates using global optimisation with joint constraints. J. Biomech. 32, 129–134. https://doi.org/10.1016/S0021-9290(98)00158-4

Lund, M.E., Andersen, M.S., Zee, M. De, Rasmussen, J., 2015. Scaling of musculoskeletal models from static and dynamic trials 37–41. https://doi.org/10.1080/23335432.2014.993706

Lund, M.E., de Zee, M., Andersen, M.S., Rasmussen, J., 2012. On validation of multibody musculoskeletal models. Proc. Inst. Mech. Eng. H. 226, 82–94. https://doi.org/10.1177/0954411911431516

Lundberg, H.J., Knowlton, C., Wimmer, M. a, 2013. Fine tuning total knee replacement contact force prediction algorithms using blinded model validation. J. Biomech. Eng. 135, 21015. https://doi.org/10.1115/1.4023388; 10.1115/1.4023388

Madaleno, F.O., Santos, B.A., Araújo, V.L., Oliveira, V.C., Resende, R.A., 2018. Prevalence of knee osteoarthritis in former athletes: a systematic review with meta-analysis. Brazilian J. Phys. Ther. 22, 437–451. https://doi.org/10.1016/j.bjpt.2018.03.012

Maly, M.R., Acker, S.M., Totterman, S., Tamez-Peña, J., Stratford, P.W., Callaghan, J.P., Adachi, J.D., Beattie, K.A., 2015. Knee adduction moment relates to medial femoral and tibial cartilage morphology in clinical knee osteoarthritis. J. Biomech. 48, 3495–3501. https://doi.org/10.1016/j.jbiomech.2015.04.039

Manal, K., Buchanan, T.S., 2013. An electromyogram-driven musculoskeletal model of the knee to predict in vivo joint contact forces during normal and novel gait patterns. J. Biomech. Eng. 135, 021014. https://doi.org/10.1115/1.4023457

Marra, M.A., Strzelczak, M., Heesterbeek, P.J.C., van de Groes, S.A.W., Janssen, D.W., Koopman, B.F.J.M., Wymenga, A.B., Verdonschot, N.J.J., 2017. Anterior referencing of tibial slope in total knee arthroplasty considerably influences knee kinematics: a musculoskeletal simulation study. Knee Surgery, Sport. Traumatol. Arthrosc. 1–9. https://doi.org/10.1007/s00167-017-4561-3

Marra, M.A., Vanheule, V., Fluit, R., Koopman, B.H.F.J.M., Rasmussen, J., Verdonschot, N., Andersen, M.S., 2015. A Subject-Specific Musculoskeletal Modeling Framework to Predict In Vivo Mechanics of Total Knee Arthroplasty. J. Biomech. Eng. 137, 020904. https://doi.org/10.1115/1.4029258

Martel-Pelletier, J., Barr, A.J., Cicuttini, F.M., Conaghan, P.G., Cooper, C., Goldring, M.B., Goldring, S.R., Jones, G., Teichtahl, A.J., Pelletier, J.-P., 2016. Osteoarthritis. Nat. Rev. Dis. Prim. 2, 1–18. https://doi.org/10.1038/nrdp.2016.72

Maxwell, S.E., Delaney, H.D., Planer, J., 2013. Stats: Designing Experiments Ch9-10. J. Chem. Inf. Model. 53, 1689–1699. https://doi.org/10.1017/CBO9781107415324.004

McAlindon, T.E., Bannuru, R.R., Sullivan, M.C., Arden, N.K., Berenbaum, F., Bierma-Zeinstra, S.M., Hawker, G.A., Henrotin, Y., Hunter, D.J., Kawaguchi, H., Kwoh, K., Lohmander, S., Rannou, F., Roos, E.M., Underwood, M., 2014. OARSI guidelines for the non-surgical management of knee osteoarthritis. Osteoarthr. Cartil. 22, 363–388. https://doi.org/10.1016/j.joca.2014.01.003

Michael J Rainbow, Ph.D, Daniel L Miranda, Ph.D, Roy T.H. Cheung, Ph.D, Joel B Schwartz, Sc.B., Joseph J Crisco, Ph.D., Irene S Davis, Ph.D, P.T., and B.C., Fleming, P.D., 2013. Automatic Determination of an Anatomical Coordinate System for a Three-Dimensional Model of the Human Patella Michael. J. Biomech. 46, 2093–2096. https://doi.org/10.1037/a0013262.Open

Millard, M., Uchida, T., Seth, A., Delp, S.L., 2013. Flexing Computational Muscle : Modeling and Simulation of Musculotendon Dynamics 135, 1–11. https://doi.org/10.1115/1.4023390

Miller, R.H., Esterson, A.Y., Shim, J.K., 2015. Joint contact forces when minimizing the external knee adduction moment by gait modification: A computer simulation study. Knee 22, 481–489. https://doi.org/10.1016/j.knee.2015.06.014

Mills, K., Hunt, M.A., Ferber, R., 2013. Biomechanical deviations during level walking associated with knee osteoarthritis: A systematic review and meta-analysis. Arthritis Care Res. 65, 1643–1665. https://doi.org/10.1002/acr.22015

Miranda, D.L., Rainbow, M.J., Leventhal, E.L., Crisco, J.J., Fleming, B.C., 2010. Automatic determination of anatomical coordinate systems for three-dimensional bone models of the isolated human knee. J. Biomech. 43, 1623–1626. https://doi.org/10.1016/j.jbiomech.2010.01.036

Moissenet, F., Chèze, L., Dumas, R., 2016. Influence of the Level of Muscular Redundancy on the Validity of a Musculoskeletal Model. J. Biomech. Eng. 138, 021019. https://doi.org/10.1115/1.4032127

Moissenet, F., Chèze, L., Dumas, R., 2014. A 3D lower limb musculoskeletal model for simultaneous estimation of musculo-tendon, joint contact, ligament and bone forces during gait. J. Biomech. 47, 50–58. https://doi.org/10.1016/j.jbiomech.2013.10.015

Moissenet, F., Chèze, L., Dumas, R., 2012. Anatomical kinematic constraints: Consequences on musculo-tendon forces and joint reactions. Multibody Syst. Dyn. 28, 125–141. https://doi.org/10.1007/s11044-011-9286-3

Moissenet, F., Modenese, L., Dumas, R., 2017. Alterations of musculoskeletal models for a more accurate estimation of lower limb joint contact forces during normal gait: A systematic review. J. Biomech. 63, 8–20. https://doi.org/10.1016/j.jbiomech.2017.08.025

Mononen, M.E., Jurvelin, J.S., Korhonen, R.K., 2015. Computer Methods in Biomechanics and Biomedical Engineering Implementation of a gait cycle loading into healthy and meniscectomised knee joint models with fibril-reinforced articular cartilage. Comput. Methods Biomech. Biomed. Engin. https://doi.org/10.1080/10255842.2013.783575

Mononen, M.E., Jurvelin, J.S., Korhonen, R.K., 2013. Effects of radial tears and partial meniscectomy of lateral meniscus on the knee joint mechanics during the stance phase of the gait cycle - A 3D finite element study. J. Orthop. Res. 31, 1208–1217. https://doi.org/10.1002/jor.22358

Mononen, M.E., Mikkola, M.T., Julkunen, P., Ojala, R., Nieminen, M.T., Jurvelin, J.S., Korhonen, R.K., 2012. Effect of superficial collagen patterns and fibrillation of femoral articular cartilage on knee joint mechanics — A 3D finite element analysis. J. Biomech. 45, 579–587. https://doi.org/10.1016/j.jbiomech.2011.11.003

Mootanah, R., Imhauser, C.W., Reisse, F., Carpanen, D., Walker, R.W., Koff, M.F., Lenhoff, M.W., Rozbruch, R., Fragomen, A.T., Kirane, Y.M., Rozbruch, S.R., Dewan, Z., Cheah, K., Dowell, J.K., Hillstrom, H.J., 2014. Development and Verification of a Computational Model of the Knee Joint for the Evaluation of

Surgical Treatments for Osteoarthritis. Comput. Methods Biomech. Biomed. Engin. https://doi.org/10.1080/10255842.2014.899588

Moro-oka, T.-A., Hamai, S., Miura, H., Shimoto, T., Higaki, H., Fregly, B.J., Iwamoto, Y., Banks, S.A., 2008. Dynamic Activity Dependence of In Vivo Normal Knee Kinematics. J. Orthop. Res. 26, 428–434. https://doi.org/10.1002/jor.20488

Mow, V.C., 1989. A NUMERICAL ALGORITHM AND AN EXPERIMENTAL 22, 853–861.

Mow, V.C., Holmes, M.H., Lai, W.M., 1984. FLUID TRANSPORT AND MECHANICAL PROPERTIES OF ARTICULAR CARTILAGE: A REVIEW. J. Biomech. 17, 377–394.

Mow, V.C., Kuei, S.C., Lai, W.M., Armstrong, C.G., 1980. Biphasic Creep and Stress Relaxation of Articular Cartilage in Compression: Theory and Experiments. J. Biomech. Eng. 102, 73–84.

Mündermann, A., Asay, J.L., Mündermann, L., Andriacchi, T.P., 2008. Implications of increased medio-lateral trunk sway for ambulatory mechanics. J. Biomech. 41, 165–170. https://doi.org/10.1016/j.jbiomech.2007.07.001

Murawski, C.D., Kennedy, J.G., 2013. Operative treatment of osteochondral lesions of the talus. J. Bone Jt. Surg. - Ser. A 95, 1045–1054. https://doi.org/10.2106/JBJS.L.00773

Myers, C. a., Torry, M.R., Shelburne, K.B., Giphart, J.E., LaPrade, R.F., Woo, S.L.-Y., Steadman, J.R., 2012. In Vivo Tibiofemoral Kinematics During 4 Functional Tasks of Increasing Demand Using Biplane Fluoroscopy. Am. J. Sports Med. 40, 170–178. https://doi.org/10.1177/0363546511423746

Myers, C.A., Torry, M.R., Peterson, D.S., Shelburne, K.B., Giphart, J.E., Krong, J.P., Woo, S.L.-Y., Steadman, J.R., 2011. Measurements of tibiofemoral kinematics during soft and stiff drop landings using biplane fluoroscopy. Am. J. Sports Med. 39, 1714–22. https://doi.org/10.1177/0363546511404922

National Institute for Health and Clinical Excellence, 2014. Osteoarthritis Care and management in adults. London NICE CG177.

Nelson, F.R.T., 2018. The Value of Phenotypes in Knee Osteoarthritis Research. Open Orthop. J. 12, 105–114. https://doi.org/10.2174/1874325001812010105

Neptune, R.R., Bogert, A.J. Van Den, 1998. Standard mechanical energy analyses do

not correlate with muscle work in cycling 31, 239–245.

Neptune, R.R., McGowan, C.P., Kautz, S.A., 2010. Forward Dynamics Simulations Provide insight into Muscle Mechanical Work during Human Locomotion Richard. Exerc. Sport Sci. Rev. 37, 203–210. https://doi.org/10.1097/JES.0b013e3181b7ea29.Forward

Nolte, D., Tsang, C.K., Zhang, K.Y., Ding, Z., Kedgley, A.E., Bull, A.M.J., 2016. Non-linear scaling of a musculoskeletal model of the lower limb using statistical shape models. J. Biomech. 49, 3576–3581. https://doi.org/10.1016/j.jbiomech.2016.09.005

Ogaya, S., Naito, H., Iwata, A., Higuchi, Y., Fuchioka, S., Tanaka, M., 2014. Knee adduction moment and medial knee contact force during gait in older people. Gait Posture 40, 341–345. https://doi.org/10.1016/j.gaitpost.2014.04.205

Olesen, C.G., De Zee, M., Rasmussen, J., 2014. Comparison between a computational seated human model and experimental verification data. Appl. Bionics Biomech. 11, 175–183. https://doi.org/10.3233/ABB-140105

Oliveria, S.A., Felson, D.T., Reed, J.I., Cirillo, P.A., Walker, A.M., 1995. Incidence of symptomatic hand, hip, and knee osteoarthritis among patients in a health maintenance organization. Arthritis Rheum. 38, 1134–1141. https://doi.org/10.1002/art.1780380817

Pabinger, C., Berghold, A., Boehler, N., Labek, G., 2013. Revision rates after knee replacement: Cumulative results from worldwide clinical studies versus joint registers. Osteoarthr. Cartil. 21, 263–268. https://doi.org/10.1016/j.joca.2012.11.014

Palazzo, C., Nguyen, C., Lefevre-Colau, M.M., Rannou, F., Poiraudeau, S., 2016. Risk factors and burden of osteoarthritis. Ann. Phys. Rehabil. Med. 59, 134–138. https://doi.org/10.1016/j.rehab.2016.01.006

Parkes, M.J., Maricar, N., Lunt, M., LaValley, M.P., Jones, R.K., Segal, N. a, Takahashi-Narita, K., Felson, D.T., 2013. Lateral wedge insoles as a conservative treatment for pain in patients with medial knee osteoarthritis: a meta-analysis. JAMA 310, 722–30. https://doi.org/10.1001/jama.2013.243229

Parra, W.C.H., Chatterjee, H.J., Soligo, C., 2012. Calculating the axes of rotation for the subtalar and talocrural joints using 3D bone reconstructions. J. Biomech. 45, 1103–1107. https://doi.org/10.1016/j.jbiomech.2012.01.011

Pedersen, D., Vanheule, V., Wirix-Speetjens, R., Taylan, O., Delport, H.P., Scheys,

L., Andersen, M.S., 2018. A novel non-invasive method for measuring knee joint laxity in 6-DOF: in vitro proof-of-concept and validation. J. Biomech. https://doi.org/10.1016/j.jbiomech.2018.10.016

Pellikaan, P., van der Krogt, M.M., Carbone, V., Fluit, R., Vigneron, L.M., Van Deun, J., Verdonschot, N., Koopman, H.F.J.M., 2013. Evaluation of a morphing based method to estimate muscle attachment sites of the lower extremity. J. Biomech. 47, 1144–1150. https://doi.org/10.1016/j.jbiomech.2013.12.010

Peña, E., Calvo, B., Martínez, M. a., Doblaré, M., 2006. A three-dimensional finite element analysis of the combined behavior of ligaments and menisci in the healthy human knee joint. J. Biomech. 39, 1686–1701. https://doi.org/10.1016/j.jbiomech.2005.04.030

Penny, P., Geere, J., Smith, T.O., 2013. A systematic review investigating the efficacy of laterally wedged insoles for medial knee osteoarthritis. Rheumatol. Int. 33, 2529–2538. https://doi.org/10.1007/s00296-013-2760-x

Perez-blanca, A., Eng, M., Espejo-baena, A., Espejo-reina, A., López, C.Q., Juanco, F.E., Eng, M., Ph, D., 2016. Alterations After Lateral Meniscus Posterior Root. Arthrosc. J. Arthrosc. Relat. Surg. 32, 624–633. https://doi.org/10.1016/j.arthro.2015.08.040

Peterfy, C.G., Guermazi, A., Zaim, S., Tirman, P.F.J., Miaux, Y., White, D., Kothari, M., Lu, Y., Fye, K., Zhao, S., Genant, H.K., 2004. Whole-organ magnetic resonance imaging score (WORMS) of the knee in osteoarthritis. Osteoarthr. Cartil. 12, 177–190. https://doi.org/10.1016/j.joca.2003.11.003

Peterfy, C.G., Schneider, E., Nevitt, M., 2008. The osteoarthritis initiative: report on the design rationale for the magnetic resonance imaging protocol for the knee. Osteoarthr. Cartil. 16, 1433–1441. https://doi.org/10.1016/j.joca.2008.06.016

Pianigiani, S., Croce, D., D'Aiuto, M., Pascale, W., Innocenti, B., 2017. Sensitivity analysis of the material properties of different soft-tissues: Implications for a subject-specific knee arthroplasty. Muscles. Ligaments Tendons J. 7, 546–557.

Piazza, S.J., 2006. Muscle-driven forward dynamic simulations for the study of normal and pathological gait. J. Neuroeng. Rehabil. 3, 5. https://doi.org/10.1186/1743-0003-3-5

Pizzolato, C., Reggiani, M., Saxby, D.J., Ceseracciu, E., Modenese, L., Lloyd, D.G., 2017. Biofeedback for Gait Retraining Based on Real-Time Estimation of Tibiofemoral Joint Contact Forces. IEEE Trans. Neural Syst. Rehabil. Eng. A Publ. IEEE Eng. Med. Biol. Soc. 25, 1612–1621.

https://doi.org/10.1109/TNSRE.2017.2683488

Pontonnier, C., Dumont, G., 2010. From motion capture to muscle forces in the human elbow aimed at improving the ergonomics of workstations. Virtual Phys. Prototyp. 5, 113–122. https://doi.org/10.1080/17452759.2010.504082

Pontonnier, C., Zee, M. De, Samani, A., Dumont, G., Madeleine, P., Beaulieu, C. De, Lann, C.D.K., Technologies, P., 2011. Trend Validation of a Musculoskeletal Model With a Workstation Design Parameter 3–4.

Qi, W., Hosseini, A., Tsai, T.Y., Li, J.S., Rubash, H.E., Li, G., 2013. In vivo kinematics of the knee during weight bearing high flexion. J. Biomech. 46, 1576–1582. https://doi.org/10.1016/j.jbiomech.2013.03.014

Quijano, S., Serrurier, A., Aubert, B., Laporte, S., Thoreux, P., Skalli, W., 2013. Three-dimensional reconstruction of the lower limb from biplanar calibrated radiographs. Med. Eng. Phys. https://doi.org/10.1016/j.medengphy.2013.07.002

Rasmussen, J., Damsgaard, M., Voigt, M., 2001. Muscle recruitment by the min/max criterion - A comparative numerical study. J. Biomech. 34, 409–415. https://doi.org/10.1016/S0021-9290(00)00191-3

Rayfield, E.J., 2007. Finite Element Analysis and Understanding the Biomechanics and Evolution of Living and Fossil Organisms. Annu. Rev. Earth Planet. Sci. 35, 541–576. https://doi.org/10.1146/annurev.earth.35.031306.140104

Reinbolt, J. a., Schutte, J.F., Fregly, B.J., Koh, B. Il, Haftka, R.T., George, A.D., Mitchell, K.H., 2005. Determination of patient-specific multi-joint kinematic models through two-level optimization. J. Biomech. 38, 621–626. https://doi.org/10.1016/j.jbiomech.2004.03.031

Richards, R., Andersen, M., Harlaar, J., van den Noort, J., 2018. Relationship between knee joint contact forces and external knee joint moments in patients with medial knee osteoarthritis: Effects of gait modifications. Osteoarthr. Cartil. https://doi.org/10.1016/j.joca.2018.04.011.This

Richards, R.E., van den Noort, J.C., van der Esch, M., Booij, M.J., Harlaar, J., 2017. Effect of real-time biofeedback on peak knee adduction moment in patients with medial knee osteoarthritis: Is direct feedback effective? Clin. Biomech. 0–1. https://doi.org/10.1016/j.clinbiomech.2017.07.004

Richmond, B.G., Wright, B.W., Grosse, I., Dechow, P.C., Ross, C.F., Spencer, M.A., Strait, D.S., 2005. Finite element analysis in functional morphology. Anat. Rec.

- Part A Discov. Mol. Cell. Evol. Biol. 283, 259–274. https://doi.org/10.1002/ar.a.20169

Robertson, D.G., Caldwell, G., Hamill, J., Kamen, G., Whittlesey, S., 2014. Research Methods in Biomechanics, 2nd ed. Human Kinetics.

Roemer, F.W., Crema, M.D., Trattnig, S., Guermazi, A., 2011. Advances in Imaging of Osteoarthritis and Cartilage 260.

Roemer, F.W., Eckstein, F., Hayashi, D., Guermazi, A., 2014. The role of imaging in osteoarthritis. Best Pract. Res. Clin. Rheumatol. 28, 31–60. https://doi.org/10.1016/j.berh.2014.02.002

Romero, F., Alonso, F.J., 2016. A comparison among different Hill-type contraction dynamics formulations for muscle force estimation 19–29. https://doi.org/10.5194/ms-7-19-2016

Rybicki, E.F., Simonen, F.A., Weis, E.B., 1972. On the mathematical analysis of stress in the human femur. J. Biomech. 5, 203–215. https://doi.org/10.1016/0021-9290(72)90056-5

Sancisi, N., Parenti-Castelli, V., 2011. A New Kinematic Model of the Passive Motion of the Knee Inclusive of the Patella. J. Mech. Robot. 3, 041003. https://doi.org/10.1115/1.4004890

Sandholm, A., Schwartz, C., Pronost, N., de Zee, M., Voigt, M., Thalmann, D., 2011. Evaluation of a geometry-based knee joint compared to a planar knee joint. Vis. Comput. 27, 161–171. https://doi.org/10.1007/s00371-010-0538-7

Sartori, M., Farina, D., Lloyd, D.G., 2014. Hybrid neuromusculoskeletal modeling best tracks joint moments using a balance between muscle excitations derived from electromyograms and optimization. J. Biomech. 47, 3613–3621. https://doi.org/10.1016/j.jbiomech.2014.10.009

Scheys, L., Van Campenhout, A., Spaepen, A., Suetens, P., Jonkers, I., 2008. Personalized MR-based musculoskeletal models compared to rescaled generic models in the presence of increased femoral anteversion: effect on hip moment arm lengths. Gait Posture 28, 358–65. https://doi.org/10.1016/j.gaitpost.2008.05.002

Seo, J., Kang, D., Kim, J., Yang, S., Kim, D., 2014. Finite element analysis of the femur during stance phase of gait based on musculoskeletal model simulation 24, 2485–2493. https://doi.org/10.3233/BME-141062

Serrancolí, G., Kinney, A.L., Fregly, B.J., Font-Llagunes, J.M., 2016. Neuromusculoskeletal Model Calibration Significantly Affects Predicted Knee Contact Forces for Walking. J. Biomech. Eng. 138, 081001. https://doi.org/10.1115/1.4033673

Seth, A., Sherman, M., Reinbolt, J.A., Delp, S.L., 2011. OpenSim: A musculoskeletal modeling and simulation framework for in silico investigations and exchange. Procedia IUTAM 2, 212–232. https://doi.org/10.1016/j.piutam.2011.04.021

Shirazi, R., 2009. Computational biomechanics of articular cartilage of human knee joint : Effect of osteochondral defects. J. Biomech. 42, 2458–2465. https://doi.org/10.1016/j.jbiomech.2009.07.022

Shirazi, R., Shirazi-adl, A., Hurtig, M., 2008. Role of cartilage collagen fibrils networks in knee joint biomechanics under compression 41, 3340–3348. https://doi.org/10.1016/j.jbiomech.2008.09.033

Shull, P.B., Huang, Y., Schlotman, T., Reinbolt, J.A., 2015. Muscle force modi fi cation strategies are not consistent for gait retraining to reduce the knee adduction moment in individuals with. J. Biomech. 48, 3163–3169. https://doi.org/10.1016/j.jbiomech.2015.07.006

Shull, P.B., Lurie, K.L., Cutkosky, M.R., Besier, T.F., 2011. Training multi-parameter gaits to reduce the knee adduction moment with data-driven models and haptic feedback. J. Biomech. 44, 1605–1609. https://doi.org/10.1016/j.jbiomech.2011.03.016

Shull, P.B., Shultz, R., Silder, A., Dragoo, J.L., Besier, T.F., Cutkosky, M.R., Delp, S.L., 2013a. Toe-in gait reduces the first peak knee adduction moment in patients with medial compartment knee osteoarthritis. J. Biomech. https://doi.org/10.1016/j.jbiomech.2012.10.019

Shull, P.B., Silder, A., Shultz, R., Dragoo, J.L., Besier, T.F., Delp, S.L., Cutkosky, M.R., 2013b. Six-week gait retraining program reduces knee adduction moment, reduces pain, and improves function for individuals with medial compartment knee osteoarthritis. J. Orthop. Res. 31, 1020–1025. https://doi.org/10.1002/jor.22340

Smith, C.R., Choi, K.W., Negrut, D., Thelen, D.G., Smith, C.R., Choi, K.W., Negrut, D., Thelen, D.G., 2018. Efficient computation of cartilage contact pressures within dynamic simulations of movement. Comput. Methods Biomech. Biomed. Eng. Imaging Vis. 6, 491–498. https://doi.org/10.1080/21681163.2016.1172346

Smith, C.R., Lenhart, B.S.R.L., Thelen, D.G., Kaiser, J., Vignos, M.F., 2016. Influence of Ligament Properties on Tibiofemoral Mechanics in Walking. J. Knee Surgeryournal Knee Surg. 29, 99–106.

Smith, C.R., Vignos, M.F., Lenhart, R.L., Kaiser, J., 2017. The Influence of Component Alignment and Ligament Properties on Tibiofemoral Contact Forces in Total Knee Replacement. J. Biomech. Eng. 138, 021017:1-10. https://doi.org/10.1115/1.4032464

Stammberger, T., Eckstein, F., Englmeier, K.H., Reiser, M., 1999. Determination of 3D cartilage thickness data from MR imaging: Computational method and reproducibility in the living. Magn. Reson. Med. 41, 529–536. https://doi.org/10.1002/(SICI)1522-2594(199903)41:3<529::AID-MRM15>3.0.CO;2-Z

Stentz-Olesen, K., Nielsen, E.T., De Raedt, S., Jørgensen, P.B., Sørensen, O.G., Kaptein, B.L., Andersen, M.S., Stilling, M., 2017. Validation of static and dynamic radiostereometric analysis of the knee joint using bone models from CT data. Bone Jt. Res. 6, 376–384. https://doi.org/10.1302/2046-3758.66.BJR-2016-0113.R3

Sturnieks, D.L., Besier, T.F., Mills, P.M., Ackland, T.R., Maguire, K.F., Stachowiak, G.W., Podsiadlo, P., Lloyd, D.G., 2008. Knee Joint Biomechanics following Arthroscopic Partial Meniscectomy 1075–1080. https://doi.org/10.1002/jor.20610

Suh, J.-K., Bai, S., 1998. Finite Element Formulation of Biphasic Poroviscoelastic Model for Articular Cartilage. J. Biomech. Eng. 120, 195–201.

Tanifuji, O., Sato, T., Kobayashi, K., Mochizuki, T., Koga, Y., Yamagiwa, H., Omori, G., Endo, N., 2011. Three-dimensional in vivo motion analysis of normal knees using single-plane fluoroscopy. J. Orthop. Sci. 16, 710–718. https://doi.org/10.1007/s00776-011-0149-9

Tanska, P., Mononen, M.E., Korhonen, R.K., 2015. A multi-scale finite element model for investigation of chondrocyte mechanics in normal and medial meniscectomy human knee joint during walking. J. Biomech. 48, 1397–1406. https://doi.org/10.1016/j.jbiomech.2015.02.043

Taylor, W.R., Schütz, P., Bergmann, G., List, R., Postolka, B., Hitz, M., Dymke, J., Damm, P., Duda, G., Gerber, H., Schwachmeyer, V., Hosseini Nasab, S.H., Trepczynski, A., Kutzner, I., 2017. A comprehensive assessment of the musculoskeletal system: The CAMS-Knee data set. J. Biomech. 65, 32–39. https://doi.org/10.1016/j.jbiomech.2017.09.022

Tecklenburg, K., Dejour, D., Hoser, C., Fink, C., 2006. Bony and cartilaginous anatomy of the patellofemoral joint. Knee Surgery, Sport. Traumatol. Arthrosc. 14, 235–240. https://doi.org/10.1007/s00167-005-0683-0

The American Society of Mechanical Engineers, 2009. V&V 20 – 2009 Standard for Verification and Validationin Computational Fluid Dynamics and Heat Transfer. NY, USA, Am. Soc. Mech. Eng.

The American Society of Mechanical Engineers, 2006. V&V 10 – 2006 Guide for Verification and Validation in Computational Solid Mechanics. NY, USA, Am. Soc. Mech. Eng.

Thelen, D.G., Anderson, F.C., 2006. Using computed muscle control to generate forward dynamic simulations of human walking from experimental data 39, 1107–1115. https://doi.org/10.1016/j.jbiomech.2005.02.010

Thelen, D.G., Won Choi, K., Schmitz, A.M., 2014. Co-simulation of neuromuscular dynamics and knee mechanics during human walking. J. Biomech. Eng. 136, 021033. https://doi.org/10.1115/1.4026358

Tsai, M.-J., Lung, H.-Y., 2014. Two-phase optimized inverse kinematics for motion replication of real human models. J. Chinese Inst. Eng. 37, 899–914. https://doi.org/10.1080/02533839.2014.904474

Tunen, J.A.C.V., Dell'isola, A., Juhl, C., Dekker, J., Steultjens, M., Lund, H., 2016. Biomechanical factors associated with the development of tibiofemoral knee osteoarthritis: Protocol for a systematic review and meta-analysis. BMJ Open 6. https://doi.org/10.1136/bmjopen-2016-011066

Turkiewicz, A., Petersson, I.F., Björk, J., Hawker, G., Dahlberg, L.E., Lohmander, L.S., Englund, M., 2014. Current and future impact of osteoarthritis on health care: A population-based study with projections to year 2032. Osteoarthr. Cartil. 22, 1826–1832. https://doi.org/10.1016/j.joca.2014.07.015

Uhlrich, S.D., Silder, A., Beaupre, G.S., Shull, P.B., Delp, S.L., 2018. Subject-specific toe-in or toe-out gait modifications reduce the larger knee adduction moment peak more than a non-personalized approach. J. Biomech. 66, 103–110. https://doi.org/10.1016/j.jbiomech.2017.11.003

Van de Velde, S.K., Hosseini, A., Kozánek, M., Gill, T.J., Rubash, H.E., Li, G., 2010. Application guidelines for dynamic knee joint analysis with a dual fluoroscopic imaging system. Acta Orthop. Belg. 76, 107–113.

van den Noort, J.C., Schaffers, I., Snijders, J., Harlaar, J., 2013. The effectiveness of

voluntary modifications of gait pattern to reduce the knee adduction moment. Hum. Mov. Sci. https://doi.org/10.1016/j.humov.2012.02.009

van den Noort, J.C., Steenbrink, F., Roeles, S., Harlaar, J., 2015. Real-time visual feedback for gait retraining: toward application in knee osteoarthritis. Med. Biol. Eng. Comput. 53, 275–286. https://doi.org/10.1007/s11517-014-1233-z

Vaziri, A., Nayeb-Hashemi, H., Singh, A., Tafti, B., 2008. Influence of Meniscectomy and Meniscus Replacement on the Stress Distribution in Human Knee Joint. Ann. Biomed. Eng. 36, 1335–1344. https://doi.org/10.1007/s10439-008-9515-y

Viano, D.C., Khalil, T.B., 1976. Investigation of Impact Response and Fracture of the Human Femur by Finite Element Modeling. https://doi.org/10.4271/760773

Viel, T., Casin, C., Ducellier, F., Steiger, V., Bigorre, N., Bizot, P., 2013. Is radiographic measurement of distal femoral torsion reliable? Orthop. Traumatol. Surg. Res. https://doi.org/10.1016/j.otsr.2013.02.009

Walter, J.P., D'Lima, D.D., Colwell, C.W., Fregly, B.J., 2010. Decreased Knee Adduction Moment Does Not Guarantee Decreased Medial Contact Force During Gait. J. Orthop. Res. 28, 1348–1354. https://doi.org/10.1002/jor.21142.Decreased

Walter, J.P., Kinney, A.L., Banks, S. a, D'Lima, D.D., Besier, T.F., Lloyd, D.G., Fregly, B.J., 2014. Muscle synergies may improve optimization prediction of knee contact forces during walking. J. Biomech. Eng. 136, 021031. https://doi.org/10.1115/1.4026428

Wang, Y., Wluka, A.E., Cicuttini, F.M., Jones, G., Ding, C., 2012. Use magnetic resonance imaging to assess articular cartilage. Ther. Adv. Musculoskelet. Dis. 4, 77–97. https://doi.org/10.1177/1759720X11431005

Waryasz, G.R., McDermott, A.Y., 2008. Patellofemoral pain syndrome (PFPS): A systematic review of anatomy and potential risk factors. Dyn. Med. 7, 1–14. https://doi.org/10.1186/1476-5918-7-9

Weinstein, A.M., Rome, B.N., Reichmann, W.M., Collins, J.E., Burbine, S.A., Thornhill, T.S., Wright, J., Katz, J.N., Losina, E., 2013. Estimating the burden of total knee replacement in the United States. J. Bone Joint Surg. Am. 95, 385–92. https://doi.org/10.2106/JBJS.L.00206

Wheeler, J.W., Shull, P.B., Besier, T.F., 2011. Real-Time Knee Adduction Moment Feedback for Gait Retraining Through Visual and Tactile Displays. J. Biomech.

Eng. 133, 041007. https://doi.org/10.1115/1.4003621

Willson, J., Torry, M.R., Decker, M.J., Kernozek, T., Steadman, J.R., 2001. Effects of walking poles on lower extremity gait mechanics. Med. Sci. Sports Exerc. 33, 142–7. https://doi.org/10.1097/00005768-200101000-00021

Wilson, D.R., Feikes, J.D., Connor, J.J., 1998. Ligaments and articular contact guide passive knee flexion. J. Biomech. 31, 1127–1136. https://doi.org/10.1016/S0021-9290(98)00119-5

Wilson, W., Rietbergen, B. Van, Donkelaar, C.C. Van, Huiskes, R., 2003. Pathways of load-induced cartilage damage causing cartilage degeneration in the knee after meniscectomy 36, 845–851. https://doi.org/10.1016/S0021-9290(03)00004-6

Wilson, W., van Donkelaar, C.C., van Rietbergen, B., Ito, K., Huiskes, R., 2005. Erratum to "Stresses in the local collagen network of articular cartilage: a poroviscoelastic fibril-reinforced finite element study" [Journal of Biomechanics 37 (2004) 357–366] and "A fibril-reinforced poroviscoelastic swelling model for articular cartil. J. Biomech. 38, 2138–2140. https://doi.org/10.1016/j.jbiomech.2005.04.024

Wilson, W., van Donkelaar, C.C., van Rietbergen, B., Ito, K., Huiskes, R., 2004. Stresses in the local collagen network of articular cartilage: a poroviscoelastic fibril-reinforced finite element study. J. Biomech. 37, 357–366. https://doi.org/10.1016/S0021-9290(03)00267-7

Wu, G., Cavanagh, P.R., 1995. ISB Recommendations in the Reporting for Standardization of Kinematic Data. J Biomech. 28, 1257–1261. https://doi.org/10.1016/0021-9290(95)00017-C

Wybier, M., Bossard, P., 2013. Musculoskeletal imaging in progress: The EOS imaging system. Jt. Bone Spine. https://doi.org/10.1016/j.jbspin.2012.09.018

Xavier Gasparutto, Sancisi, N., Jacquelin, E., Parenti-Castelli, V., Dumas, R., 2015. Validation of a multi-body optimization with knee kinematic models including ligament constraints. J. Biomech. 48, 1141–1146.

Yang, N., Nayeb-hashemi, H., Canavan, P.K., 2009. The Combined Effect of Frontal Plane Tibiofemoral Knee Angle and Meniscectomy on the Cartilage Contact Stresses and Strains The Combined Effect of Frontal Plane Tibiofemoral Knee Angle and Meniscectomy on the Cartilage Contact Stresses and Strains. https://doi.org/10.1007/s10439-009-9781-3

Yang, N.H., Canavan, P.K., Nayeb-Hashemi, H., Najafi, B., Vaziri, a, 2010. Protocol for constructing subject-specific biomechanical models of knee joint. Comput. Methods Biomech. Biomed. Engin. 13, 589–603. https://doi.org/10.1080/10255840903389989

Yue, B., Varadarajan, K.M., Moynihan, A.L., Liu, F., Rubash, H.E., Li, G., 2011. Kinematics of medial osteoarthritic knees before and after posterior cruciate ligament retaining total knee arthroplasty. J. Orthop. Res. 29, 40–46. https://doi.org/10.1002/jor.21203

Yusuf, E., 2016. Pharmacologic and Non-Pharmacologic Treatment of Osteoarthritis. Curr. Treat. Options Rheumatol. 2, 111–125. https://doi.org/10.1007/s40674-016-0042-y

Zajac, F.E., 1989. Muscle and tendon properties: models, scaling, and application to biomechanics and motor control. CRC Crit. Rev. Biomed. Eng. 17, 359–411.

Zee, M. De, Lund, M., Schwartz, C., 2010. Validation of musculoskeletal models: the importance of trend validations. IUTAM Symp. Hum. Mov. Anal. Simul. 3–4.

Zeighami, A., Dumas, R., Kanhonou, M., Hagemeister, N., Lavoie, F., de Guise, J.A., Aissaoui, R., 2017. Tibio-femoral joint contact in healthy and osteoarthritic knees during quasi-static squat: A bi-planar X-ray analysis. J. Biomech. 53, 178–184.

Zeng, X., Ma, L., Lin, Z., Huang, W., Huang, Z., Zhang, Y., Mao, C., 2017. Relationship between Kellgren-Lawrence score and 3D kinematic gait analysis of patients with medial knee osteoarthritis using a new gait system. Sci. Rep. 7, 4080. https://doi.org/10.1038/s41598-017-04390-5

ISSN (online): 2446-1636
ISBN (online): 978-87-7210-373-0

AALBORG UNIVERSITY PRESS